NAVAL POSTGRADUATE SCHOOL
Monterey, California

(2)

THESIS

EVOLUTION OF DIURNAL SURFACE WINDS
AND SURFACE CURRENTS FOR
MONTEREY BAY

by

Michael D. Foster

December, 1993

Thesis Advisor: Jeffrey D. Paduan
Thesis Co-Advisor: Carlyle A. Wash

Approved for public release; distribution is unlimited.

REPORT DOCUMENTATION PAGE

Form Approved OMB No. 0704

1. AGENCY USE ONLY *(Leave blank)*	2. REPORT DATE	3. REPORT TYPE AND DATES COVERED
	December 1993.	Master's Thesis

4. EVOLUTION OF DIURNAL SURFACE WINDS AND SURFACE CURRENTS FOR MONTEREY BAY

5. FUNDING NUMBERS

6. AUTHOR(S) Michael D. Foster

7. PERFORMING ORGANIZATION NAME(S) AND ADDRESS(ES)
Naval Postgraduate School
Monterey CA 93943-5000

8. PERFORMING ORGANIZATION REPORT NUMBER

9. SPONSORING/MONITORING AGENCY NAME(S) AND ADDRESS(ES)

10. SPONSORING/MONITORING AGENCY REPORT NUMBER

11. SUPPLEMENTARY NOTES The views expressed in this thesis are those of the author and do not reflect the official policy or position of the Department of Defense or the U.S. Government.

12a. DISTRIBUTION/AVAILABILITY STATEMENT
Approved for public release; distribution is unlimited.

12b. DISTRIBUTION CODE
A

13. ABSTRACT *(maximum 200 words)*

The diurnal-period fluctuations of winds and surface currents are analyzed for September 1992 in and around Monterey Bay. Wind records are compared for three coastal stations and two mooring sites. Remotely-sensed surface current observations from two CODAR (HF radar) sites are used to explore the ocean's response to diurnal-period forcing.

An average diurnal cycle is formed at each wind station and at all CODAR bins. The earliest sea breeze response is seen at the coastal wind stations where morning winds accelerate toward the coastal mountain ranges. A few hours later, the coastal winds accelerate to the southeast down the Salinas Valley. Offshore afternoon winds rotate from their normal alongshore orientation to also become aligned with the valley.

The CODAR-derived surface currents respond in less than the two-hour sampling rate to the onset of the diurnal onshore winds. Currents accelerate in the direction of the Salinas Valley. As the day progresses, the more offshore currents rotate clockwise out from under the winds in a possible Ekman or inertial adjustment that continues throughout the night and spreads onshore. In the afternoon, a complicated eddy pattern develops near shore in a possible response to the coastal boundary.

14. SUBJECT TERMS CODAR, Diurnal winds, HF Surface Current Radar, Mesoscale circulations, Monterey Bay Circulation, Sea breeze, Surface currents, Thermally-induced circulations.

15. NUMBER OF PAGES 109

16. PRICE CODE

17. SECURITY CLASSIFICATION OF REPORT	18. SECURITY CLASSIFICATION OF THIS PAGE	19. SECURITY CLASSIFICATION OF ABSTRACT	20. LIMITATION OF ABSTRACT
Unclassified	Unclassified	Unclassified	UL

NSN 7540-01-280-5500

Standard Form 298 (Rev. 2-89)
Prescribed by ANSI Std. 239-18

Approved for public release; distribution is unlimited.

EVOLUTION OF DIURNAL SURFACE WINDS AND
SURFACE CURRENTS FOR MONTEREY BAY

by

Michael D. Foster
Lieutenant Commander, United States Navy
B.S., United States Naval Academy, 1982

Submitted in partial fulfillment
of the requirements for the degrees of

MASTER OF SCIENCE IN METEOROLOGY
AND
MASTER OF SCIENCE IN PHYSICAL OCEANOGRAPHY

from the

NAVAL POSTGRADUATE SCHOOL
December 1993

Author: 

Michael D. Foster

Approved by: 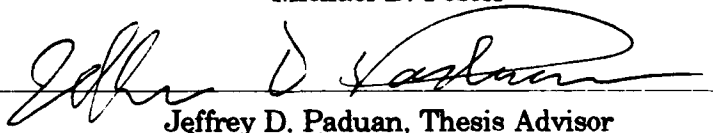

Jeffrey D. Paduan, Thesis Advisor

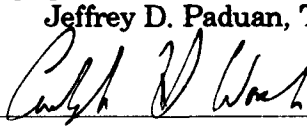

Carlyle A. Wash, Thesis Co-Advisor

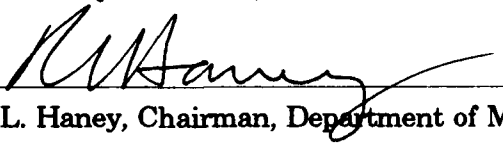

Robert L. Haney, Chairman, Department of Meteorology

Curtis A. Collins, Chairman, Department of Oceanography

ABSTRACT

The diurnal-period fluctuations of winds and surface currents are analyzed for September 1992 in and around Monterey Bay. Wind records are compared for three coastal stations and two mooring sites. Remotely-sensed surface current observations from two CODAR (HF radar) sites are used to explore the ocean's response to diurnal-period forcing.

An average diurnal cycle is formed at each wind station and at all CODAR bins. The earliest sea breeze response is seen at the coastal wind stations where morning winds accelerate toward the coastal mountain ranges. A few hours later, the coastal winds accelerate to the southeast down the Salinas Valley. Offshore afternoon winds rotate from their normal alongshore orientation to also become aligned with the valley.

The CODAR-derived surface currents respond in less than the two-hour sampling rate to the onset of the diurnal onshore winds. Currents accelerate in the direction of the Salinas Valley. As the day progresses, the more offshore currents rotate clockwise out from under the winds in a possible Ekman or inertial adjustment that continues throughout the night and spreads onshore. In the afternoon, a complicated eddy pattern develops near shore in a possible response to the coastal boundary.

TABLE OF CONTENTS

ACKNOWLEDGMENT

My sincere thanks go to both of my thesis advisors, Doctors Jeffery D. Paduan and Carlyle A. Wash, for their forbearance and counsel. My eternal gratitude goes to Mr. Mike Cook, who made this thesis possible by sharing his computer expertise and unselfishly answering (seemingly) millions of computer questions. Most of all, I would like to thank my wonderful wife, Bobbi Jean, for her encouragement, support and love.

I. INTRODUCTION

The United States Navy has shifted its primary operating regions from the deep oceans (blue water navy) to that of coastal or littoral operations (brown water navy). Since 1990, a large part of the four major United States military operations have occurred in the near-shore or littoral regions around the world. In 1990 to 1991, most of the naval operations in the Persian Gulf War took place within the littoral regions of the Persian Gulf and confined regions of the Red Sea. In 1991 and 1992, the United States military was involved with two major disaster relief missions in India and the Philippines in the coastal regions. Recently the United States military conducted an amphibious assault in Somalia to deliver famine relief supplies. In short, the major focus of operations in the early 1990's has been in the littoral regions where the effects of thermally-induced circulations such as the sea breeze are a major contributor to the coastal wind patterns and subsequent current fields. Increased understanding of the sea breeze circulation and its effects on the near-shore surface currents will enhance the United States' ability to conduct safe and sustained operations in the littoral region.

While many studies have been performed on sea breeze circulations in coastal regions, little research has been done to relate the local sea breeze with ocean currents within the coastal regime. In the coastal regime, the sea breeze circulations are responsible for periodic winds near airports and harbors as well as the induction of the

marine stratus and fog into coastal valleys and low lying areas. The sea breeze circulation may have a profound effect upon the nearshore surface current structure. The ocean currents will, in turn, have a pronounced effect upon coastal shipping, docking, moorings and, in certain military applications, amphibious landings.

This thesis investigates relationships between the sea breeze circulation and surface currents in Monterey Bay for the month of September 1992. It describes the mesoscale wind field pattern within Monterey Bay by examining continuous wind measurements from five separate observing stations positioned along the periphery, inside and oceanward of Monterey Bay. The surface ocean current field throughout the Bay is examined using measurements from two Coastal Ocean Dynamics Applications Radar (CODAR) systems along the shoreline. The final aspect of the thesis is the relationships between the wind and current fields.

The thesis results are organized as follows: the background of sea breeze circulations in the atmosphere and remote sensing of ocean currents using HF radars are presented in Section II; diurnal variability of the wind field and the ocean surface current field is presented in Sections III and IV, respectively; Section V describes the relationship between wind and currents; and Section VI summarizes the results and presents the conclusions.

II. BACKGROUND

A. SEA BREEZE CIRCULATION

The near-surface air flow in the coastal environment is influenced by both large-scale and mesoscale wind phenomena. The most common and easily observed aspect of the coastal wind flow is that of the thermally-induced sea and land breeze circulations. Sea and land breeze circulations are produced by temperature contrasts between the land and the ocean. A number of parameters affect the onset, strength and direction of the sea/land breeze. Seasonal changes in solar heating change the land-sea contrast necessary for sea breeze circulations. The combined effects of clouds and prevailing synoptic flow will influence the time of onset and intensity of sea and land breeze circulations. Round (1993) examined a number of these features for the Monterey Bay region.

1. Classic Sea/Land Breeze

Normally, the sea breeze occurs along a coastal boundary during daylight hours when the temperature contrast between land and ocean caused by solar heating is greatest. Solar irradiance will provide the thermal stimulus to warm the surfaces of land and ocean. Land areas will warm up considerably faster than the oceans. As the land warms, a thermally-induced meso-low pressure area of less dense air is established, in which there is upward motion. Meanwhile, over the ocean, the temperature is relatively cool compared to the temperatures over land. This cool air

immediately over the surface of the ocean is more dense and forms a thermally-induced meso-high pressure area. Within this meso-high, there is subsidence from aloft. The pressure gradient from the thermally-induced meso-high and meso-low, produced by the differences in temperature over the land and water, generates onshore wind flow. To complete the sea breeze cell, the return flow to the ocean occurs above the onshore flow. An example of the growth of the classic sea breeze circulation is shown in Figure 1 (Hsu, 1988).

The land breeze can be thought of as the reverse case of the sea breeze. Since the land cools faster at night than the ocean, surface winds flow offshore, while onshore return flow occurs above the offshore flow.

2. Sea Breeze Dynamics

The development of the wind circulation associated with the sea breeze can be related to Newton's second law for a linked series of fluid parcels as applied by Kelvin (Gill, 1982). Thus the circulation, C, in this context, is the line integral of the wind velocity, $\vec{v}$, through its closed path, l, as in Equation 1:

$$C \equiv \oint \vec{V} \cdot d\vec{l} \qquad [1]$$

Using the basic concept of temperature difference between the land and ocean, the acceleration of the wind parcels along the surface in the coastal regime can be shown to be proportional to the temperature contrast across the circulation (Holton 1979). Assuming V represents the mean horizontal velocity in the plane, $\bar{T}_2$ represents the

mean atmospheric temperature over the land, $\bar{T}_1$ represents the mean atmospheric temperature over the ocean, p_0 represents the atmospheric pressure at the surface, p_1 represents the atmospheric pressure at the height of the return flow, h represents the height of the return flow, and L represents the horizontal extent of the sea breeze circulation; the acceleration due to the sea breeze circulation can be expressed as

$$\frac{dV}{dt} = \frac{R \ln(p_0/p_1)}{2(h+L)} (\bar{T}_2 - \bar{T}_1) . \qquad [2]$$

Thus, the acceleration of onshore flow would increase very rapidly and would persist until the acceleration was balanced by factors such as friction and temperature changes. The idealized sea breeze circulation is illustrated in Figure 2 by Holton (1979).

3. Effect of Coastal Upwelling on Sea Breeze

The climate of the western coast of the United States is dominated by the North Pacific high during the summer months (Elliott and O'Brien, 1977). The associated large-scale pressure pattern produces a large-scale northerly gradient wind flowing parallel to the coast. Ekman turning of the top layer of the ocean due to these northerly winds force ocean surface waters away from the coast. As the surface waters diverge, colder sub-surface waters upwell along the coast. Hot interior valleys combine with the cold offshore waters to produce a strong temperature gradient that contributes to northerly to north-northwesterly geostrophic winds along the coast, and therefore low-level onshore (sea breeze) winds (Banta et al., 1993). The upwelling-

influenced sea breeze circulations can penetrate the interior of the coast as much as 50 miles or more inland (Gill, 1982).

Around Monterey Bay, the topography of the area strongly influences the sea breeze circulation. Relatively high mountains to the north and south help funnel the sea breeze circulation into the Santa Clara Valley and the mouth of the Salinas Valley. The heating in the Salinas Valley and Santa Clara Valley provide strong temperature contrasts to the water in Monterey Bay. The breaking of internal waves at the head of the Monterey Canyon could lead to cold upwelling pulses that could serve to increase further the temperature contrasts between ocean and land (Petruncio, 1993).

4. Recent Research into Monterey Bay Sea Breeze Circulations

Banta et al. (1993) constructed vertical cross-sections of the atmosphere using pulsed Doppler lidar perpendicular to the coast in order to get a clear picture of the wind flow in a sea breeze circulation. Their studies showed the beginnings of the sea breeze along the surface flowing inland. For most of their study, they could not detect a return aloft above the sea breeze, nor any Coriolis turning of the sea breeze. Banta et al. concluded that the lack of return flow aloft was due to large-scale influences overwhelming meso-scale local influences in completing the circulation.

Round (1993) described the sea breeze circulation in Monterey Bay based on meteorological observations taken at the vertical wind profiler site at Fritsche Field on Fort Ord. He attempted to categorize the sea breeze by development, onset, surge inland, wind speed, intensity, boundary layer effects, and large scale effects. A speed index was developed to estimate circulation intensity. Four separate types of

sea breezes were identified: gradual development, clear onset, frontal and double surge. Gradual development and frontal sea breezes accounted for over 65% of the observed sea breeze occurrences.

B. TOPOGRAPHY AROUND MONTEREY BAY

The topography and its influences upon both synoptic and mesoscale wind circulations are critical to the study. As shown in Figure 3, the region around Monterey Bay is complex, varying from sea level to over 4,000 feet in the Santa Lucia Range. The prominent features include the Santa Cruz mountains extending from San Francisco along the coast to the southeast of Santa Cruz; the Salinas Valley which extends to the southeast from Moss Landing to King City; and the Santa Lucia Coastal Mountain Range which extends south of Monterey Peninsula forming the western boundary of Salinas Valley. The Salinas and Santa Clara Valleys are important for they are the source regions for the heating required to bring about the sea breeze circulations in Monterey Bay.

C. HF RADAR MEASUREMENT OF OCEAN CURRENTS

1. Introduction

Obtaining an accurate picture of the ocean surface current structure is often a very expensive and time consuming process. Through the use of Eulerian and Lagrangian current measurement devices, the surface current can be obtained for one specific point or its trajectory can be traced over the period of the observation. No

practical method exists using these techniques to obtain a two-dimensional time series over large areas. Advances in electronic technology have enabled the independent development and utilization of high frequency (HF) radar current measurement devices in several different countries around the world. These instruments are capable of providing a two-dimensional time series over large parts of the coastal zone.

2. History

In his studies of surface gravity waves, Crombie (1955) of New Zealand pioneered and developed the principles of using radio wave scatter in the HF frequency band (3-30 MHz) to measure the speed of surface ocean currents. The Doppler shift of radio waves emitted from a stationary transmitter, reflected off a moving object and received at a stationary receiving station is defined by

$$\Delta f = 2f(v/c) = \frac{2v}{\lambda} \qquad [3]$$

where f is the central frequency, v is the velocity of object toward the transmitter, c is the speed of the radio waves, and λ is the wavelength of the radio waves. The speed of surface gravity waves in deep water is given by

$$v = \sqrt{\frac{gL}{2\pi}} \qquad [4]$$

where v is the phase velocity of the waves, g is the acceleration due to gravity, and L

is the wavelength of waves. The Doppler shift due to reflections from deep water gravity waves is given by

$$\Delta f = = \frac{2}{\lambda}\sqrt{\frac{gL}{2\pi}} = \sqrt{\frac{g}{\pi\lambda}} \qquad [5]$$

where the second equation holds for gravity waves of half the radar wavelength, L= $\lambda/2$, which are the dominant reflectors.

After performing several tests, Professor Crombie discovered that there were multiple peaks in the frequency spectrum about the central frequency of the incident radio waves due to echoes from surface waves. A typical frequency spectrum of backscattered energy is shown in Figure 4 (Fernandez, 1993). Several peaks corresponded to different orders of approximation representing frequency wave lengths of surface gravity waves. The spectral peaks in the echoes received corresponded to multiples of $n\lambda/2$. The different multiples n represents the different orders of approximation of resolving the spectral peaks. When n = 1 (1st order approximation) the signal received was 10-15 dB (several orders of magnitude) stronger than the nearest second order approximation (Barrick and Growler, 1986). As such, the first order approximation serves as the basis for all ocean surface current measurements using high frequency radio waves. The reason for the very high 1st order return is resonant Bragg scattering from surface gravity waves with wavelength exactly one half the wavelength of the incident radio waves.

In the HF band, Bragg scattering is produced by deep water gravity waves whose phase speeds are known precisely (Equation 5). Observed deviations from the expected Doppler shift can be used to measure surface currents (Stewart and Joy, 1974). Figure 5 (Barrick et al., 1977) illustrates the Bragg scatter effect and illustrates the types of Doppler shifts expected from advancing and receding oceanic waves. The current velocity can only be measured radially towards or away from any one transmitting and receiving site. Utilizing two transmitting/receiving stations, the horizontal velocities of the current can be computed using simple trigonometric relationships. It is important to note that there is a baseline region of instability. The baseline region of instability exists in the straight line path between the two stations. In the baseline region, accurate current vectors cannot be resolved since there are no observations of the velocity components perpendicular to the baseline.

3. CODAR in Monterey Bay

Remote current measurements in Monterey for the period of this thesis research were obtained from two CODAR transmitting/receiving sites located at Hopkins Marine Laboratory in Monterey and at the Monterey Bay Aquarium Research Institute (MBARI) station in Moss Landing. Each of these two sites obtained radial current velocity components for a field of 195 gridpoints that were observed for the month of September. Each gridpoint is a 2 km by 2 km square which represents the intersection of the two radar beams. The locations of these gridpoints are shown in Figure 6. The figure also indicates numerically and graphically the percentage of time

a radar-derived current vector was recorded out of a maximum of 360 possible observations.

Neal (1992) performed a study of CODAR-derived surface currents in Monterey Bay using data from the same radar installations. He compared them with Acoustic Doppler Current Profiler (ADCP) measurements during three months in the spring of 1992 in an attempt to explain the temporal and spatial coverage of CODAR-derived surface currents and confirm the validity of CODAR measurements in Monterey Bay. CODAR measurements compared favorably with the moored ADCP measurements for low frequency motions (period greater than one week). Neal observed onshore surface currents in the afternoon and weak offshore current flow at night. He also alluded to current forcing caused by the diurnal sea breeze influence and both semi-diurnal and diurnal tidal influences. This work follows on the work of Neal using more frequent CODAR data (2 hourly versus 3 hourly) and a suite of wind measurements.

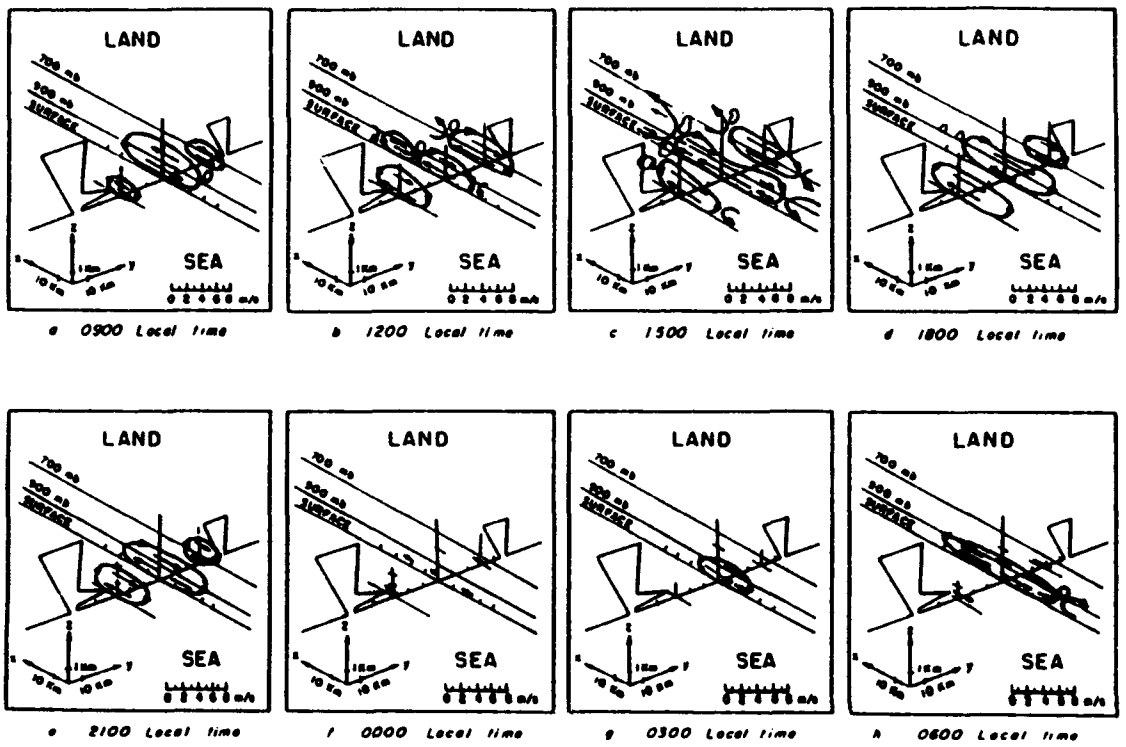

Figure 1. An idealized thermally-induced circulation model. Shown are portions of the Texas coastline, including Galveston Bay and Sabine Lake, and the land and sea areas in a two-dimensional (x,y) plane. Three different thermally-induced circulations are show vertically in the (x,z) plane. Panels *a-d* show the onshore component (sea breeze) of the thermally-induced circulation, while panels *e-h* show the offshore component (land breeze). The smaller circulations on each flank are modified by the local effects of Galveston Bay and Sabine Lake (Hsu, 1988).

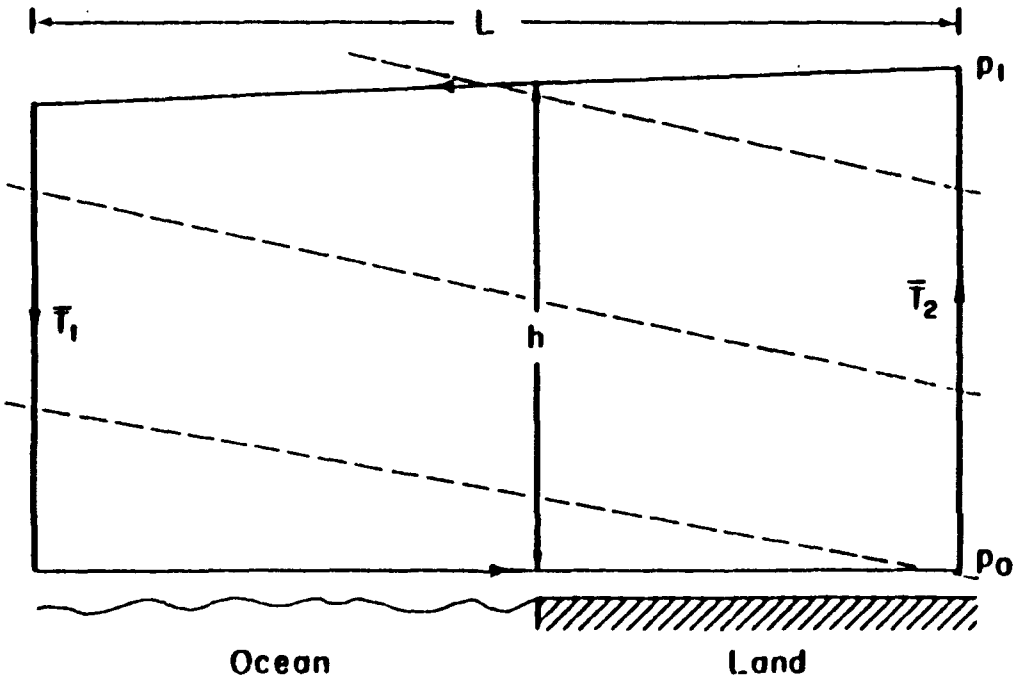

Figure 2. The circulation theorem applied to an idealized sea breeze circulation. The circulation will be evaluated around the outer box, following the arrows. $\bar{T}_2$ ($\bar{T}_1$) is the mean atmospheric temperature over the land (ocean), p_0 is the atmospheric pressure at the surface, p_1 is the atmospheric pressure at the height of the return flow, h is the height of the return flow, and L is the horizontal extent of the sea breeze circulation. The dashed lines indicate isosteric surfaces, or isolines of specific volume (Holton, 1979).

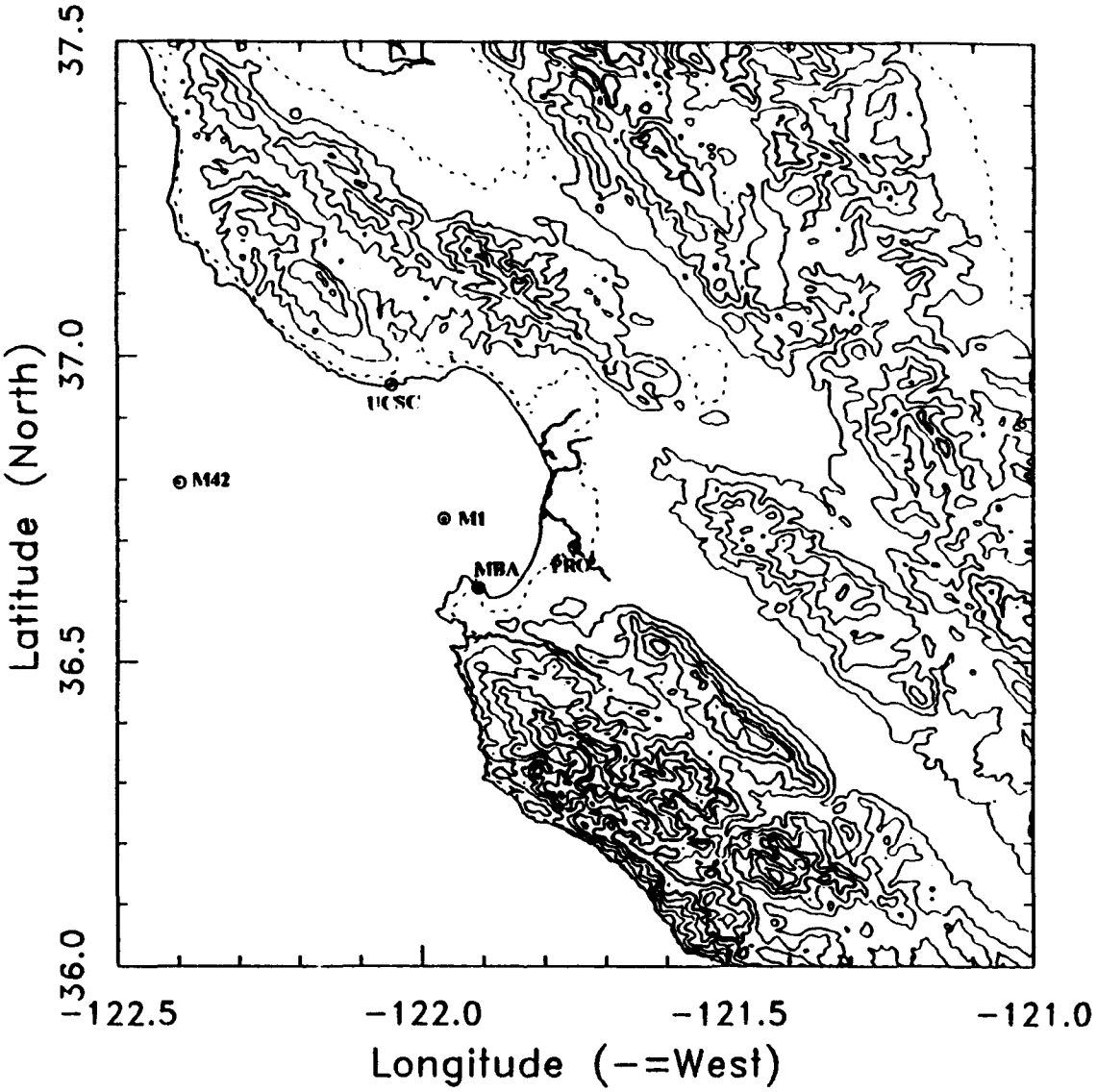

Figure 3. The terrain surrounding Monterey Bay. The Santa Cruz Mountains are to the north, the Santa Lucia Mountains to the south, and the Salinas Valley stretches to the southeast. The Pajaro Valley extends due east of Monterey Bay with some connection to the larger Santa Clara Valley to the north. The five wind observation stations used in this study are plotted in bold lettering. The dashed line represents 50 meters above sea level, while the solid lines represent 100 meter contour intervals. 500 meter contours are highlighted in bold.

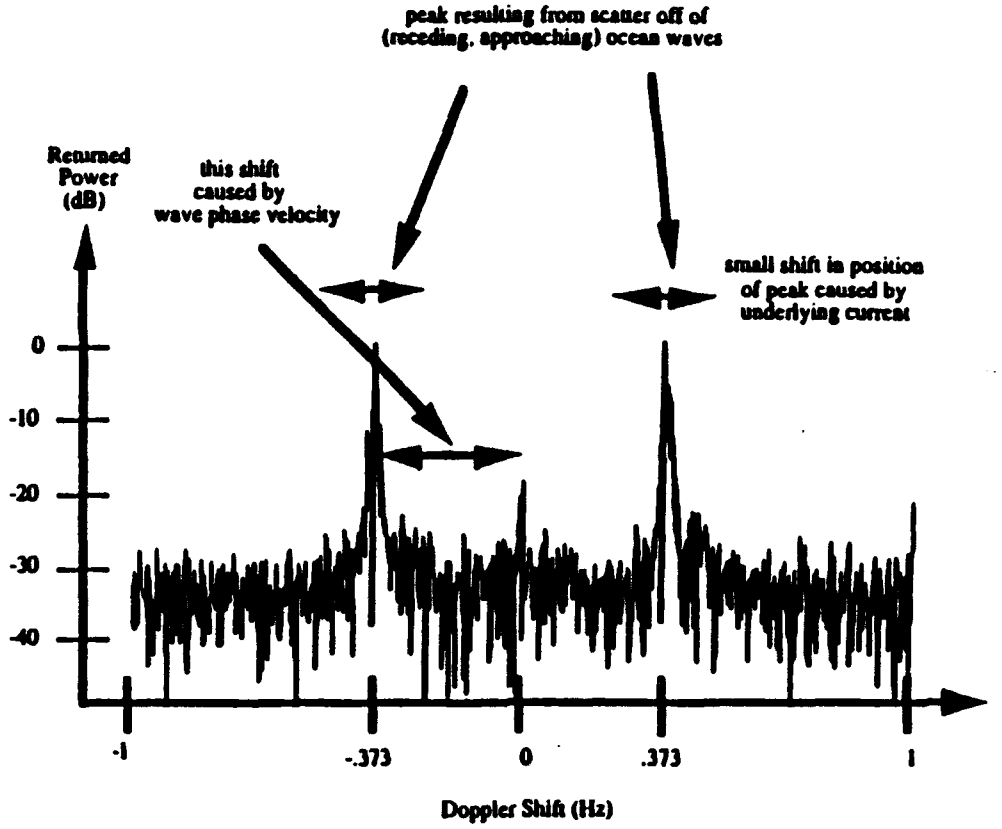

Figure 4. An example of a returned radar echo spectrum and the Doppler shifts associated with scatter off of advancing and receding ocean waves (Fernandez, 1993).

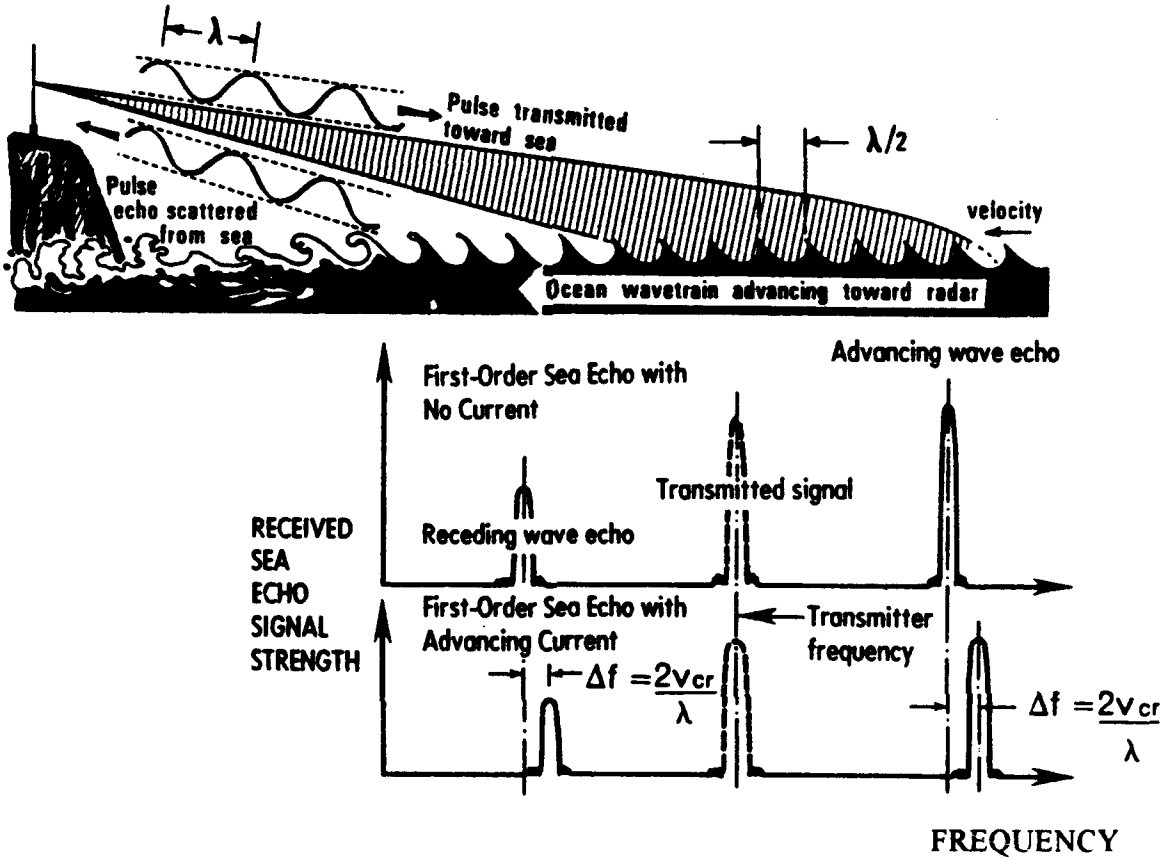

Figure 5. Schematic representation of Bragg Scatter from the ocean surface producing a first-order return and the determination of the Doppler shift associated with an underlying current. λ is the wavelength of the radio wave, Δf is the Doppler shift of the reflected echo relative to the expected Doppler shift from surface waves of one half the radar wavelength, and V_{cr} is the mean effective current velocity radial to the radar (Barrick et al., 1977).

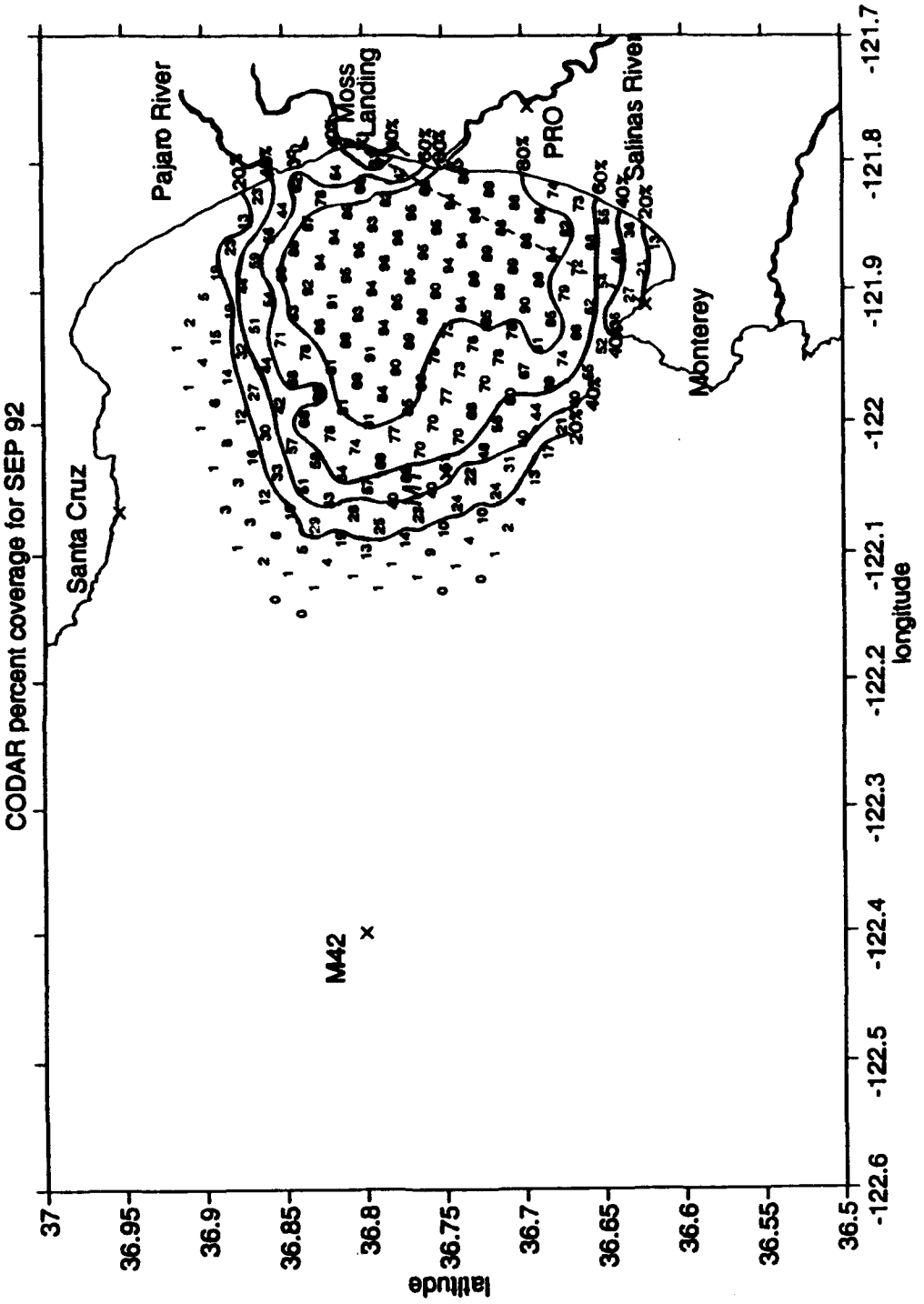

Figure 6. CODAR percent coverage map of Monterey Bay for September 1992. Each contour interval represents a 20% change in coverage. The baseline region of uncertainty of the CODAR-derived current vectors is plotted with a dashed line.

III. WIND SEA BREEZE EFFECTS

A. GENERAL WIND INFORMATION

Wind data in and around Monterey Bay was collected at five different locations, three on the coast and two afloat. The location of the five wind stations is given in Figure 3. The first station was the National Oceanographic and Atmospheric Administration (NOAA) NDBO 46042 mooring buoy site (abbreviated M42) located near 36.8° North latitude, 122.4° West longitude, 48 km due west of Moss Landing. The second ocean wind measuring buoy was located near 36.75° North and 122.04° West. This mooring is operated by the MBARI and is known as the M1 site. The northernmost land station was located at the Long Marine Research Laboratory at the University of California at Santa Cruz, referred to as the UCSC site. The southern land station was located at the Monterey Bay Aquarium (MBA) and referred to as the MBA site. The last wind measuring station was located at the Fritsche Field vertical wind profiling site located on Fort Ord and referred to as the PRO site.

Wind data was received in several different formats. The UCSC, MBA, and PRO wind data was available in five minute temporal resolution, while M1 was available in ten minute resolution. M1 observed the wind at 2 Hz sampling for one minute every ten minutes and derived a vector average over that one minute. The M42 wind data was available in one hour temporal resolution only. It derived from a vector average over an eight minute period. The winds for each of the observation

stations were taken at different heights and the data was averaged over different sampling intervals shown in Table I. All times were converted to Pacific Daylight Time (PDT).

TABLE I

Wind Station	Height above Sea Level (meters)	Height above roof top/ground (meters)	Interval averaged over (minutes)
M42	5	-	8
M1	3.8	-	1
UCSC	20	7	5
MBA	20	3	5
PRO	53	4	2

The data at UCSC was collected for the last half of September 1992 only (from 1800 PDT on 14 September onward). The PRO data was continuous and the M1 data was nearly continuous with only 1 five minute gap in the entire series, which was filled by linear interpolation. The other three wind stations M42, UCSC and MBA had larger gaps in the time series.

Gaps in the time series were filled using linear interpolation if the gap was less than three hours. When the gap was greater than three hours, a complex gap filling scheme was used that preserved the canonical nature of the winds. This scheme filled shorter gaps first then filled larger gaps. The longer gaps were filled using one-third linear interpolation plus one-third pre-gap canonical observation plus one-third post-gap canonical observation. (In this context, canonical observation refers to the value

observed at the same time one day earlier or later.) Gaps in time series at MBA and UCSC were filled using ten minute resolution data and at M42 using one hour resolution data.

The gap-filled wind time series data for U and V components are plotted in Figure 7 for all five wind stations. The obvious signal at most locations is the diurnal-period fluctuations. The exception is at M42 where more of the variance seen in fluctuations with periods of about five days.

Upon retrieval of the M1 mooring for normal maintenance in April 1993, it was discovered that the compass used in the wind measurements had developed irregularities with possible drift in the instrument calibration. It is not known to what extent the compass drifted nor when it first occurred. The reader should be aware of possible wind direction inaccuracies at M1. The calibration error had no effect on the magnitude of the wind speed.

B. ROTARY WIND SPECTRA

According to Gill (1982), the rotary spectra examines how the kinetic energy density of a time series of velocity vectors is distributed among various frequencies. The horizontal velocity vectors are split into east-west (U) and north-south (V) components. U and V components are then expressed in the complex plane by taking U as the real part and V as the imaginary part. The velocities of wave disturbances in the real and imaginary planes are proportional to $\exp(i\omega t)$ (a counterclockwise rotating wave) and $\exp(-i\omega t)$ (a clockwise rotating wave). Thus the rotary spectra will tell how

much energy associated with a time series of velocity vectors is contributed by clockwise and counterclockwise rotating portions of the time series. Examining the rotary spectra for the wind time series will indicate if there is a preference for a particular direction of rotation of the wind vectors at the wind stations at the diurnal frequency.

Rotary spectra for the four longest wind time series are presented in Figure 8. The solid (dashed) line is energy spectra associated with clockwise (counterclockwise) rotation. The rotary spectra indicate strong clockwise rotation (solid line greater than dashed line in Figure 8) of the winds at the diurnal frequency at the oceanic moorings, M42 and M1. The rotary spectra at MBA indicated strong counterclockwise rotation (dashed line greater than solid line in Figure 8) at the diurnal frequency. At the PRO site, the clockwise and counterclockwise rotational components are essentially the same. Therefore, there is statistically no preference for either clockwise or counter-clockwise rotation of the diurnal-period winds at the PRO site, which corresponds to a rectilinear shift of the winds up and down the Salinas Valley.

C. SYNOPTIC CONDITIONS

Synoptically, September 1992 was uneventful for most of the month. A general northwesterly flow along the coast of California predominated and was typified by the surface data plot for 00Z on 8 September (Figure 9). Figures 10 to 12 show vector stick plots of the winds for Monterey Bay for the month of September in ten day

segments. The general northwesterly flow is the result of the eastern North Pacific high and the thermally-induced low over the southwestern United States.

The major exception to northwesterly flow occurred on 26 and 27 September, at which time a coastal southerly surge of winds occurred at the M1 and M42 sites. Examination of the synoptic charts reveals a coastal southerly wind event that began near San Diego on 25 September, progressed slowly northward along the coast to Monterey Bay arriving on 26 September just slightly ahead of the daily sea breeze, and progressed northward of Monterey Bay by the end of the 27th of September. In Figure 12, the coastal southerly event is readily apparent in the M42 and M1 wind data on 26 and 27 September, while northwesterly flow returned on 28 September. The event is not obvious in the land coastal wind records. One probable explanation for the coastal southerly event is the northward propagation of a trapped Kelvin wave (Gill, 1982) in the marine layer bounded by onshore flow and coastal mountains and an initial instability in the inversion near San Diego.

D. STATION TO STATION WIND COMPARISONS

In order to begin wind station to station comparisons, one needs to look at the wind effects at each individual station. All winds are oriented so the winds flow towards a direction, in contrast to the standard meteorological convention of naming direction from which the wind flows. The wind-rose illustrations in Figure 13 show the relationships between the number of times hourly observations occurred for each direction, where directions are binned into 30-degree-wide sectors. It should be noted

that for UCSC in Santa Cruz, the wind rose represents only the second half of September 1992.

At M42, a synoptic wind flow dominates as indicated by most of the observations being towards the southeast. At M1 the wind pattern is still influenced by the overall background synoptic flow, but more variability is evident due to the effects of the sea breeze. At UCSC and MBA, the winds are influenced by the combined effects of a local onshore sea breeze, the larger-scale sea breeze produced by heating in the Salinas and Santa Clara Valleys, the prevailing background flow, and local topography. The winds at PRO are strongly influenced by the topography, here the flow is either southeast down the Salinas Valley, or northwest up the valley toward the ocean.

1. Canonical Day Winds

The wind-rose representations in Figure 13 do not describe the strength of the winds at each station nor do they expose the timing of the daily sea breeze variations at each station. To obtain this information, the canonical, or typical, day winds were computed by averaging all observations at similar times for each station. i.e. all 0000 observations were averaged together, etc... The canonical-day results are presented as hodographs and stick vectors in Figures 14 and 15, respectively. In Figure 14, the monthly mean wind is represented by $\oplus$, and the mean hourly winds in PDT are connected by solid lines with numeric values representing midnight (0), 6 AM (6), noon (12), and 6 PM (18).

The sea breeze begins at MBA and UCSC by shifting towards the land approximately 0900, then rotating towards the Salinas Valley. This is apparent at UCSC by clockwise rotation of the canonical-day hodographs (Figure 14), stick vectors (Figure 15) and wind spectra (Figure 8). At MBA, the shift toward the Salinas Valley is accomplished by a counterclockwise rotation. At the PRO site, the winds also shift counterclockwise towards the valley with the sea breeze beginning near 1000 and peaking near 1300, although these winds are more nearly rectilinear.

Offshore, the winds shift clockwise in response to the sea breeze influence. The wind shift begins near 1000 at M1 and near 1100 at M42. This difference is due to the fact that the sea breeze circulation begins at the coast under the influence of morning inland heating and then the circulation expands inland and outward from the coast as the circulation becomes larger. At M1, the afternoon winds develop an unexpected small component of flow toward the north. It has been postulated (Nuss, Naval Postgraduate School) that this flow may help counterbalance the mean wind divergence in Monterey Bay during sea breeze hours. However, there is also uncertainty in the direction for the winds at M1 as described earlier. The maximum and minimum coastal winds at MBA and PRO occur near the same time and their counterclockwise rotation about the mean is similar. In contrast, at M42 and M1 the rotation about the mean is clockwise and the maximum and minimum wind speeds occur just slightly later at M42, probably due to the fact that it is further out to sea.

2. 17 to 20 September

In order to quantify and check the validity of the canonical day winds for use in this study, an extensive look at the diurnal wind signature in hourly wind data for four days was performed. The specific period of 17 to 20 September was chosen for closer wind analysis because it contains a clear sea breeze signal and has data from all five sites (refer to Figure 11). The observed wind patterns in hourly data for the four day period of intensive scrutiny are consistent with those generated by the canonical-day averaging process over the entire period.

At M42 on 17th, the winds decrease after 0100 PDT to a minimum near 1000 PDT. Winds begin to strengthen after 1100 PDT beginning the slight counterclockwise rotation early in the sea breeze cycle. The strongest winds occur near 1800 to 1900 PDT as the winds begin a strong clockwise wind rotation that continues through 2000-2200 PDT. On the 18th, the winds weaken till 1400 PDT, then begin to build with the onset of a counterclockwise rotation early on then shift to clockwise rotation. The onset of a period of uniformly strong winds begins near 1800 PDT indicating a strong, prevalent synoptic flow pattern that lasts for 48 hours. On the 20th, strong prevailing synoptic flow peaks near 0700 PDT with a slight easing of the winds afterwards. By 1500 PDT, there is an initial counterclockwise rotation toward land shifting to clockwise rotation with maximum wind speeds near 2200 PDT.

At M1 on the 17th, the winds begin a counterclockwise rotation towards the northeast near 1000 to 1100 PDT, while a clockwise rotation begins around 1500 PDT with onset of the strongest wind speeds that last until 0300 PDT the next

morning. The strongest winds occur in the afternoon hours from 1500 to 1900 PDT with an east-northeast orientation. On the 18th, the winds begin their weak counterclockwise shift toward the east between 0800 and 0900 PDT. The winds peak near 1800 PDT, after which the winds begin their clockwise rotation as their speeds abate. The 19th is a repeat of the previous day with slightly higher wind speeds. The orientation of the peak winds in the afternoon is toward the east. Early in the morning of the 20th, the onshore component of wind field is higher than normal. By 1000 PDT, the counterclockwise rotation begins as the winds shift toward the east-northeast and more onshore flow.

The winds at UCSC are remarkably diurnal and consistent with the offshore winds. Between 0800 and 0900 PDT every morning, the winds begin their clockwise rotation toward the land to the north. By 1000 PDT, the winds veer to northeast. By 1100 PDT, the winds begin to build significantly and continue to veer and point toward the east-southeast at 1400 PDT. After the winds peak near 1400, they begin to abate and continue to rotate clockwise until midnight and reach their daily minimum wind speed.

On the 17th at the MBA site, the day starts with a very weak land breeze with a slight offshore component. Beginning at 0800 PDT, the winds begin to back toward the southeast. By 1000 PDT, the winds build to a maximum while pointing toward the southeast. Remarkably, the winds decrease slightly in the afternoon and align themselves down the Salinas Valley. The winds begin to abate and back toward the northeast after 1800 PDT. On the 18th, the land breeze continues until 0800 PDT.

Again, by 0900 PDT, the winds begin to back toward the south. The strongest winds occur near noontime and point toward the southeast. The 19th and 20th are similar to the 17th and 18th, except that the initial southeast morning wind shift occurs between 0900 and 1000 PDT on the 20th. On the 20th, the lack of land breeze is noticeable and may be related to the stronger than normal onshore flow at M1.

At PRO on the 17th, the winds shift from a land breeze component at 0700 PDT to a strong sea breeze component at 0800 PDT down the Salinas valley. The strongest winds occur while pointing down the Salinas Valley at 1300 to 1400 PDT. The sea breeze begins to abate after 1400 PDT and begins a transition to the land breeze circulation. The land breeze winds peak near 0600 PDT the next day. On the 18th, the land breeze winds persist until 0900 PDT, at which time the sea breeze begins. The sea breeze circulation takes effect by 1000 PDT. The sea breeze continues until the land breeze begins near 2300 PDT. On the 19th, the sea breeze is well established by 1100 PDT with a maximum near 1400 PDT. The sea breeze winds abate after 1500 PDT until the land breeze begins near 2200 PDT. On the 20th, the strongest land breeze winds continue until 1100 PDT, at which time the sea breeze begins its daily cycle.

E. WIND ANALYSIS

In order to quantify the relationship between wind records, two different methods were used to correlate the winds from the five different sites. One method was to split the winds into east-west and north-south components (U and V) and then perform

component-to-component spectral analysis. The other method was to use a complex correlation applied to the vector winds. Both methods used hourly data. UCSC was not included since the time series was one-half as long at UCSC than the rest of the wind stations.

1. Longitudinal and Latitudinal Cross Spectra

In splitting the winds into the east-west and north-south components, it was found that the U components were more highly related to each other than the V components. This is probably due to the fact that the sea and land breezes are mostly in the east-west direction. The V components were much more variable such as in the cases of UCSC and MBA in which the winds rotate in opposite directions with the onset of the sea breeze.

In the east-west time series components, MBA leads PRO, which leads M1, which leads M42. The coherences exceed the 95% significant level of confidence. Cross spectral analyses were performed on the different time series and the results are shown in Tables II and III for the specific diurnal period of 24 hours or a diurnal frequency of 0.0417 Hz. One degree of phase difference is equal to four minutes of time difference. Based upon a sampling interval of one hour, any phase difference less than 15 degrees is within the noise of the observations. Table II shows the sea breeze starting at MBA then reaching PRO between one to two hours later. The sea breeze begins at M1 three hours after the start at MBA and begins at M42 between three and four hours from the start at MBA.

TABLE II

U Analysis at f=0.0417 cph or 1 cpd	Phase Difference (degrees)	Phase Difference (h)	Coherence	95% Sig Level of Coherence
MBA leads M42	56.8	3.8	.980	.726
MBA leads PRO	21.4	1.4	.993	.726
MBA leads M1	45.0	3.0	.978	.726
PRO leads M1	22.6	1.5	.979	.726
M1 leads M42	10.9	.7	.951	.726
PRO leads M42	35.0	2.3	.962	.726

TABLE III

V Analysis at f=0.0417 cph or 1 cpd	Phase Difference (degrees)	Phase Difference (h)	Coherence	95% Sig Level of Coherence
MBA leads M42	157.0	10.5	.802	.726
MBA leads PRO	42.5	2.8	.915	.726
M1 leads MBA	140.4	9.4	.833	.726
PRO leads M1	175.7	11.7	.922	.726
M42 leads M1	55.5	3.7	.814	.726
PRO leads M42	116.9	7.8	.888	.726

As can be seen from Table III, the results from the V component time series analysis are not as conclusive as those from the U velocity components since the values for coherency are not as high as they are for the U velocity components, even though they are still above the 95% level of confidence. The V diurnal fluctuation starts at MBA, then reaches PRO approximately three hours later. Since the direction

of rotation is opposite for M1, M42, and UCSC from MBA and PRO, the phase relationships approach 180 degrees out of phase with time lags of six to twelve hours.

2. Complex Correlation

The winds were also compared using the complex correlation described by Kundu (1976). The complex correlation scheme uses both the U and V components of the time series by assigning them real and imaginary values in the complex plane, respectively. The correlation magnitude and phase angle differences between the two time series are calculated for the lags out to plus or minus one-half the record length. Figure 16 shows the results of the complex correlations. The winds at M1 and M42 (solid line) are highly correlated, exhibiting a diurnal pattern so that the major peaks of the correlation magnitude occur with zero phase shifts or multiples of plus-or-minus 24 h. The phase difference between M1 and M42 (not shown) indicates that, on average, the winds at M42 are approximately 24° clockwise from M1.

When correlated to M1, the land wind stations have smaller correlation magnitudes near zero lag than does M42. They indicate peaks at lags of 12-h increments reflecting the semi-diurnal frequencies that could be due to the asymmetric nature of the sea and land breezes. The correlation magnitude for the land stations with M1 (dotted and dash-dotted lines) confirm the cross spectral analyses by showing 1 to 3-hour time lags corresponding to the sea breeze circulation beginning at MBA, then spreading to PRO, and finally arriving at M1.

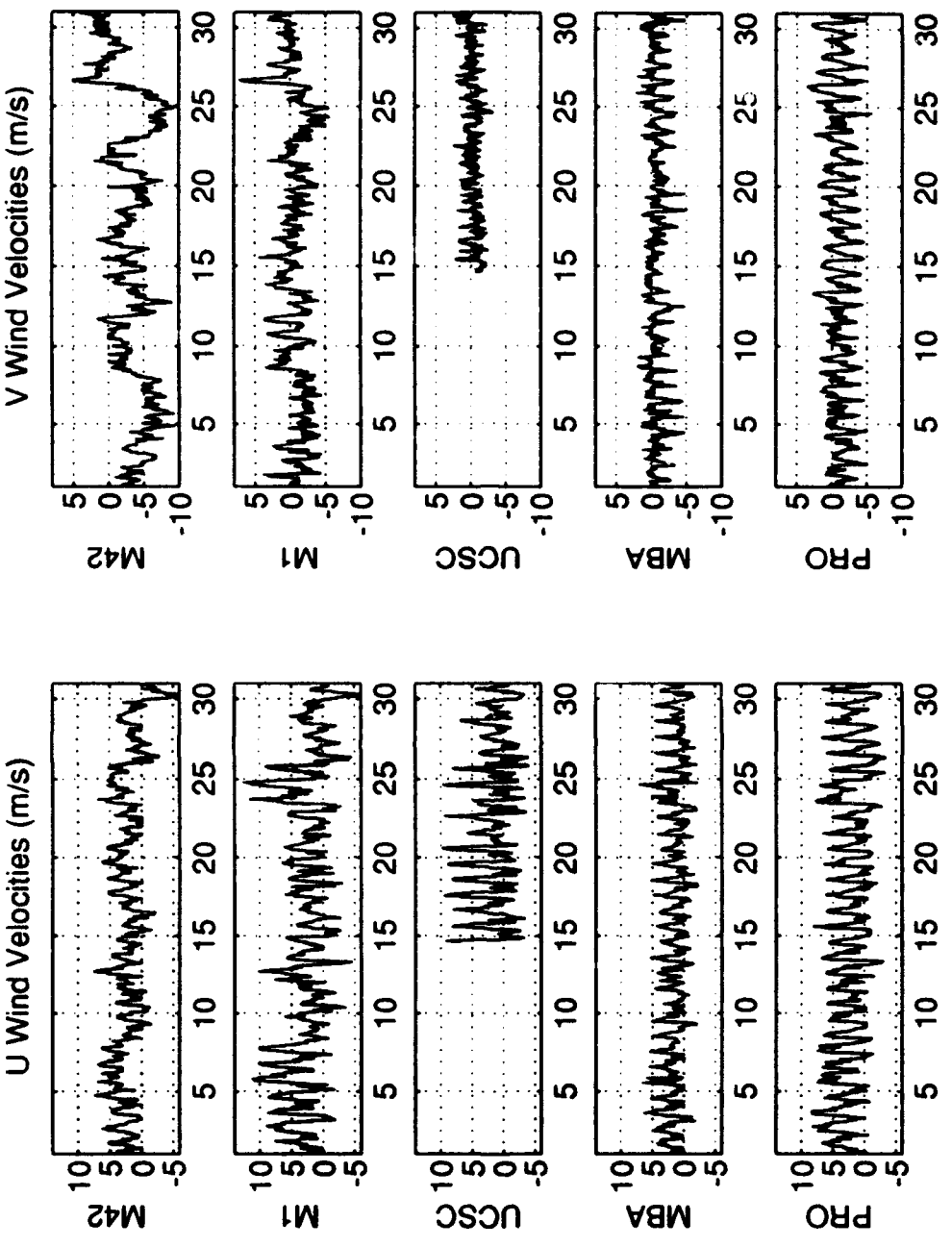

Figure 7. Wind velocities for the five reporting wind stations for September 1992. The wind velocities are split into U (north-south) and V (east-west) components. The vertical axis is in m/s, while the horizontal axis represents the days of September.

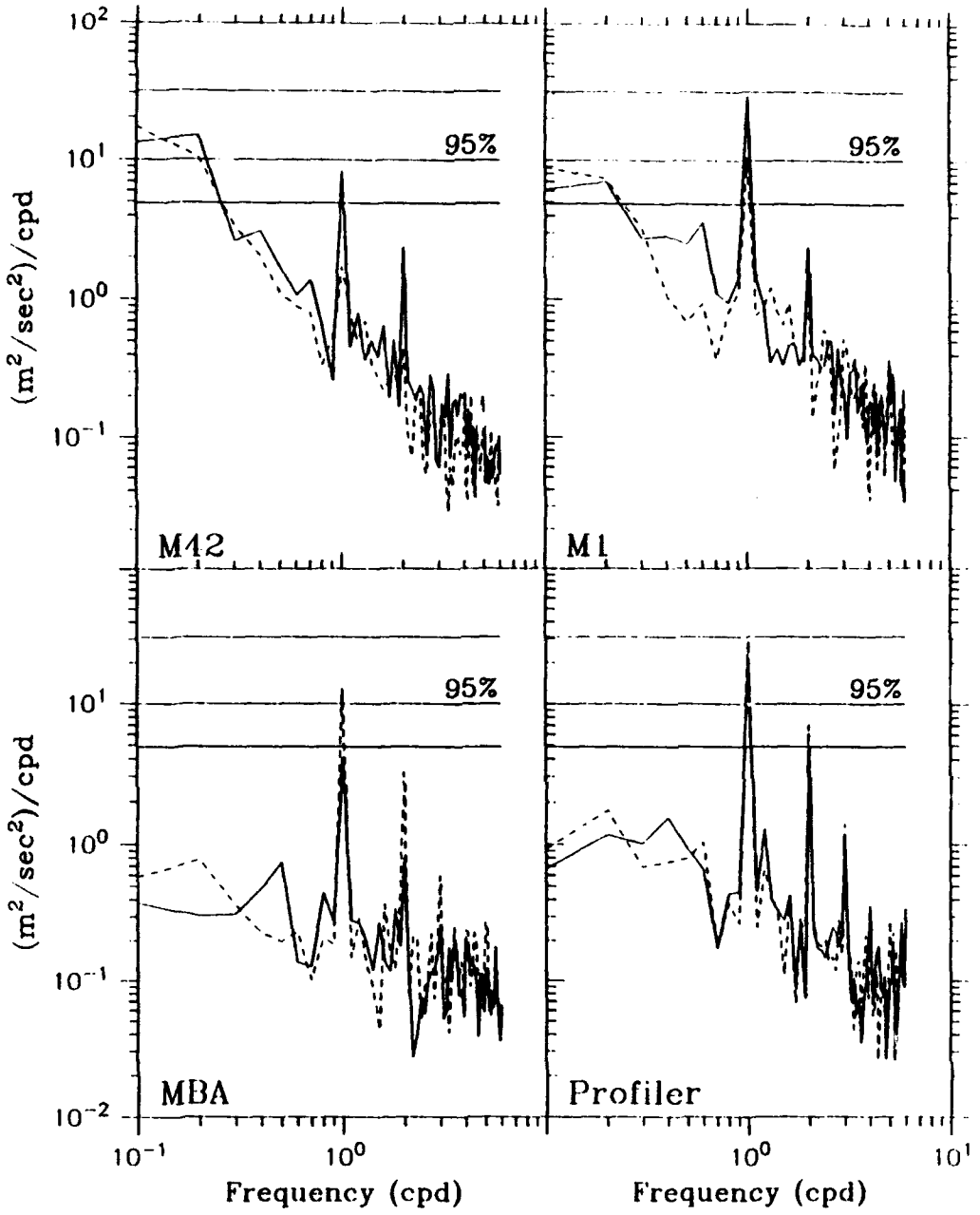

Figure 8. Rotary Spectra for MBA, PRO, M1 and M42 records. Solid lines represent the energy associated with clockwise rotation, while dashed lines represent the energy associated with counterclockwise rotation. The 95% confidence limits for the associated, one-sided auto spectra are also shown.

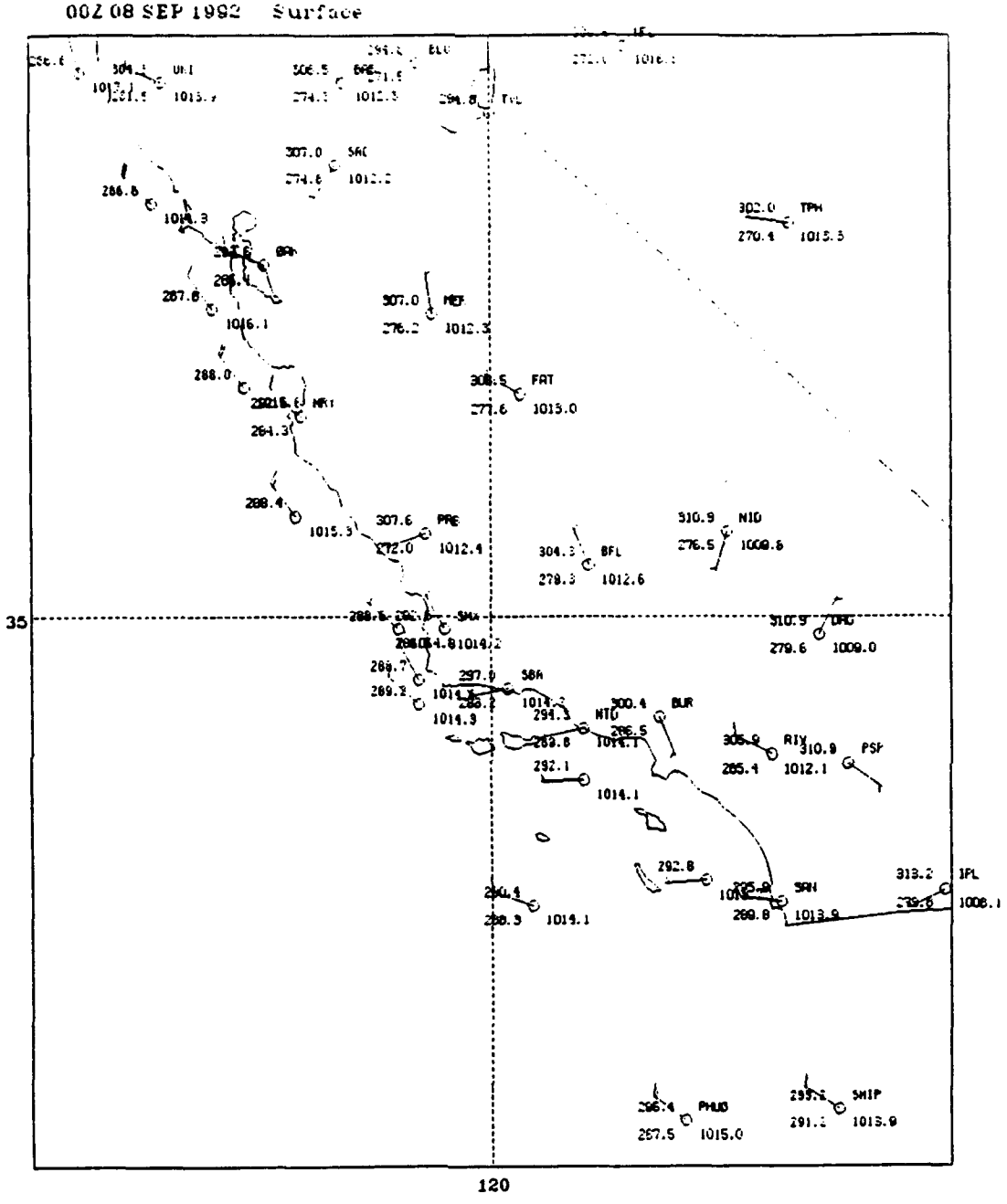

Figure 9. Surface weather map showing surface observations for 00Z on 8 September 1992.

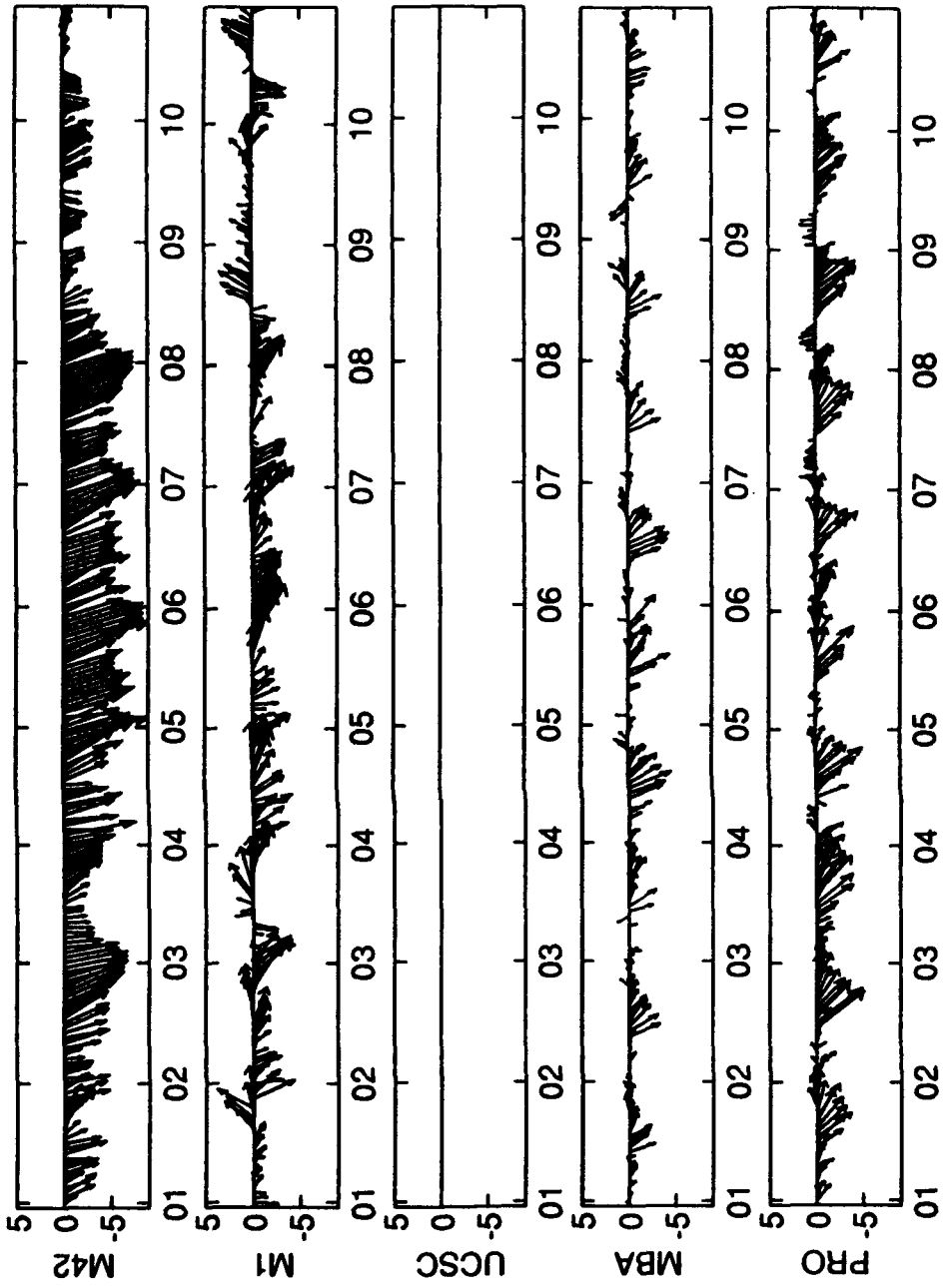

Figure 10. Plot of the surface winds for the five wind stations for 1 to 10 September 1992. The horizontal axis represents the days of the month, while the vertical axis represents wind speed in m/s. Arrows are pointing toward the direction of wind flow.

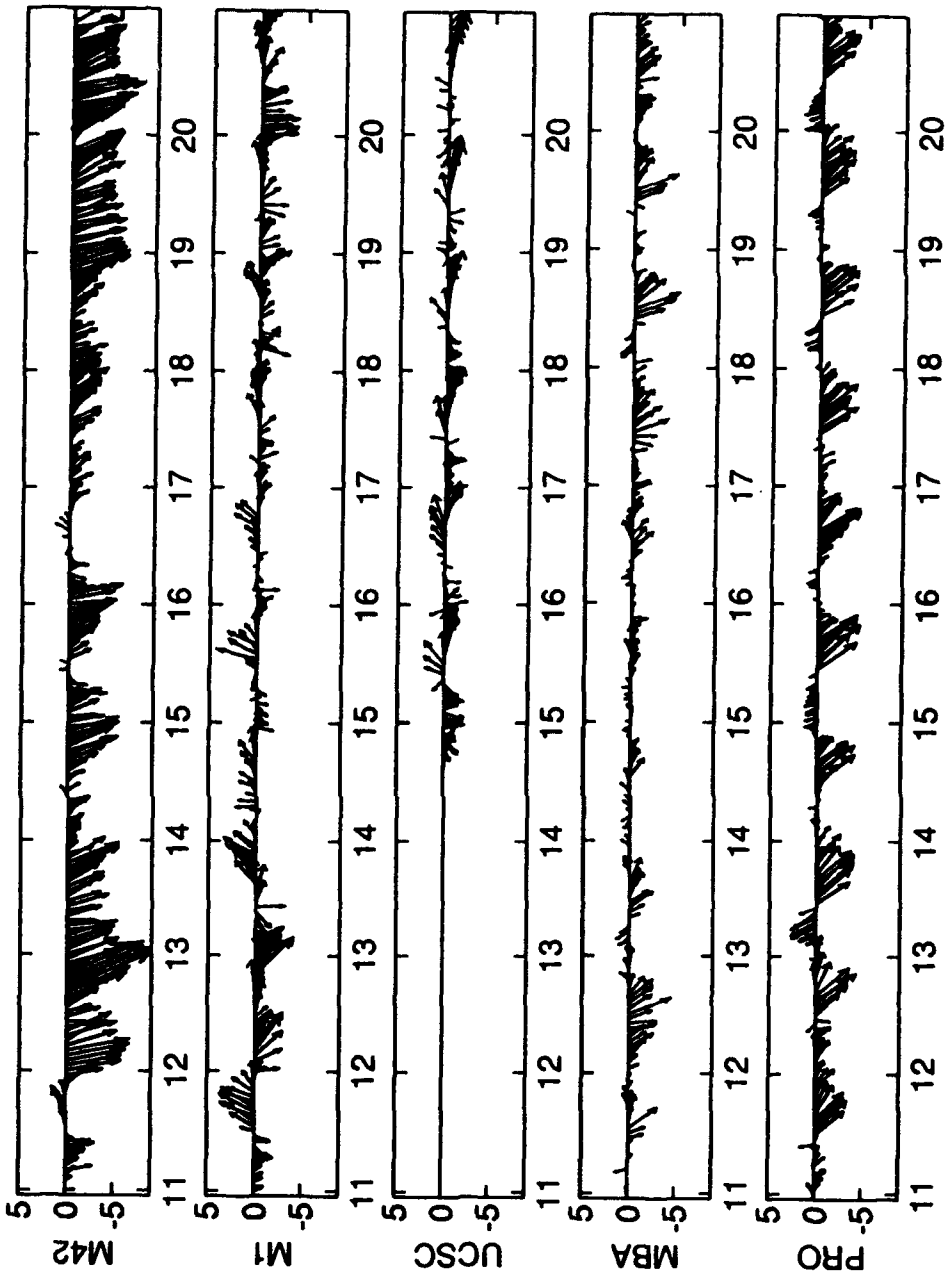

Figure 11. Same as in Figure 10, except for the period of 11 to 20 September.

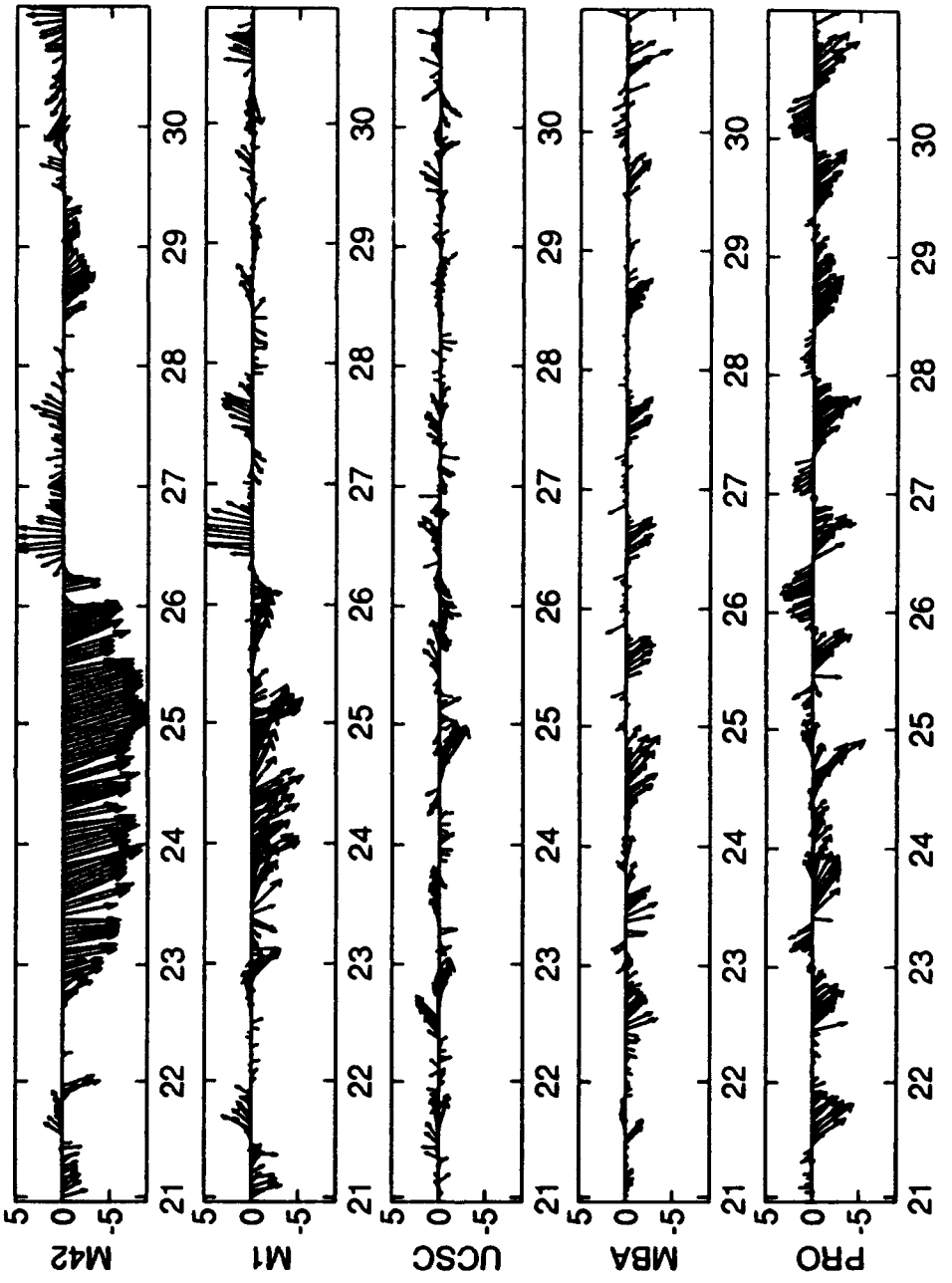

Figure 12. Same as in Figure 10, except for the period of 21 to 30 September.

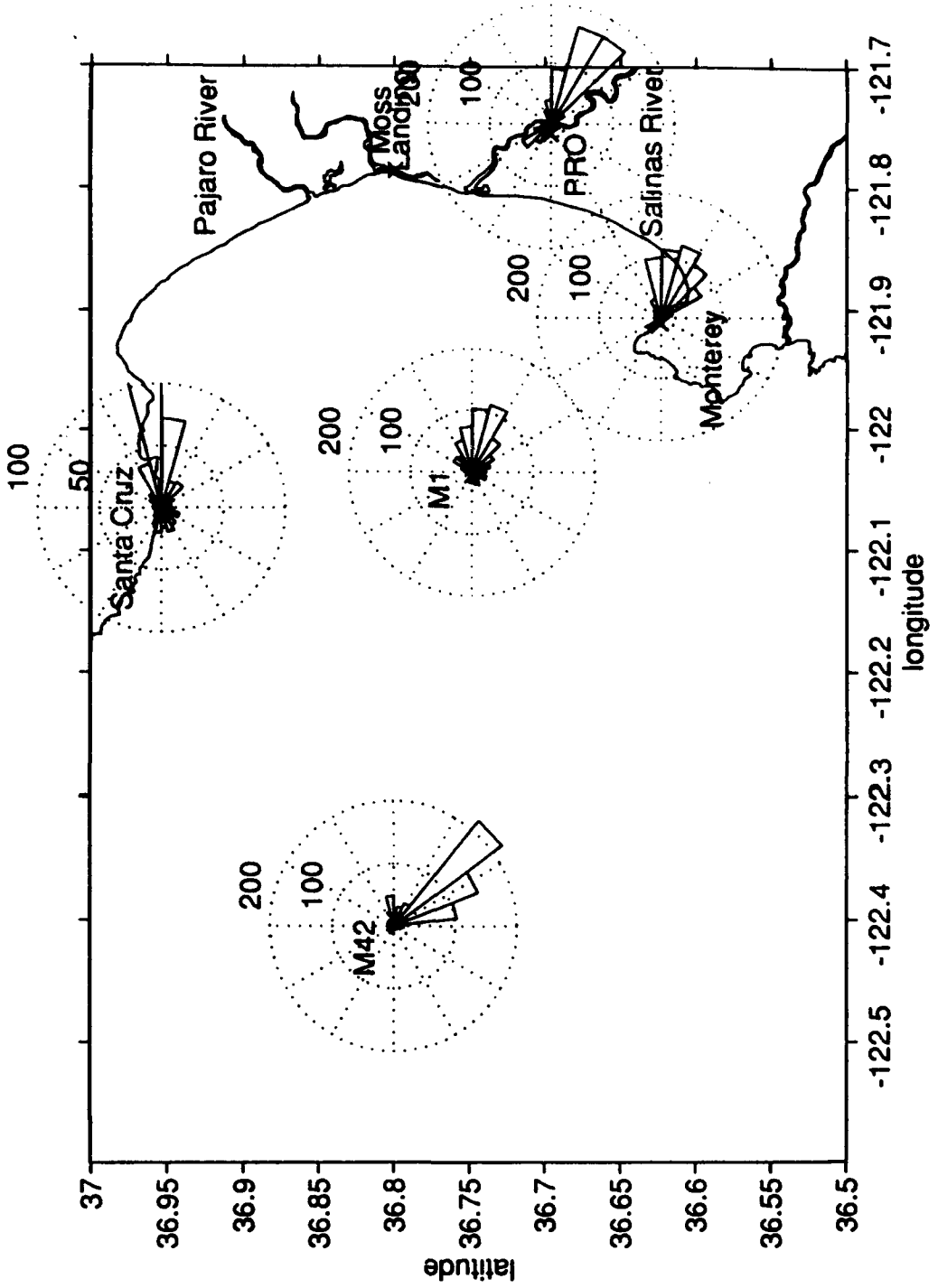

Figure 13. Wind rose showing the number of times a particular direction was observed during the month of September 1992 base on hourly observations. Wind directions are resolved into 30° bins. Note change in scale for the UCSC, which operated for only 16 days.

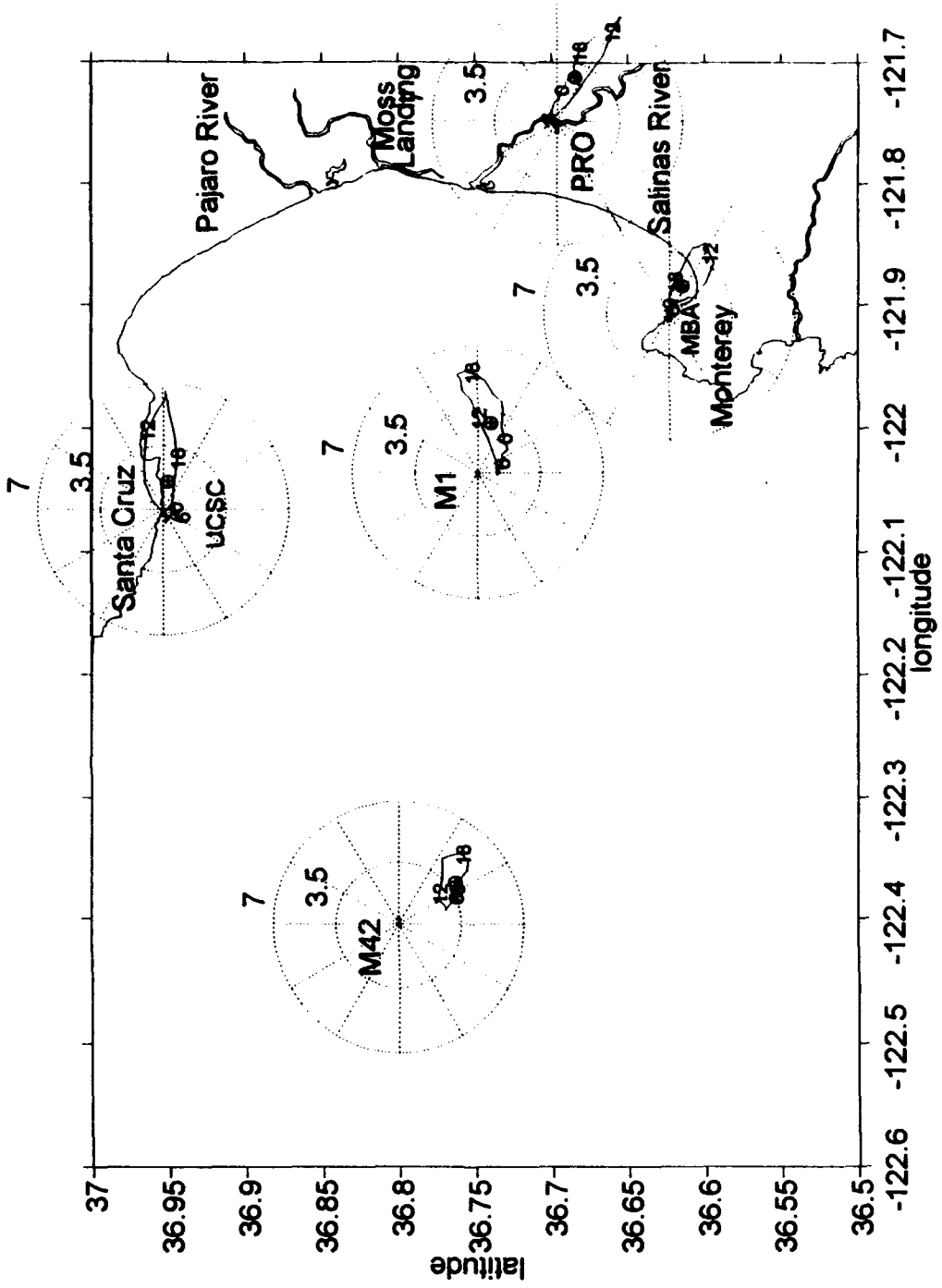

Figure 14. Wind hodographs for the month of September 1992. The solid line of the hodograph is inscribed by the tip of the canonical day wind vectors. The mean monthly wind is shown by ⊕ for each of the wind stations. Selected times of the day are overlain on the hodograph, and speeds are in m/s.

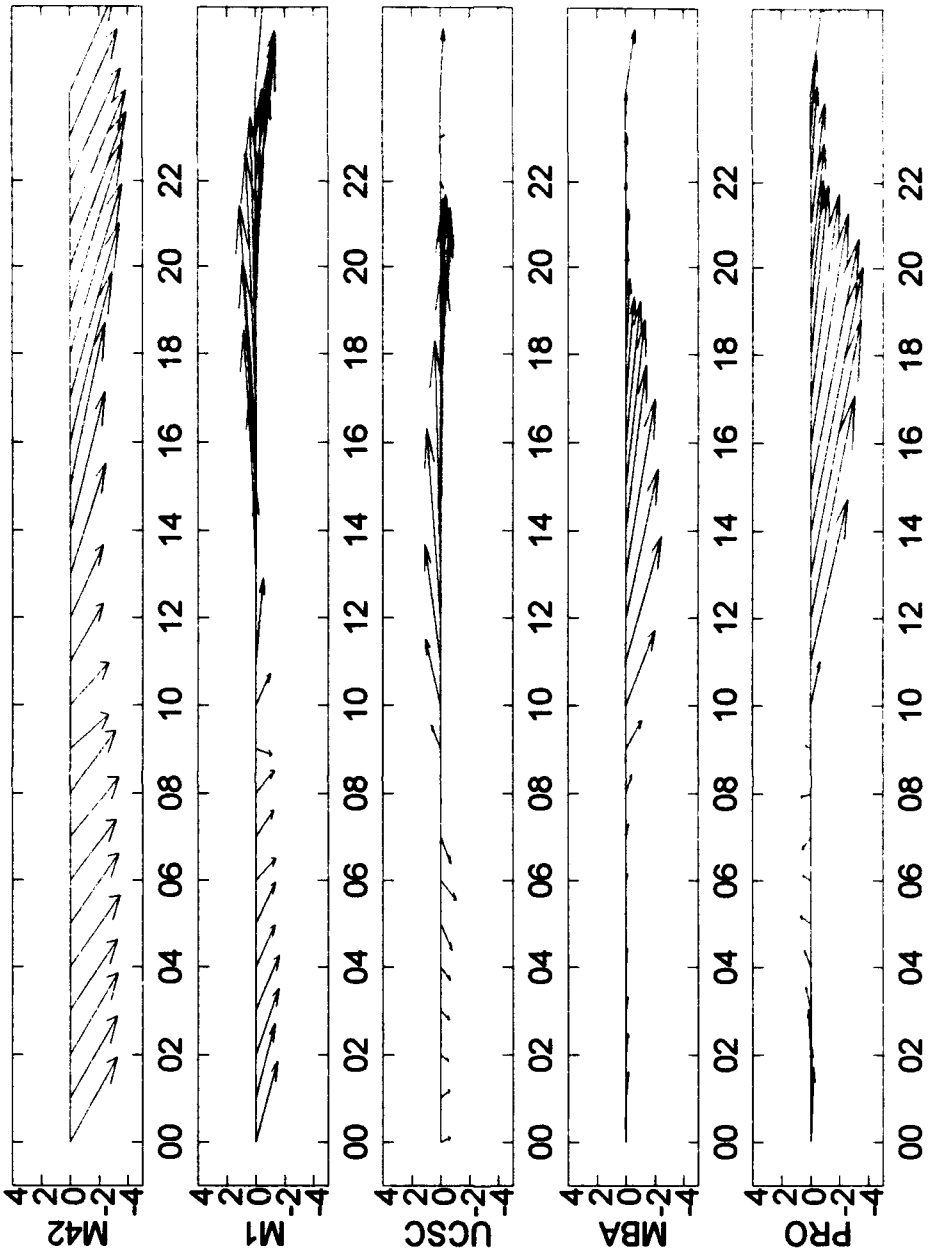

Figure 15. The canonical day wind plots for the five wind stations for September 1992. The vertical axis gives the wind speed scale in m/s. Location along the horizontal axis represents the canonical hour of the day. Arrows pointing to the right along the horizontal axis correspond to wind flow towards the east, while arrows pointing to the left correspond to wind flow towards the west.

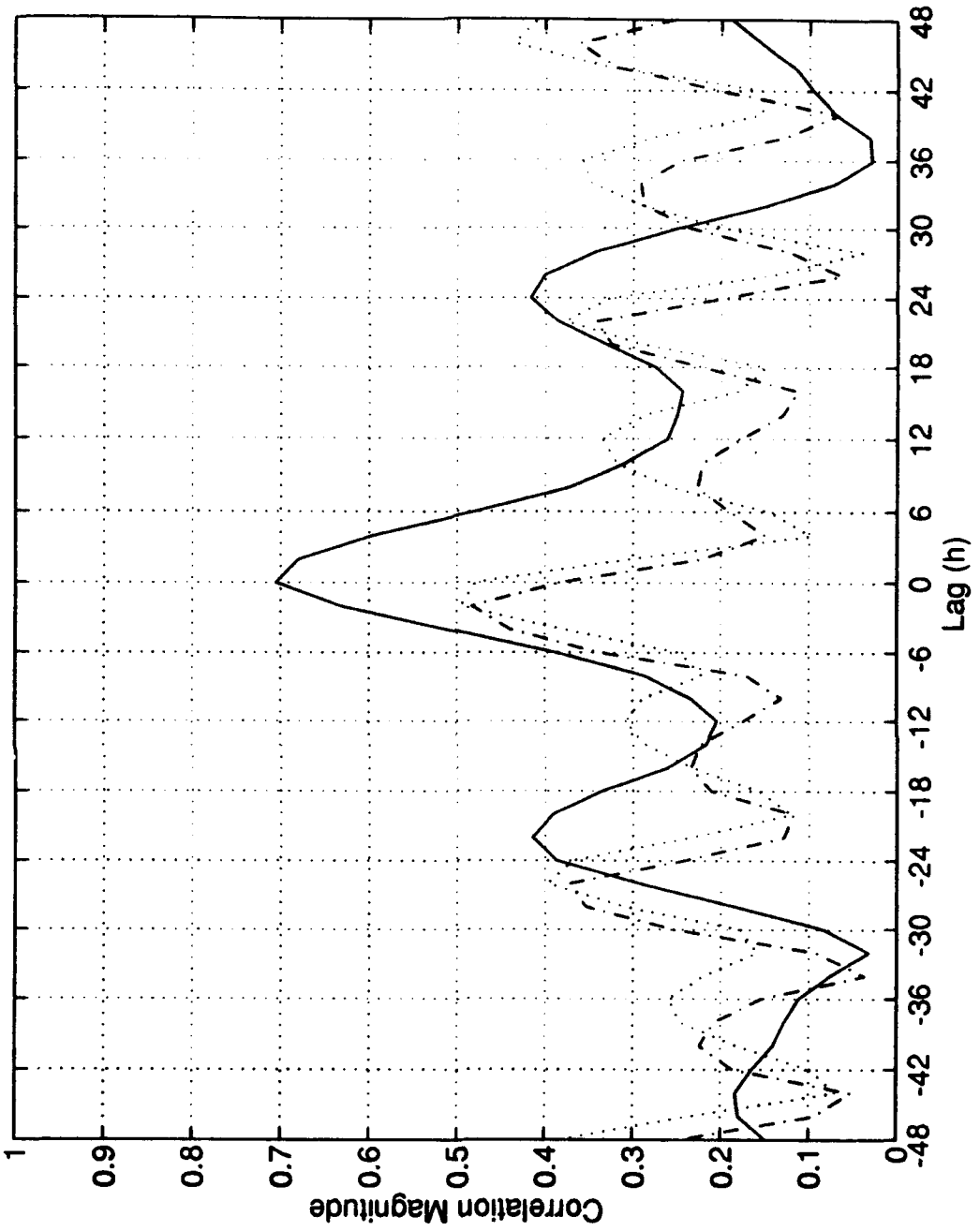

Figure 16. Magnitudes of the lagged complex correlation between selected wind records. The solid line represents the correlation between M1 and M42. The dotted line represents the correlation between M1 and PRO. The dash-dotted line represents the correlation between M1 and MBA.

IV. OCEAN CURRENT EFFECTS

A. GENERAL OCEAN CURRENT INFORMATION

CODAR current data in Monterey Bay was collected for 195 separate gridpoints for the month of September 1992 as shown in Figure 6. As mentioned before, each gridpoint represents the top meter of surface current in an approximate two-by-two km area that represents the intersection of two radar beams, originating from Moss Landing and Monterey. Figure 6 also indicates the percentage of time each gridpoint reported based on a maximum of 360 two-hour reports for the month of September. All CODAR observations were received and analyzed in PDT.

Since the CODAR current observations are the result of combining two radial current velocities, there exists some ambiguity in the directional computation the closer the gridpoints are to the direct line (base line) between the two CODAR stations. This affects data between the base line and the coast line. Computer algorithms that computed the current vectors in this region assumed that the onshore velocity components were zero at the coast and linearly interpolated those components out to one gridpoint offshore of the baseline. This assumption is questionable and care should be taken to avoid drawing conclusions from any results near the baseline, which is shown as a dashed line in this study.

Since an observation may not be provided due to low signal to noise values for a particular observation time, the time series from any one specific gridpoint will tend to

have gaps. Spectral and time series analysis of the CODAR data requires continuous data. Therefore, a gap filling routine similar to the one used to fill the wind data gaps was developed. In order to provide the most consistent current time series, linear interpolation was used to fill gaps of up to six hours. For gaps longer than six hours, the filling routine searched the previous and following records up to 3 days for canonical observations. This limited the ability to fill gaps in time series to coverage greater than 71 percent of the time. For analyses using simple means, such as the canonical day calculations, unfilled data time series were used.

1. Representative Locations

For the purposes of specific data analyses conducted on the time series, four different widely spaced CODAR gridpoints from the most densely reported gridpoints (greater than 75% reporting) were used. These four gridpoints along with the wind stations used in this study are illustrated Figure 17. The four gridpoints are 1305, 1409, 1803, and 1709, following the numbering of Neal (1992). Examples of the east-west (U) and north-south (V) current velocity components are exhibited in Figure 18. Upon inspection of the time series, the most obvious signal corresponds to diurnal-period fluctuations.

Rotary spectra for the four CODAR-derived current time series are presented in Figure 19 (a description of the rotary spectra is given in Section III.B.). They indicate strong clockwise rotational components (solid lines) of the surface currents about the diurnal frequency at all four CODAR gridpoints. Thus, the energy associated with clockwise rotating currents at the diurnal frequency dominates the

energy spectrum, while the energy associated with the counterclockwise rotating current components are smaller by nearly two orders of magnitude. It is important to note that, at the CODAR gridpoint closest to land (1803), a semi-diurnal peak is observed to be statistically significant. This semi-diurnal peak may result from the semi-diurnal tide, which is shown by Petruncio (1993) to be amplified over the head of the Monterey Submarine Canyon.

2. September Mean Currents

The mean CODAR-derived currents for September 1992 are presented in Figure 20. As a measure of confidence in these mean currents, the 95% standard errors of the means are presented in Figure 21 according to (Krauss and Böning, 1987):

$$STD\ ERR = \frac{2\sigma}{\sqrt{N_m}} \qquad [6]$$

N_m is the number of independent observations in the calculation of the mean (taken to equal the number of observations in this study). Since the standard error decreases with an increasing number of observations, the standard error velocity field plot in Figure 21 gives an indication of both the variability of the currents at each gridpoint and the number of observations. Thus, larger values of standard error will indicate fewer number of observations used in the mean computation and/or larger variability of the observations about the mean. In either case, larger values of standard error

indicate that the mean may not be truly representative. The east-west and north-south components of the error have been combined to form error vectors. Since the computed errors are all positive, the vectors are limited to point within the first quadrant. If the error vectors point more toward the east, there is more east-west variability in the observations. And likewise, if the error vectors point more toward the north, there is more north-south variability in the currents.

Figure 20 indicates that there was a mean cyclonic eddy in Monterey Bay centered slightly west-northwest of Moss Landing in September 1992. Figure 21 indicates that the standard errors associated with this cyclonic eddy are larger than mean currents producing it, indicating that the eddy may not have been statistically significant. In addition, there was a slight anticyclonic boundary flow to the west that may have provided an outflow near Point Piños along Pacific Grove Marine Garden Park, for surface waters forced into Monterey Bay, although these currents are not much larger than their error estimates.

B. CANONICAL DAY CURRENTS

Each of the standard observation periods during each day was averaged for the entire month to establish the canonical day for all current gridpoints in a manner similar to that used for the wind stations. The mean canonical day current and wind maps are shown in Figures 22 to 33 and represent the two hourly mean current and mean wind flow starting at 1000 PDT and ending at 0800. Figures 34 to 45 represent the standard error plots for the same respective time periods and are included so the

reader may infer the reliability of the canonical day maps. The following discussion describes the patterns of both typical winds and currents throughout the day, beginning in the morning.

At 1000 PDT (Figure 22), the winds at the two coastal wind sites exhibit local cross-coastal flow and begin an eastward rotation (clockwise for UCSC, counterclockwise for MBA) under the influence of the larger-scale sea breeze circulation due to the Salinas and Santa Clara Valleys. The sea breeze circulation has started with winds directed down the valley. The oceanic stations remain under the influence of the mean synoptic wind flow. Currents within the interior of Monterey Bay show a cyclonic, elongated eddy with its major axis oriented toward the southeast, centered northeast of M1. Weak currents flow into the Bay from the southwest near Point Piños.

By noontime (Figure 23), the sea breeze circulation is well established ashore. Wind flow at MBA and PRO has increased and points down the Salinas Valley. Wind flow at UCSC is veering toward the east-northeast and increasing in magnitude as well. Winds at M1 have increased in magnitude over 200% since 1000 and backed in direction over 45° toward the east as the sea breeze circulation develops at M1. Currents within the Bay have begun a definite shift toward the southeast and increased their speed over 150% near M1 since 1000. Currents in the outer portions of the Bay are parallel to the winds at the PRO site. The cyclonic eddy has weakened and moved northeast to be centered near the mouth of the Pajaro River.

The 1400 PDT winds (Figure 24) ashore have continued to increase in magnitude, reaching their peak. The southern shore stations have aligned their wind flow to the southeast, parallel to the Salinas Valley. The wind flow at UCSC has continued to veer toward the east until it is pointing directly at the opening of the Pajaro Valley and the Santa Clara Valley beyond it. The winds at M42 have increased and backed toward the land to the east under the influence of the sea breeze. The currents throughout the Bay have increased in magnitude; but it appears as though the faster currents are spreading into the interior of the Bay from the outer portions with strong onshore current flow. The currents near M1 have begun to veer toward the south. There is still a hint of a slight cyclonic rotation in the current field near Moss Landing.

By 1600 PDT (Figure 25), the winds at the shore stations have begun to decrease. The winds at M1 have reached their peak. The currents have continued to have strong flow directed toward the coast. Boundary effects may be producing a northward component in the nearshore currents in the vicinity of Moss Landing. The currents in the vicinity of M1 have continued to veer anticyclonically.

By 1800 PDT (Figure 26), the winds ashore have continued to weaken. The winds at M1 have also begun to weaken, while the winds at M42 have reached their peak. The strong currents have continued their anticyclonic rotation and are pointed almost directly south. The cyclonic eddy has reformed to the southeast of the Pajaro River, again under the influence of boundary effects probably caused by current flowing against the coast for approximately eight hours.

The 2000 PDT (Figure 27) winds at the coastal land stations have decreased in magnitude so they are no longer significant. The winds at PRO, M1 and M42 have continued to weaken, although wind speeds at M1, even after weakening, are still near ten knots. The anticyclonic current rotation near M1 has continued to the point where the current flows are perpendicular to the wind flow at M1. An exit channel has formed in the currents parallel to the Monterey Peninsula. Offshore flow in the interior of the Bay produces a line of convergence in the surface currents from M1 north toward Santa Cruz.

At 2200 PDT (Figure 28), the wind flow is weak at all wind stations. Offshore current flow spreads from the interior of the Bay to the outreaches of the CODAR coverage. The current flow near M1 continues its anticyclonic rotation while opening up a wider outflow channel northwest of the Monterey Peninsula. The currents have veered so much by this time, the current flow is now opposed by wind flow near M1.

The midnight (Figure 29) currents within the whole Bay have undergone the clockwise rotation and are flowing outward. It is important to note that the currents in the outer portions of the Bay are decreasing in magnitude rapidly as the wind stress at M1 is now opposing the current flow. The veering of the currents is now prominent in the interior of the Bay.

By 0200 PDT (Figure 30), the currents near M1 have become slack under the influence of the opposing wind stress and offshore current flow. Currents continue to flow out of the interior of the Bay, producing surface divergence and convergence near

M1, which is an area with confused flow. The cyclonic rotation continues in the interior of the Bay producing slight surface divergence in a line from MBA to UCSC.

The wind stress provided by the prevailing synoptic conditions as defined at M42 and reiterated at M1 begins to act upon the generally slack currents near M1 by 0400 PDT (Figure 31). In the vicinity of M1 and westward toward M42, the currents begin to flow onshore. This onshore flow interacts with the continued clockwise rotation of the currents within the interior of the Bay, producing a counter-clockwise rotating eddy in the canonical day currents centered slightly northeast of M1.

From 6 to 8 PDT (Figures 32 and 33, respectively), the currents associated with the synoptic wind flow progressively eastward into the interior of Monterey Bay. The line of convergence in the surface currents, associated with the onshore flow from the west and the offshore flow with the currents in the innermost portions of the Bay, continues to propagate eastward. Oceanward boundary of the line of convergence, the weak cyclonic eddy in the mean currents centered north of M1 drifts northward with the line's eastward propagation. currents within the interior of Monterey Bay appear to cease their cyclonic rotation as the line of convergence sweeps deeper into the Bay.

In summary, cyclonic flow is prevalent in the early morning most days north of M1 while offshore flow is prevalent during night time or when onshore flow is diminished. This offshore flow is probably due to the build up of water against the beach by the strong onshore flow during the afternoon. Figures 34 through 45 indicate

relatively low confidence in the weaker nighttime and morning currents and in the further out locations as compared with the strong afternoon currents.

C. CODAR CURRENT ANALYSIS

In order to quantify some of the CODAR temporal and spatial characteristics, two different methods were used to correlate the currents at the four different gridpoints located in different portions of the 75% coverage portion of the map shown in Figure 6. (The exact locations of the four gridpoints are shown in Figure 17.) The methods are the same as those applied to winds described in Section III.E. One method split the currents into east-west and north-south components (U and V) to perform component-to-component analysis. The other used complex correlation applied to vector winds. Both methods used two-hourly, gap-filled, CODAR-derived surface currents. Again, gridpoints 1305, 1409, 1803 and 1709 were used since they represented the most spatial variation while maintaining the highest percentage coverage and most continuous data available.

1. Longitudinal and Latitudinal Cross Spectra

After splitting the current data into its cartesian components, it was found that both U and V components were highly correlated with one another and all phase differences were less than the data resolution of the observations with greater than 95% confidence in the coherency. In both the U and V component cases, the data at gridpoint 1709 leads that at gridpoint 1409 which in turn leads that at gridpoints 1803 and 1305. The U components at gridpoints 1709 and 1409 as well as the V

components at gridpoints 1409 and 1803 are in phase with one another. Table IV and V show the results of the U and V cross spectral analysis when compared at the diurnal period of 24 h, respectively. All phase differences are less than 30 degrees and are within the two-hour sampling interval of the observations.

TABLE IV

U Analysis at f=0.0417 cph or 1.00 day	Phase Difference (degrees)	Phase Difference (h)	Coherence	95% Sig Level of Coherence
1709 leads 1409	.6	0.0	.977	.726
1709 leads 1803	15.9	1.1	.976	.726
1709 leads 1305	27.3	1.8	.962	.726
1409 leads 1803	14.5	1.0	.977	.726
1409 leads 1305	26.2	1.7	.941	.726
1803 leads 1305	11.7	.8	.913	.726

TABLE V

V Analysis at f=0.0417 cph or 1.00 day	Phase Difference (degrees)	Phase Difference (h)	Coherence	95% Sig Level of Coherence
1709 leads 1409	6.0	.4	.971	.726
1709 leads 1803	7.2	.5	.919	.726
1709 leads 1305	21.6	1.4	.943	.726
1409 leads 1803	.6	0.0	.892	.726
1409 leads 1305	15.4	1.0	.944	.726
1803 leads 1305	17.0	1.1	.920	.726

2. Complex Correlation

The currents were compared using the same complex correlation routine used on the winds earlier. Figures 46 and 47 show the results of the complex correlation scheme used. The currents at gridpoint 1409 are highly correlated with the currents at gridpoints 1305 and 1709 in magnitude with no time lag (solid and dashed lines, Figure 46) and also in multiples of the diurnal period. Gridpoints 1305 and 1709 (solid line, Figure 47) are also highly correlated in a similar way. Gridpoint 1803 did not correlate well with any of the other gridpoints initially nor at any time lag.

The lack of correlation of the currents at gridpoint 1803 with currents at the other gridpoints may be due to its location closest to the coast near the mouth of the Salinas Valley. The current flow onto the coastal boundary during the daylight hours may contribute to the development of a pressure gradient and near coastal current flow not in harmony with the strong diurnal signal present in the currents at the other gridpoints. This site is also over the head of the Monterey Submarine Canyon and has a stronger tidal component (Petruncio, 1993).

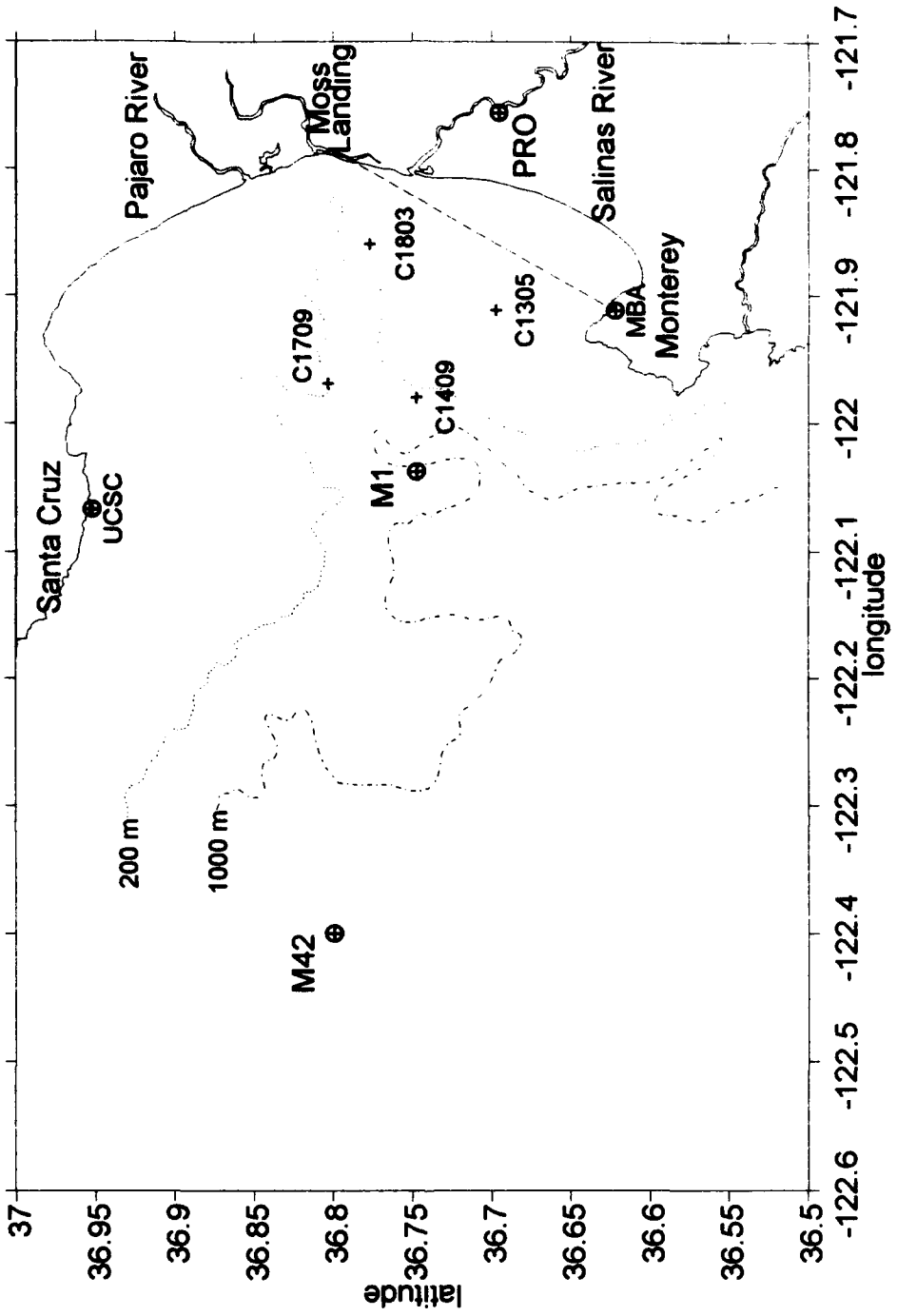

Figure 17. Location of the five wind stations (⊕) used in this study together with four CODAR gridpoints (+). The dotted and dash-dotted lines are the 200 meter and 1000 meter isobaths, respectively. The baseline region of uncertainty of the CODAR-derived current vectors is plotted with a dashed line.

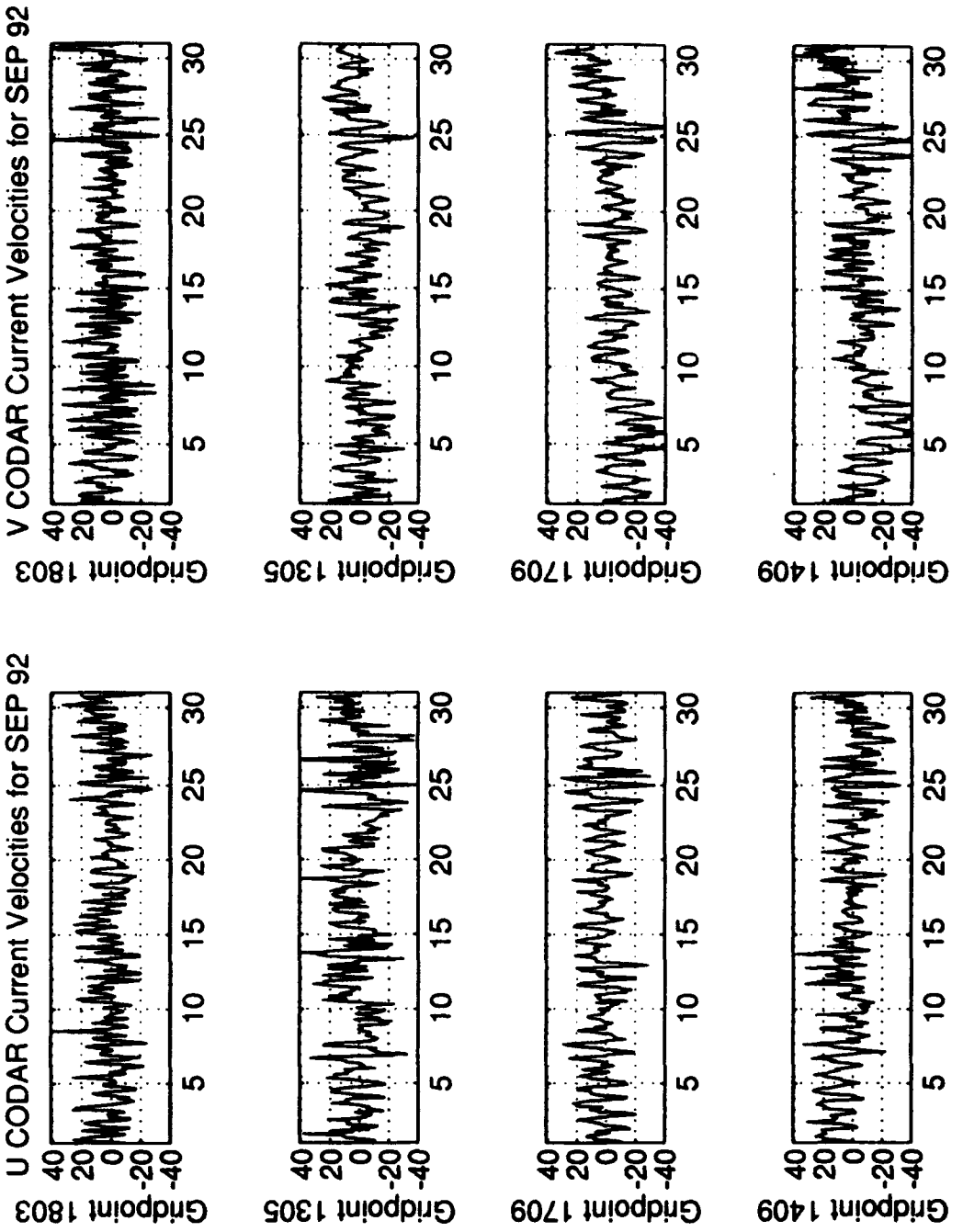

Figure 18. CODAR-derived current velocities for the four selected gridpoints in September 1992. The current velocities are split into U (north-south) and V (east-west) components. The vertical axis is in cm/s, while the horizontal axis represents the days of September.

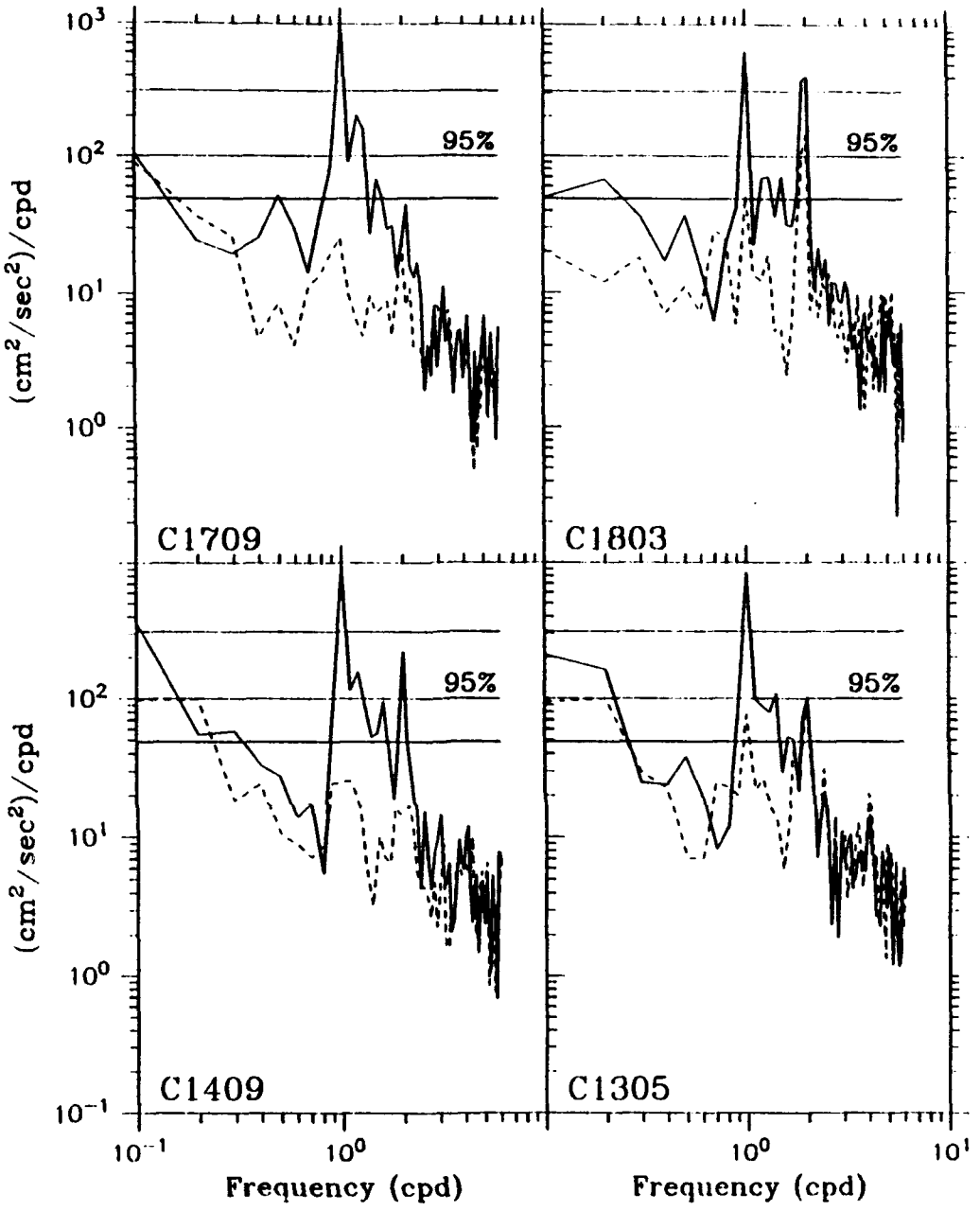

Figure 19. Rotary Spectra for CODAR gridpoints 1305, 1409, 1709 and 1803. Solid lines represent the energy associated with clockwise rotation, while dashed lines represent the energy in counter-clockwise rotation. The 95% confidence limits for the associated, one-sided auto spectra are also shown.

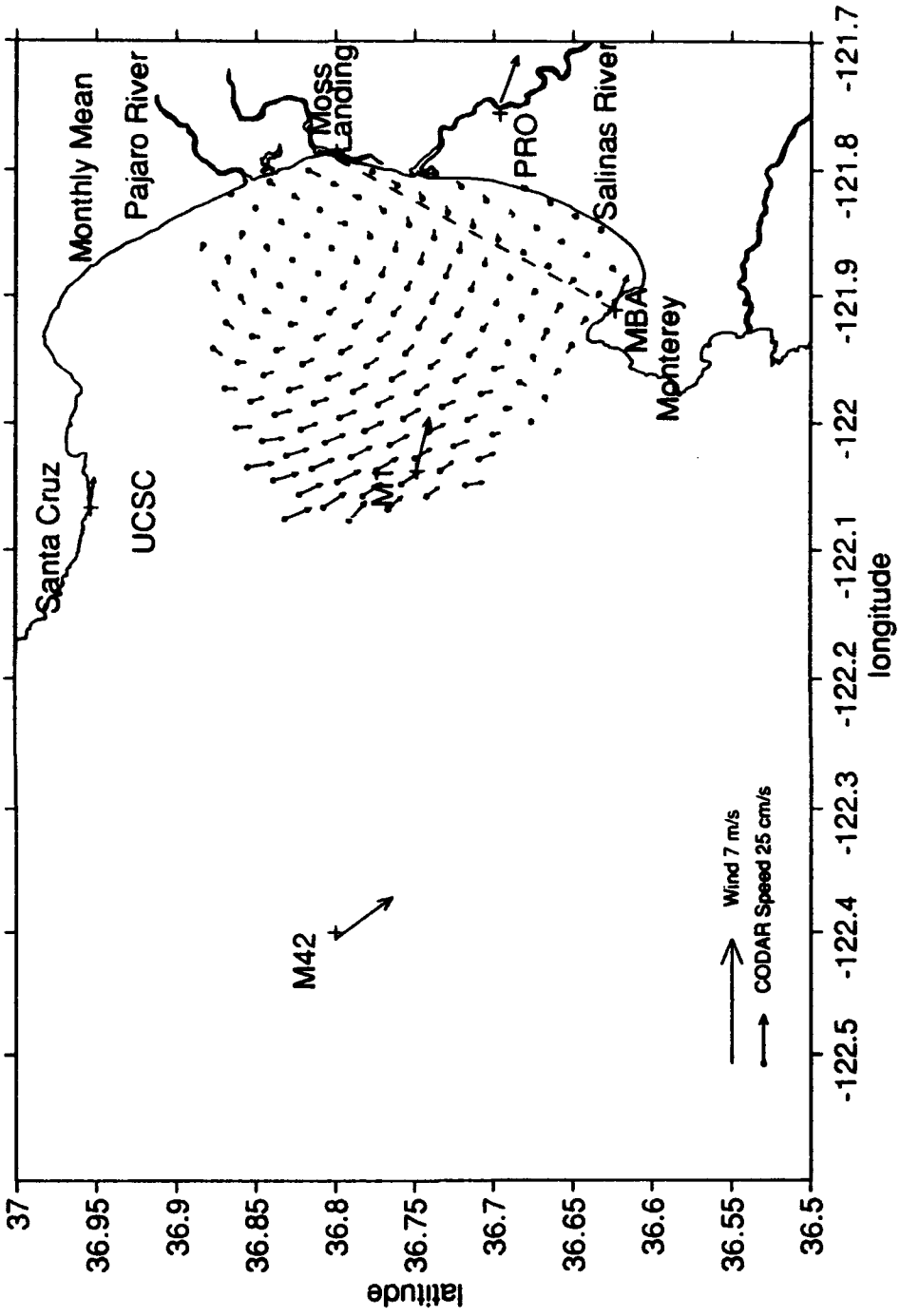

Figure 20. Mean CODAR-derived current and mean wind fields for September 1992.

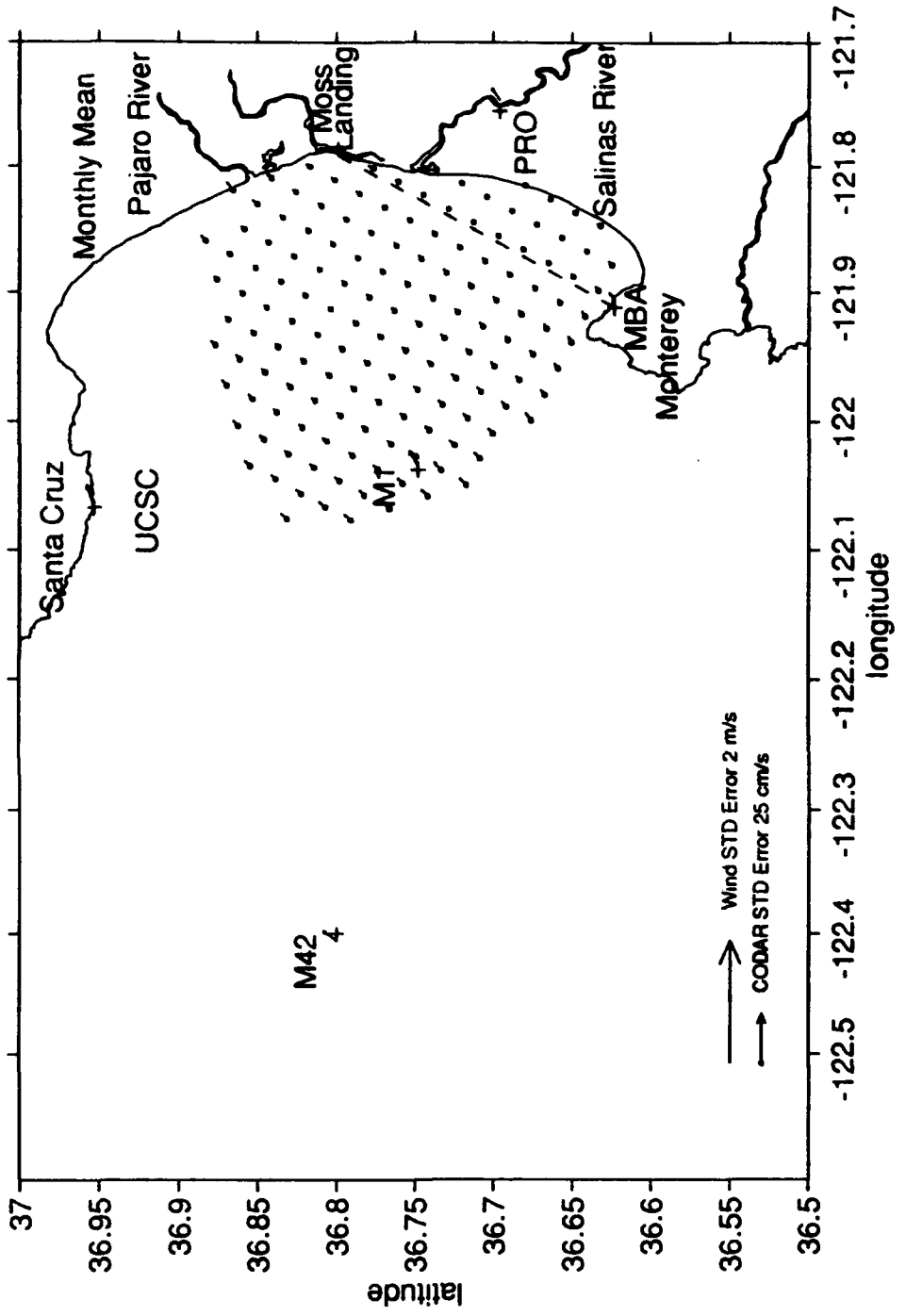

Figure 21. Standard Error fields for CODAR-derived mean currents and mean winds in September 1992. The standard error weights the variance of the observations by the number of observations (see text).

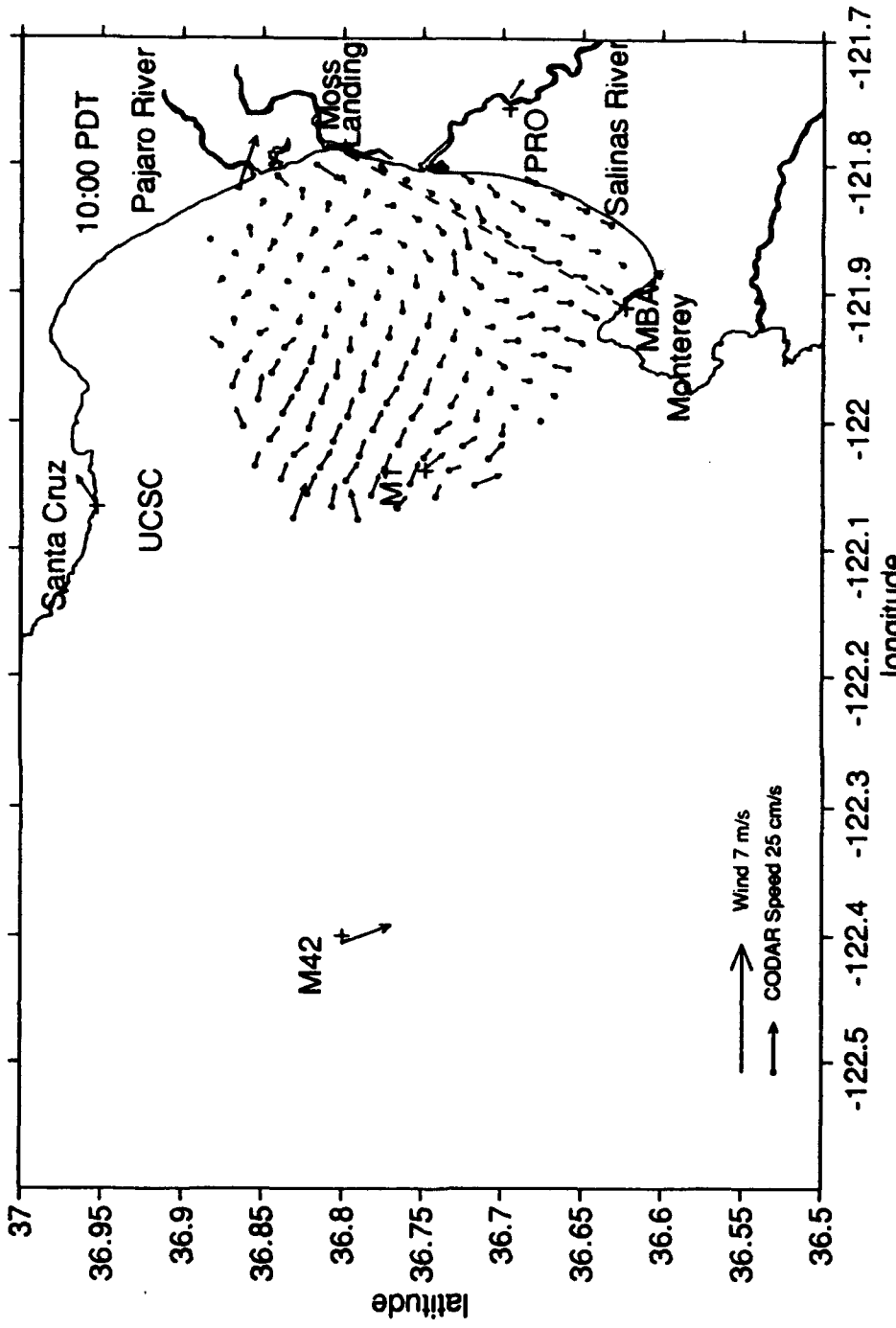

Figure 22. Mean CODAR-derived current and mean wind fields for 1000 PDT in September 1992.

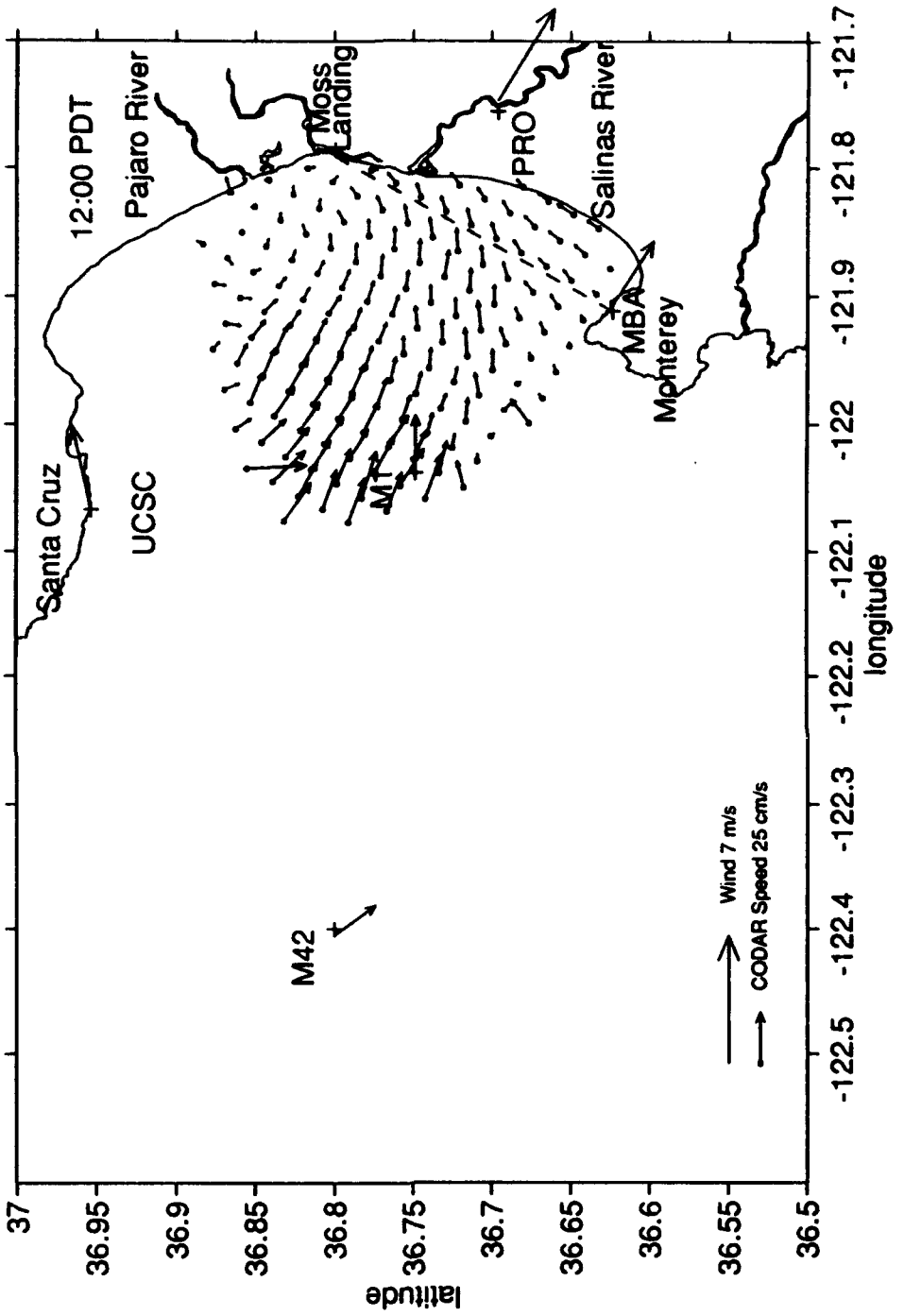

Figure 23. Mean CODAR-derived current and mean wind fields for 1200 PDT in September 1992.

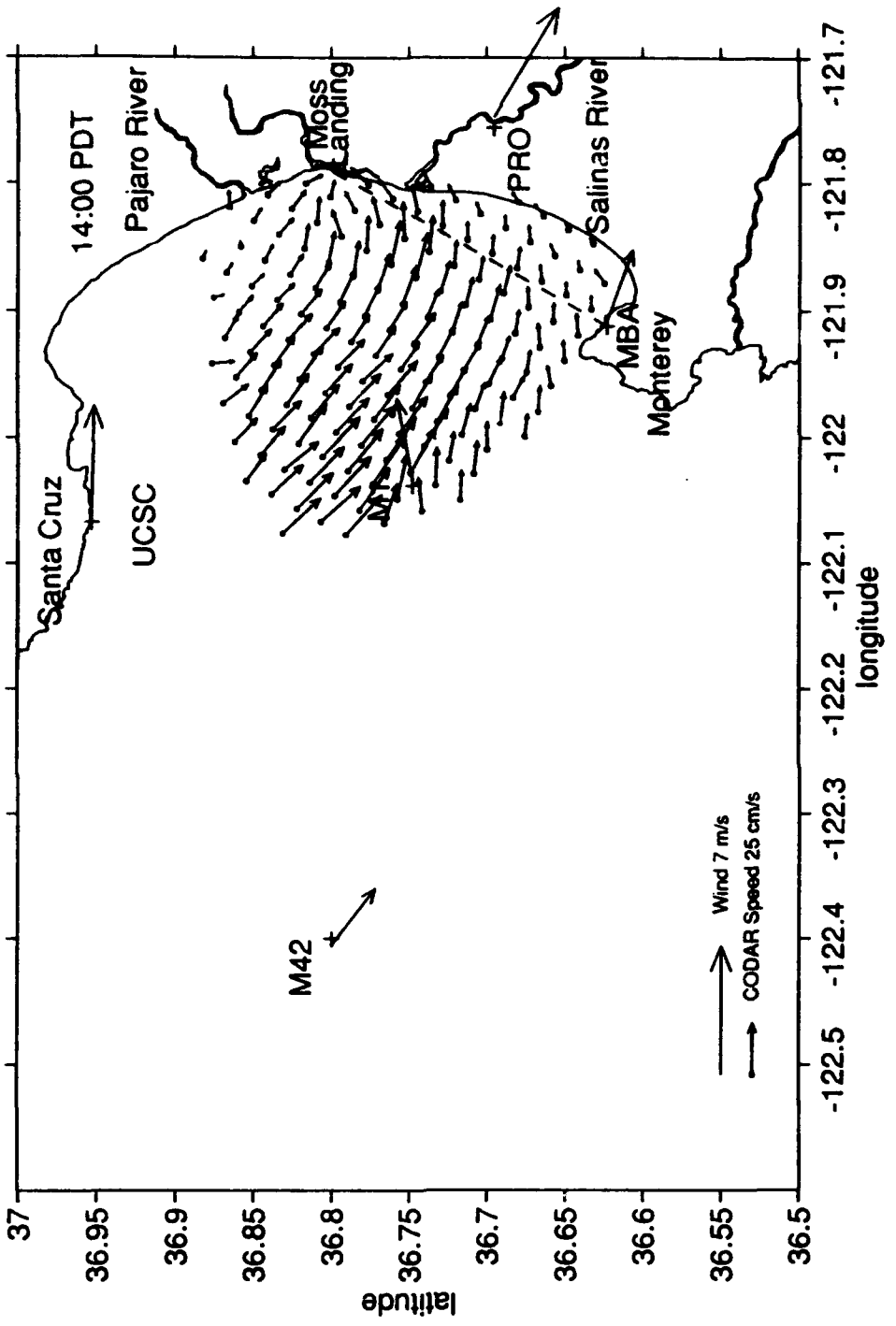

Figure 24. Mean CODAR-derived current and mean wind fields for 1400 PDT in September 1992.

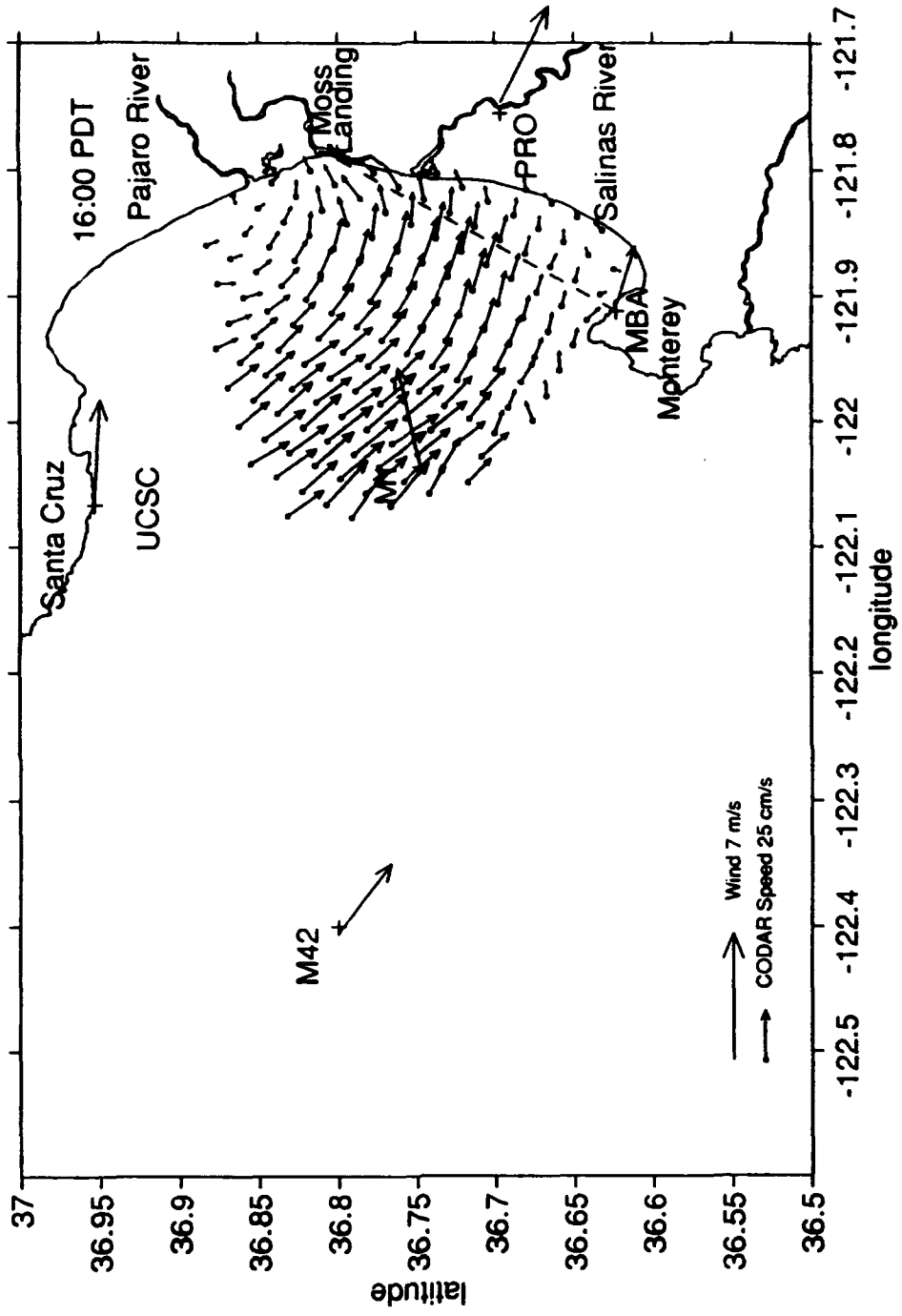

Figure 25. Mean CODAR-derived current and mean wind fields for 1600 PDT in September 1992.

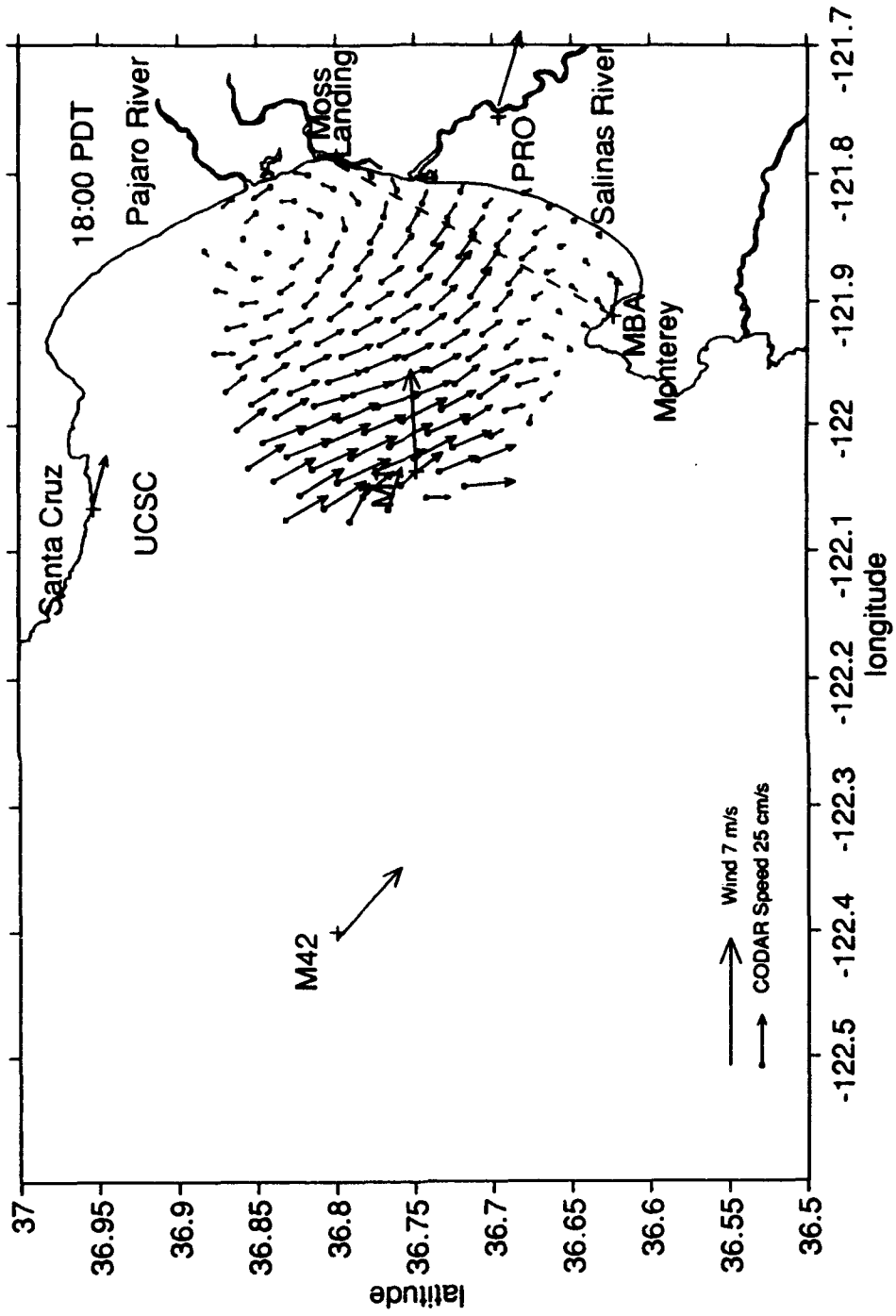

Figure 26. Mean CODAR-derived current and mean wind fields for 1800 PDT in September 1992.

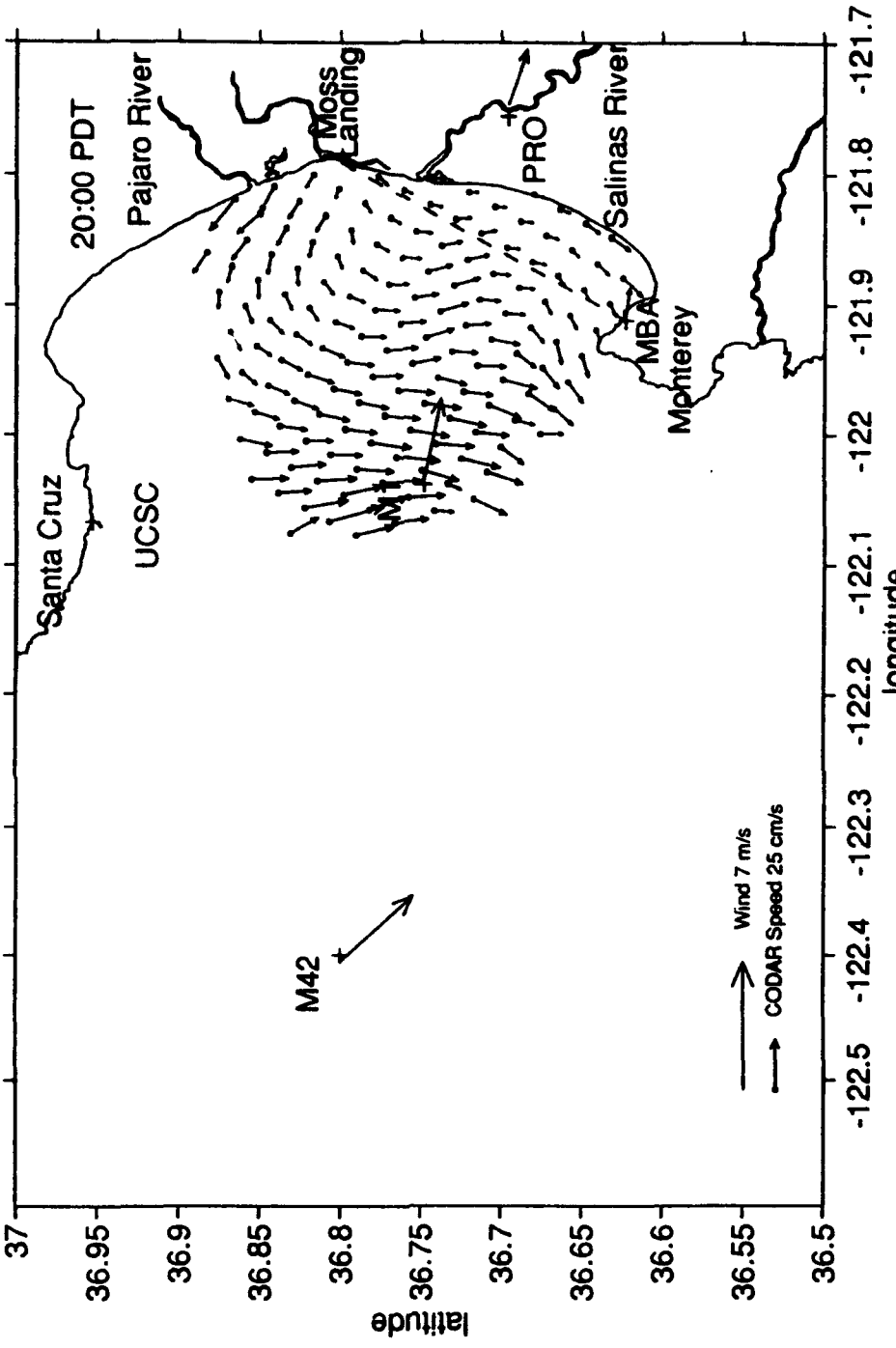

Figure 27. Mean CODAR-derived current and mean wind fields for 2000 PDT in September 1992.

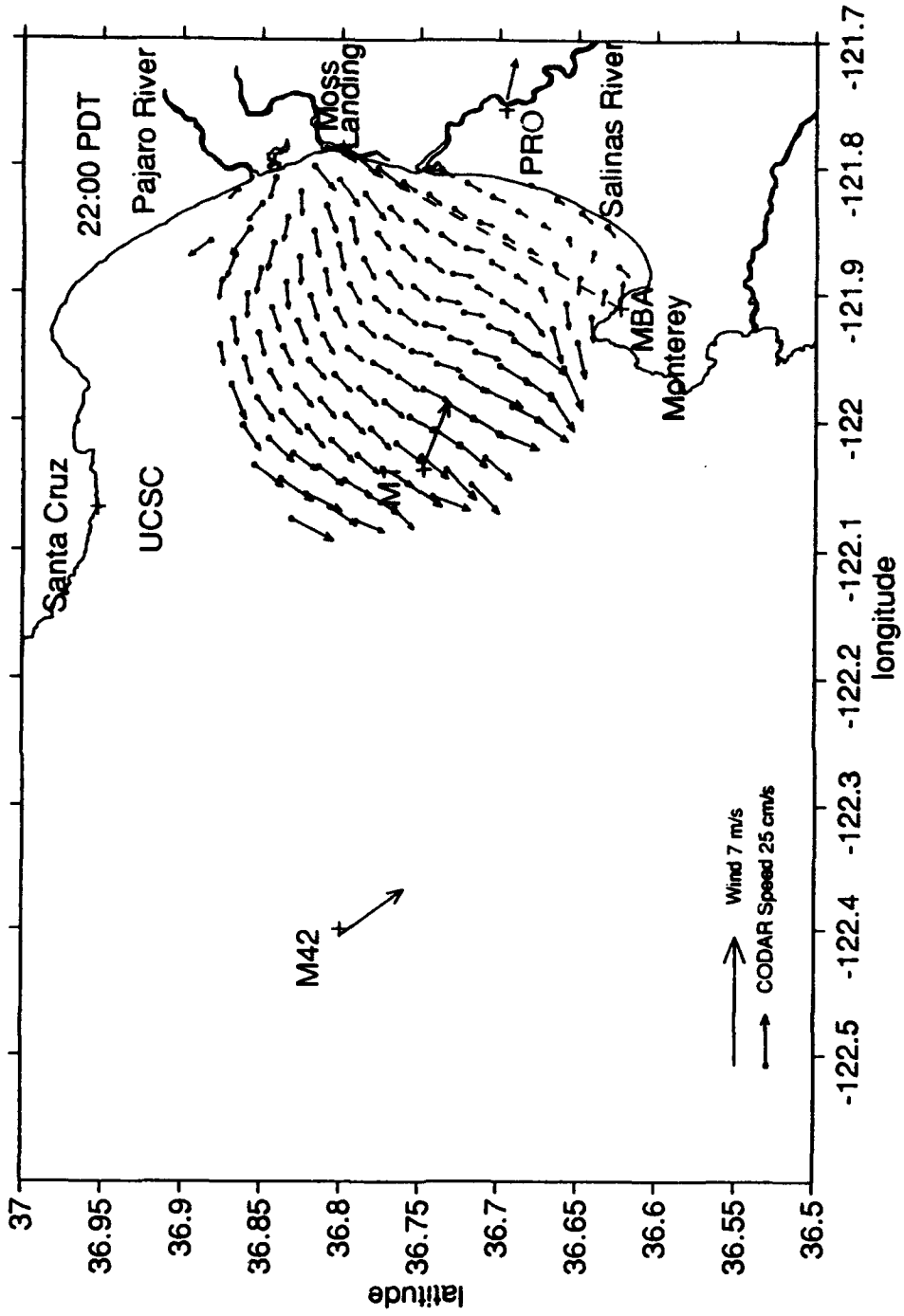

Figure 28. Mean CODAR-derived current and mean wind fields for 2200 PDT in September 1992.

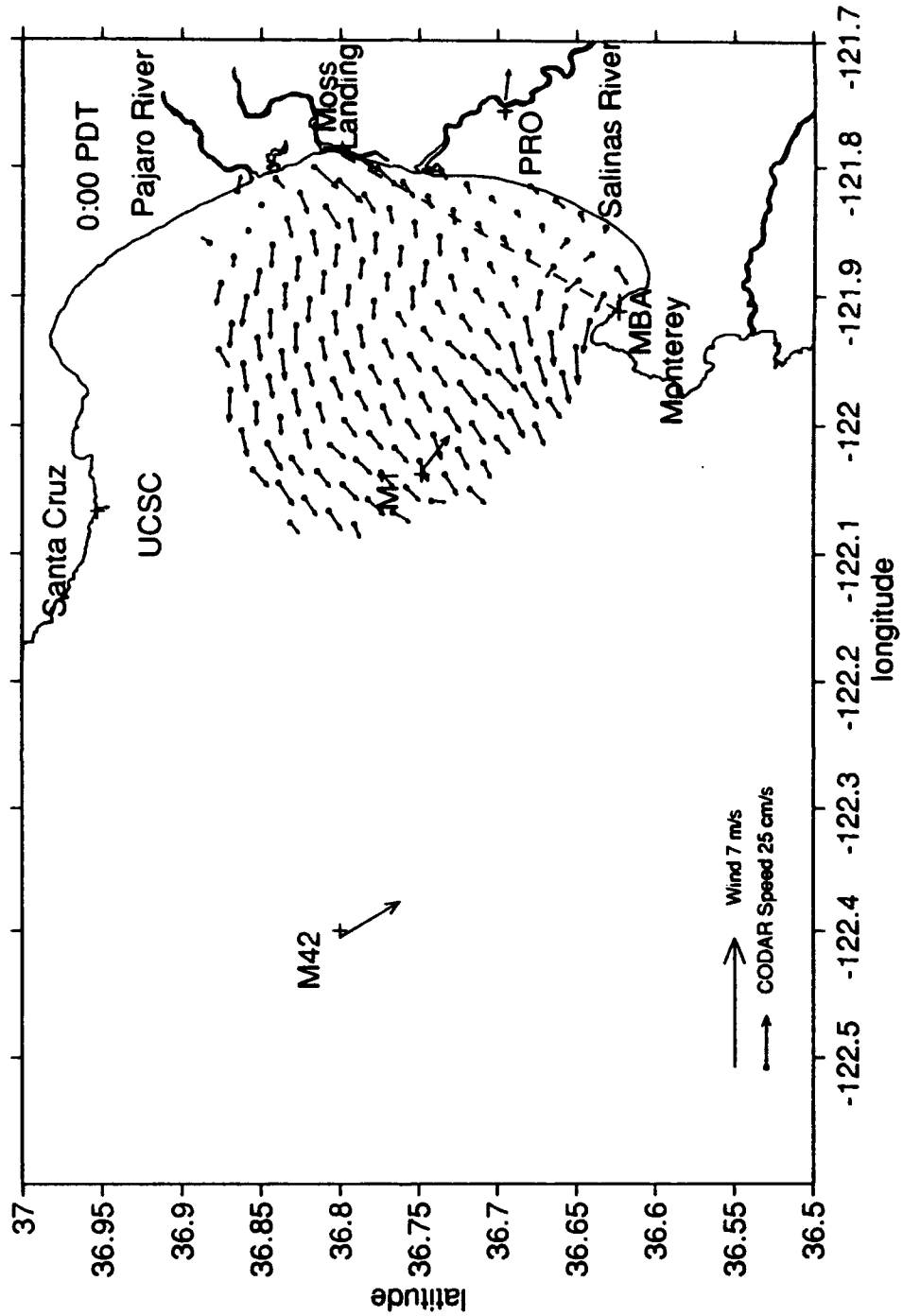

Figure 29. Mean CODAR-derived current and mean wind fields for 0000 PDT in September 1992.

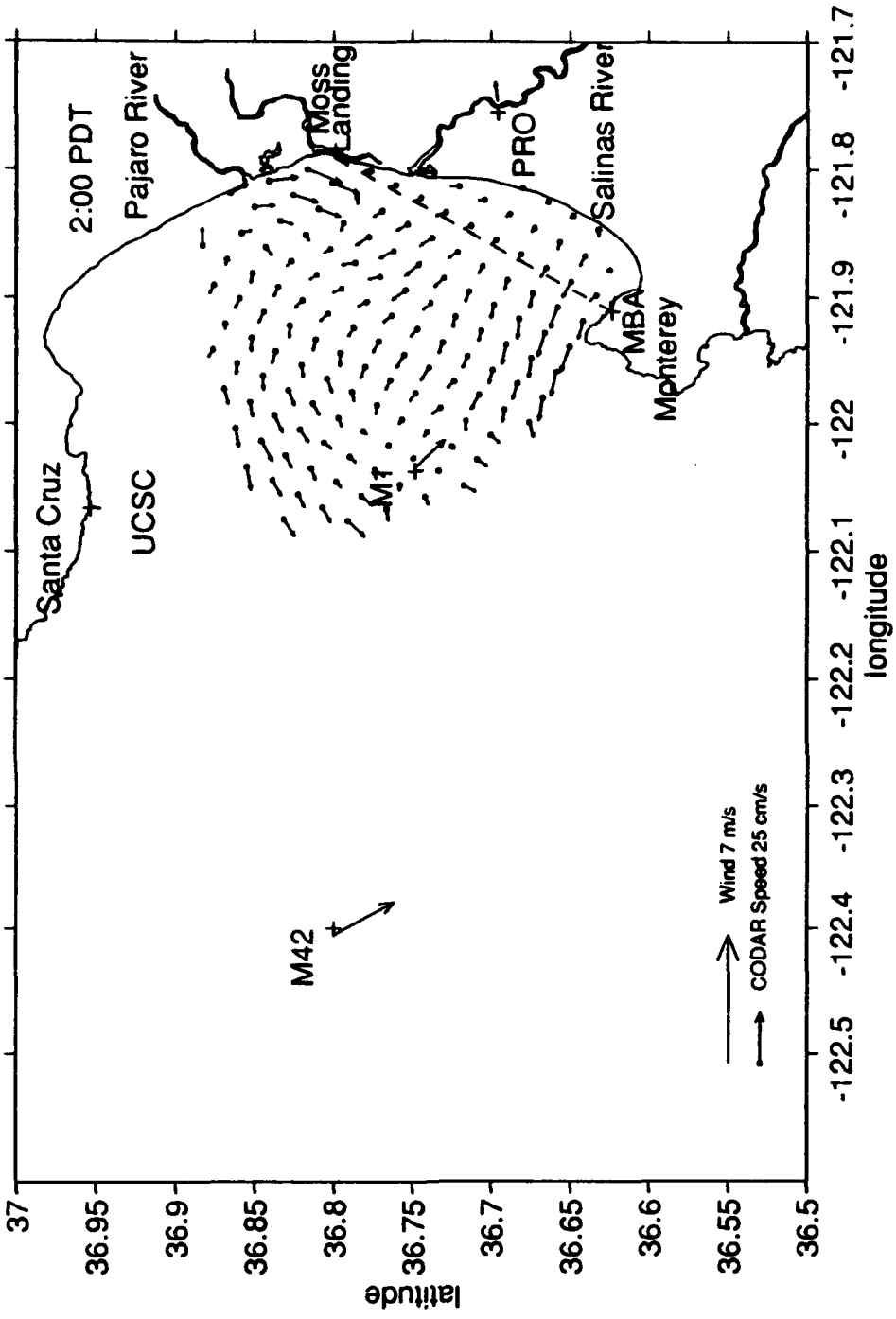

Figure 30. Mean CODAR-derived current and mean wind fields for 0200 PDT in September 1992.

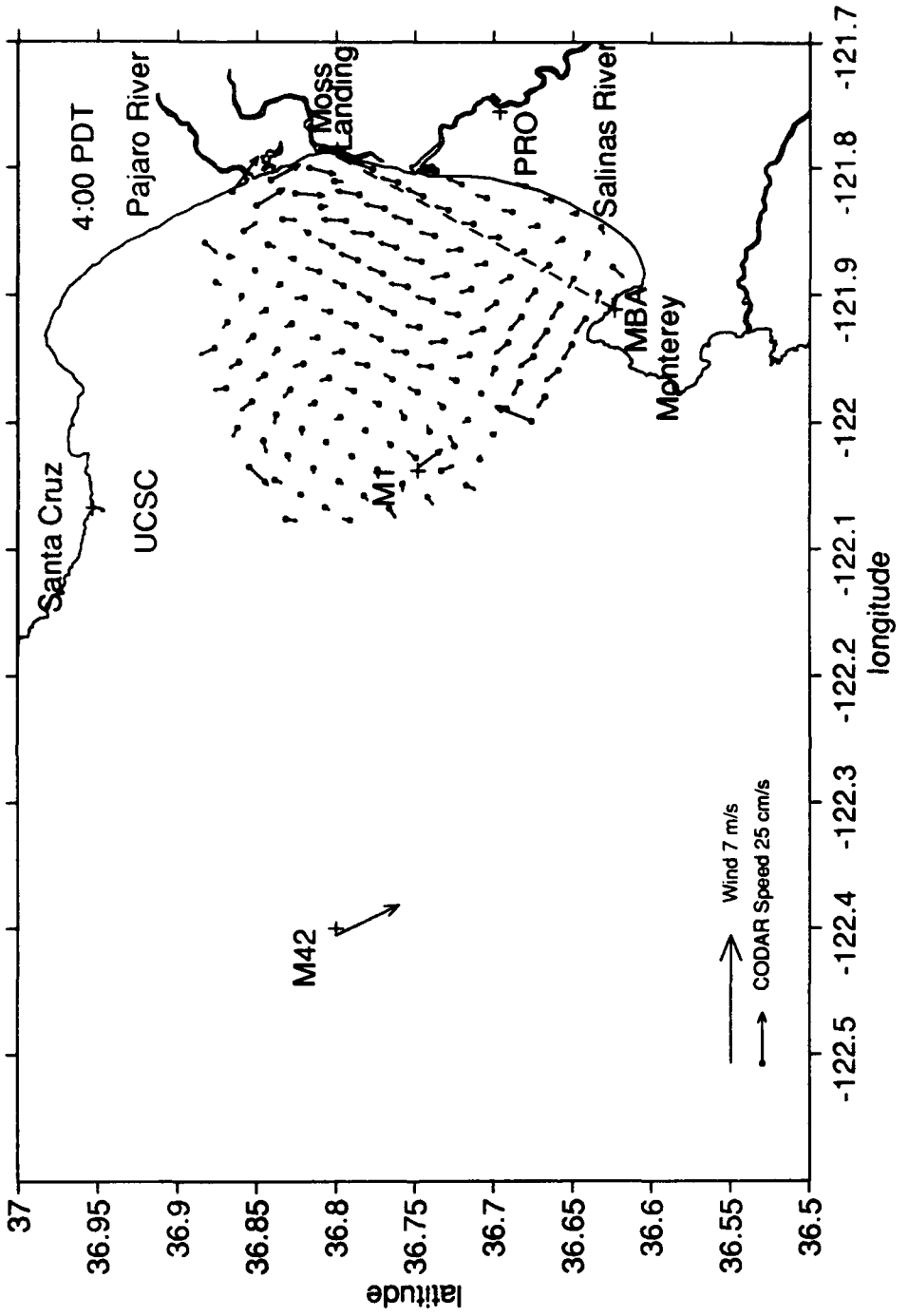

Figure 31. Mean CODAR-derived current and mean wind fields for 0400 PDT in September 1992.

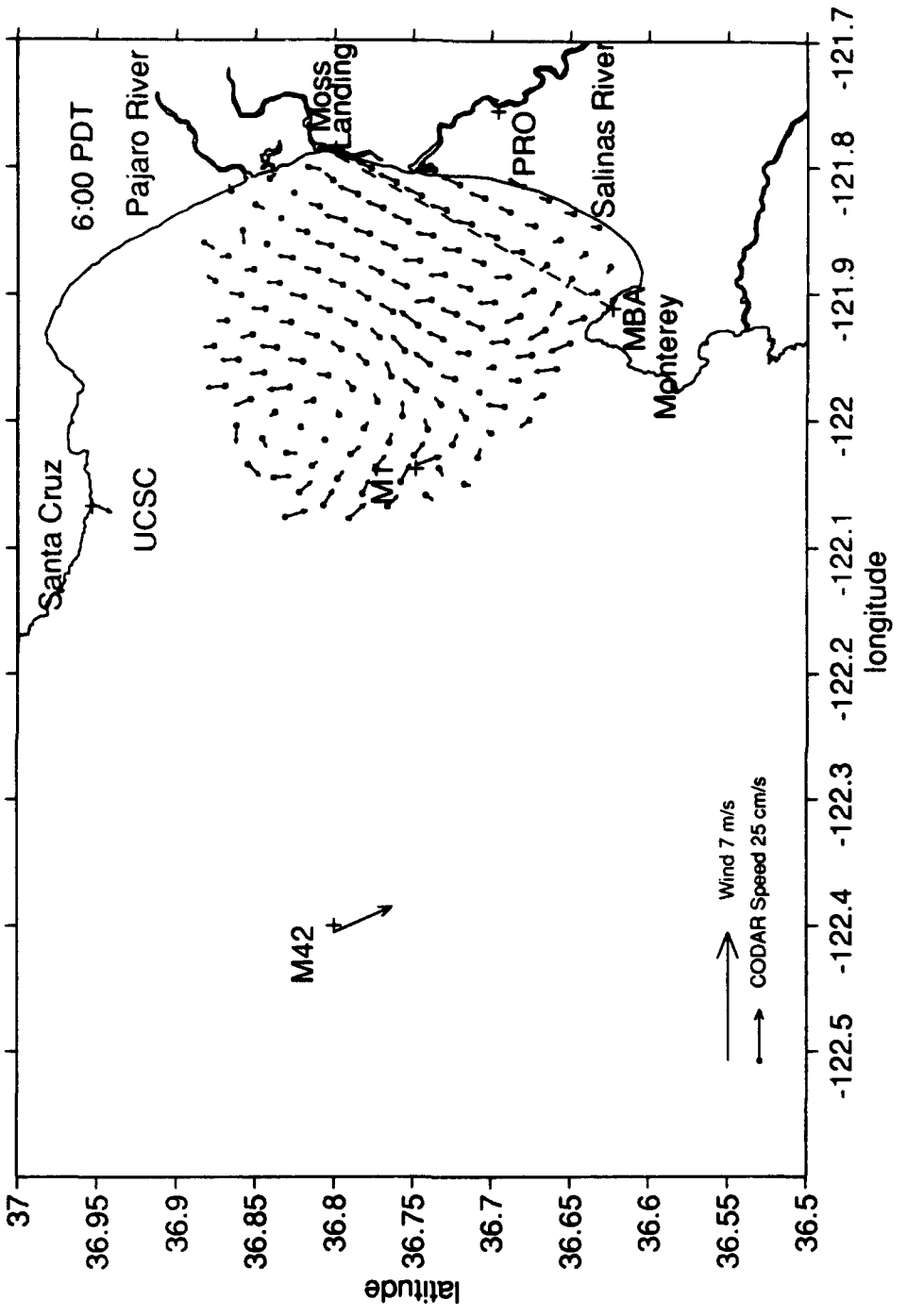

Figure 32. Mean CODAR-derived current and mean wind fields for 0600 PDT in September 1992.

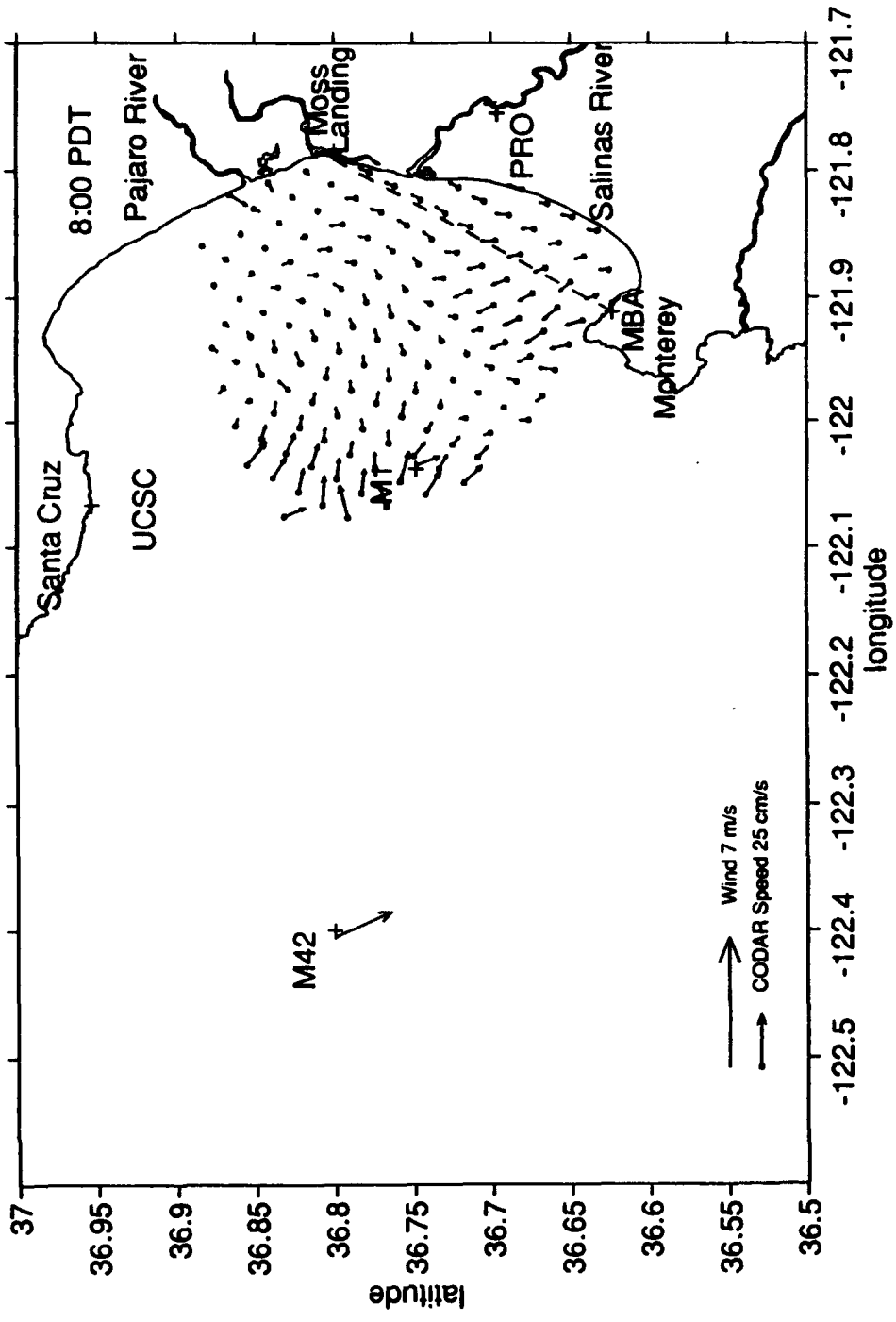

Figure 33. Mean CODAR-derived current and mean wind fields for 0800 PDT in September 1992.

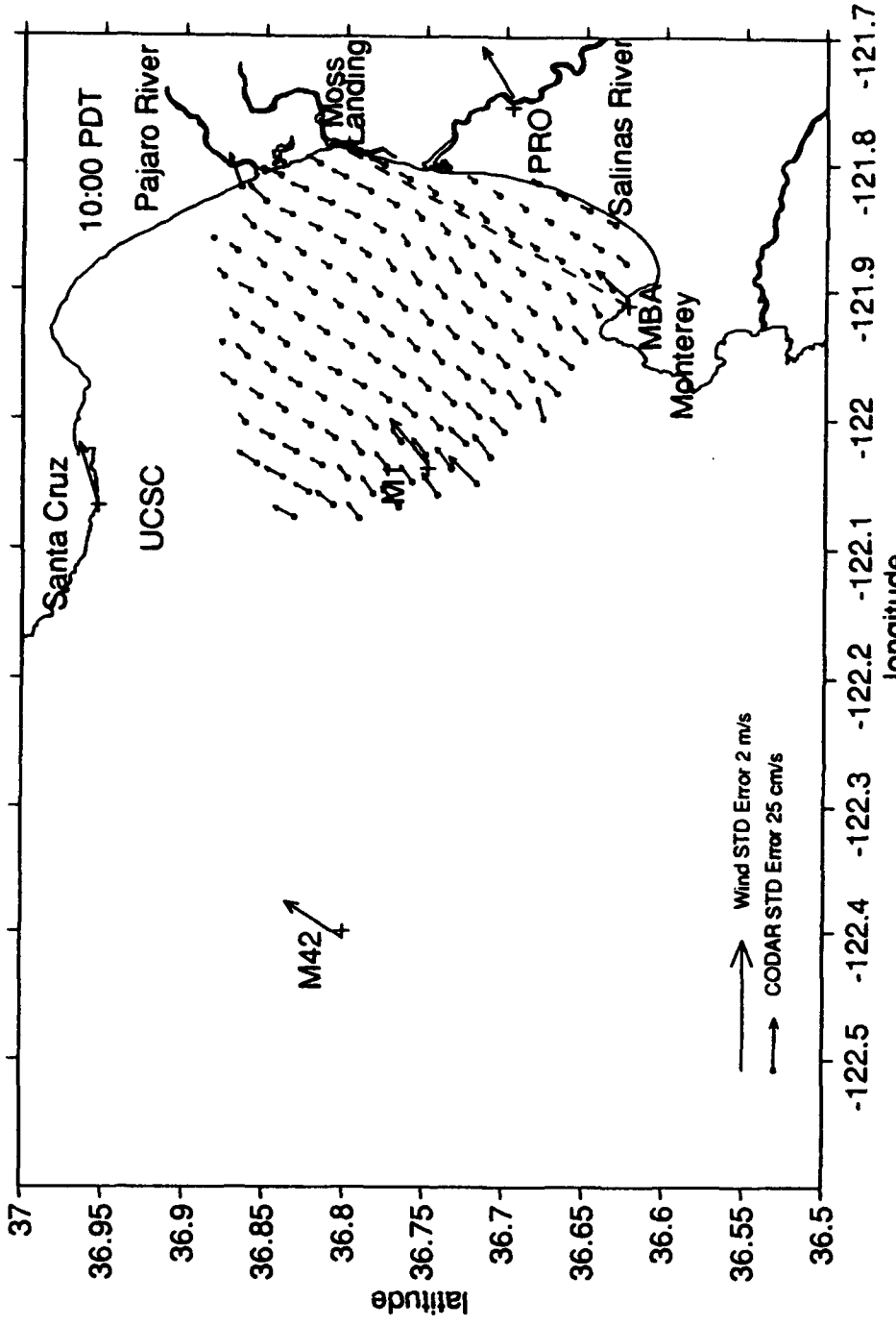

Figure 34. CODAR STD Error Velocity fields for 1000 PDT in September 1992.

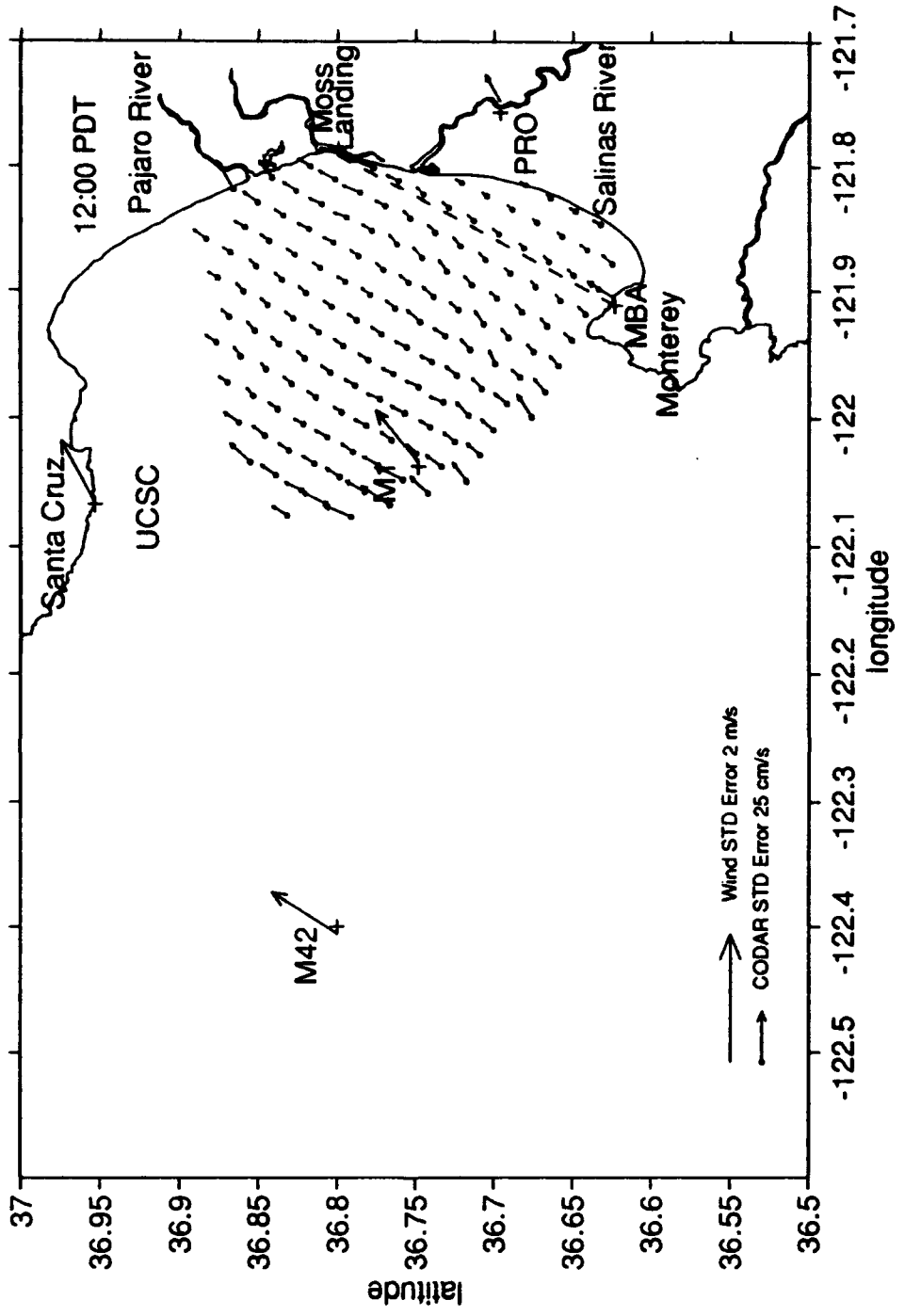

Figure 35. CODAR STD Error Velocity fields for 1200 PDT in September 1992.

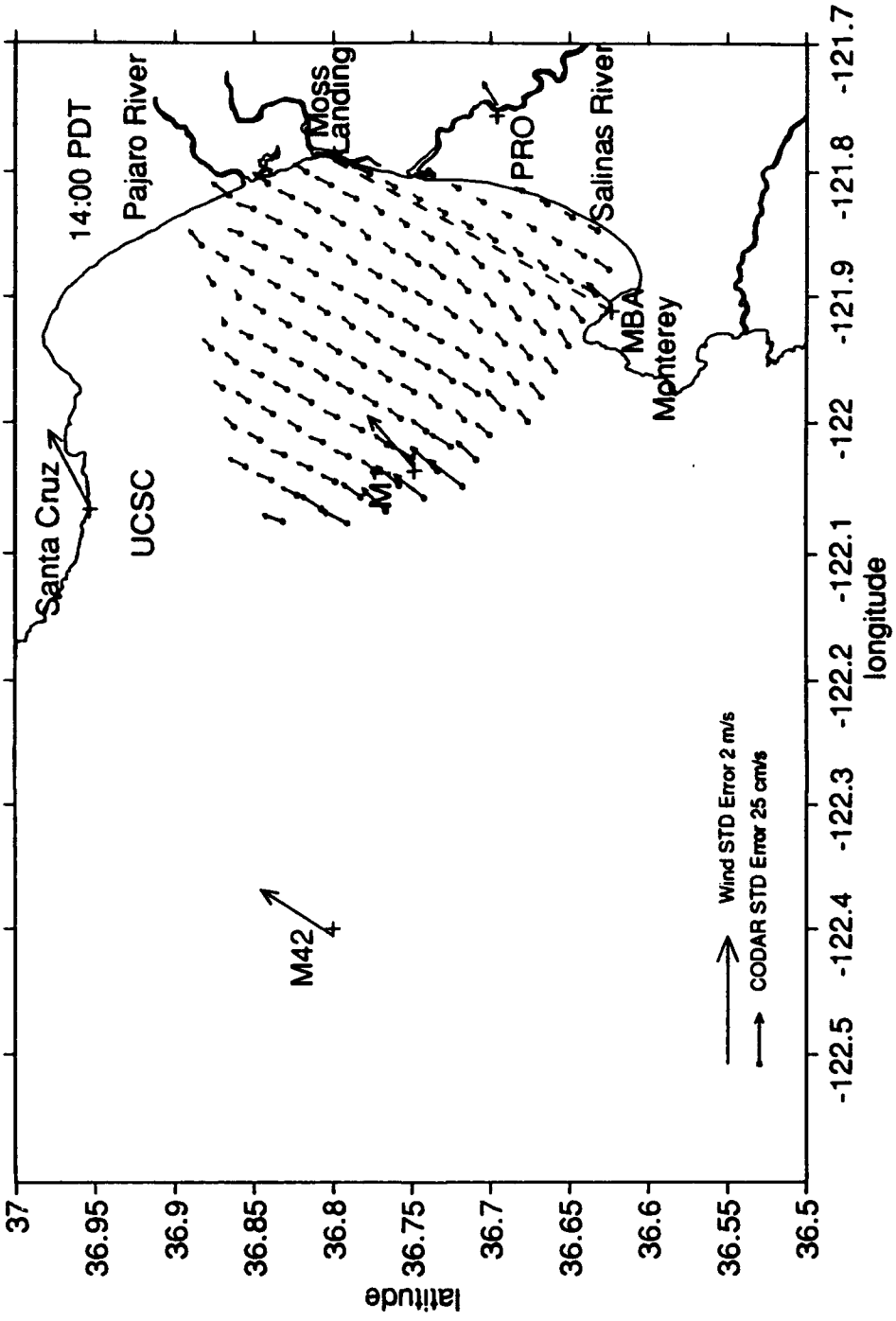

Figure 36. CODAR STD Error Velocity fields for 1400 PDT in September 1992.

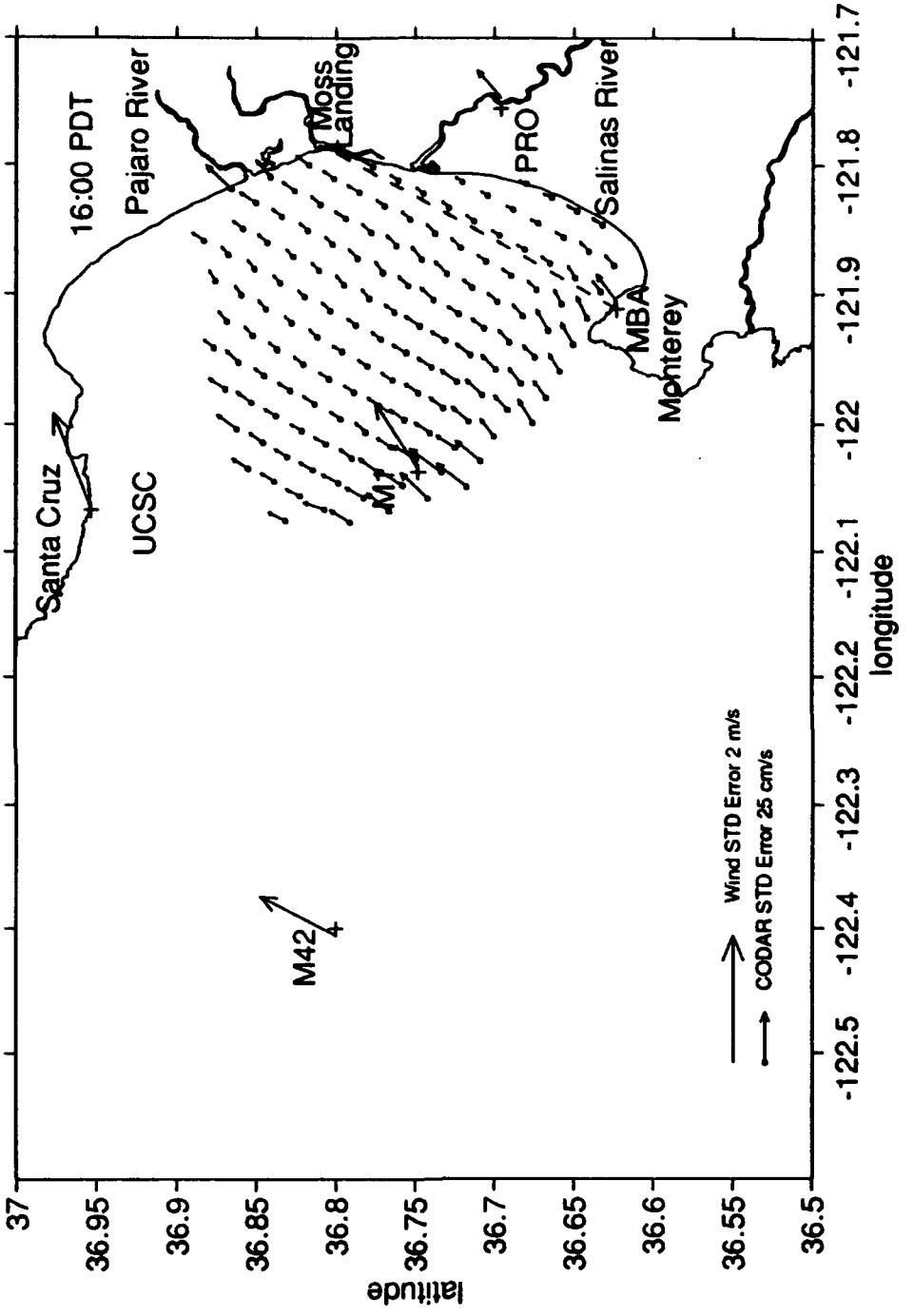

Figure 37. CODAR STD Error Velocity fields for 1600 PDT in September 1992.

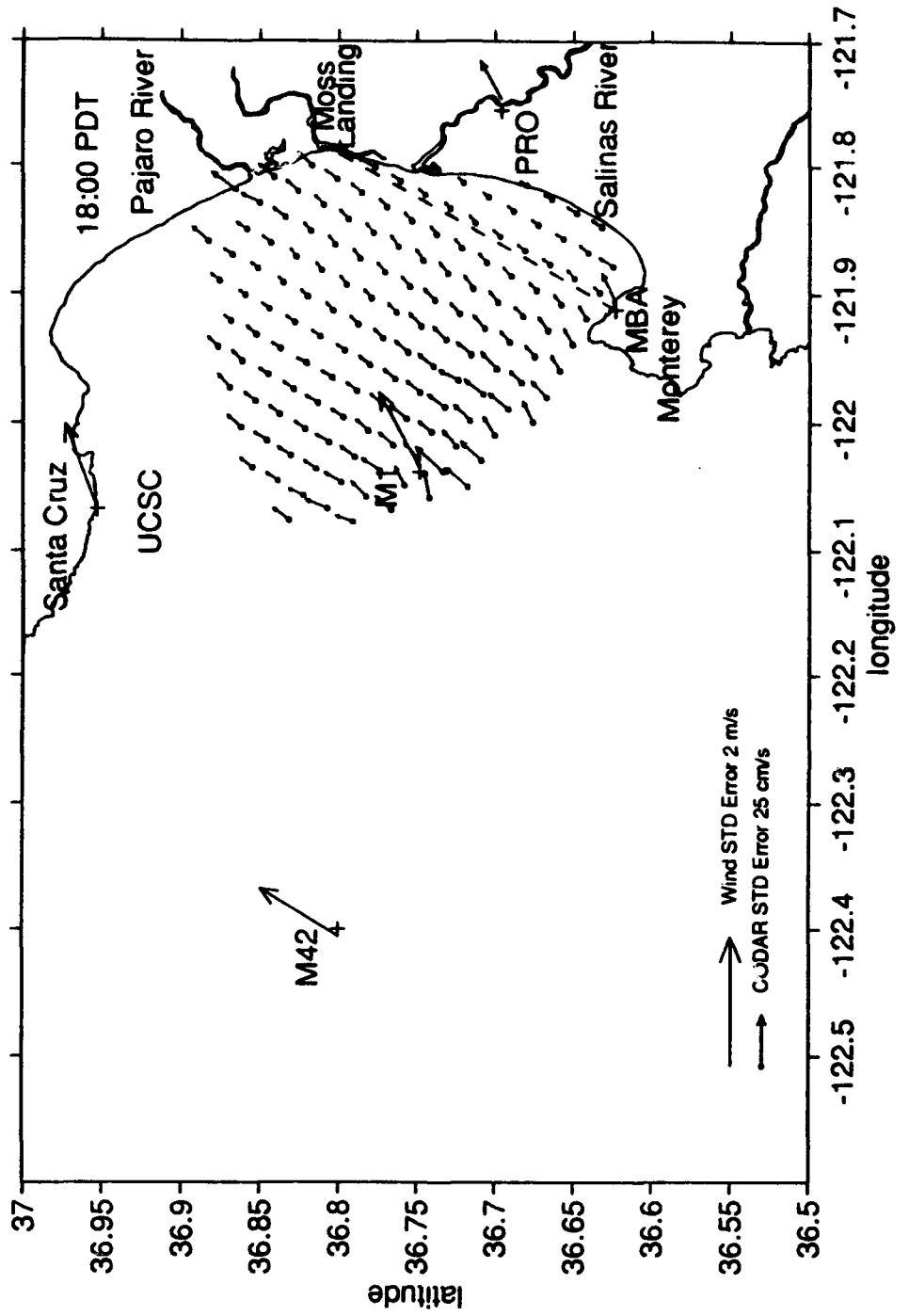

Figure 38. CODAR STD Error Velocity fields for 1800 PDT in September 1992.

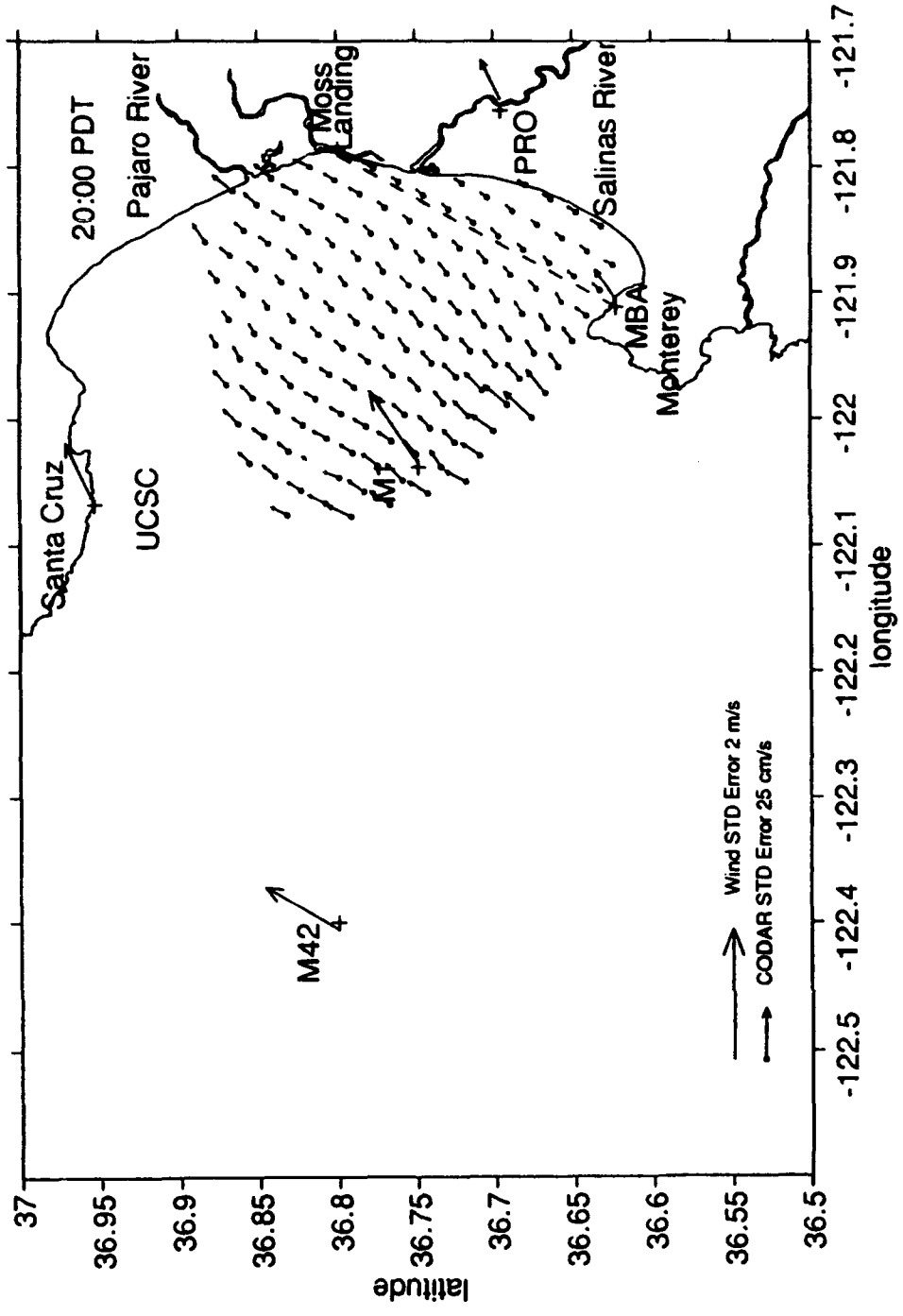

Figure 39. CODAR STD Error Velocity fields for 2000 PDT in September 1992.

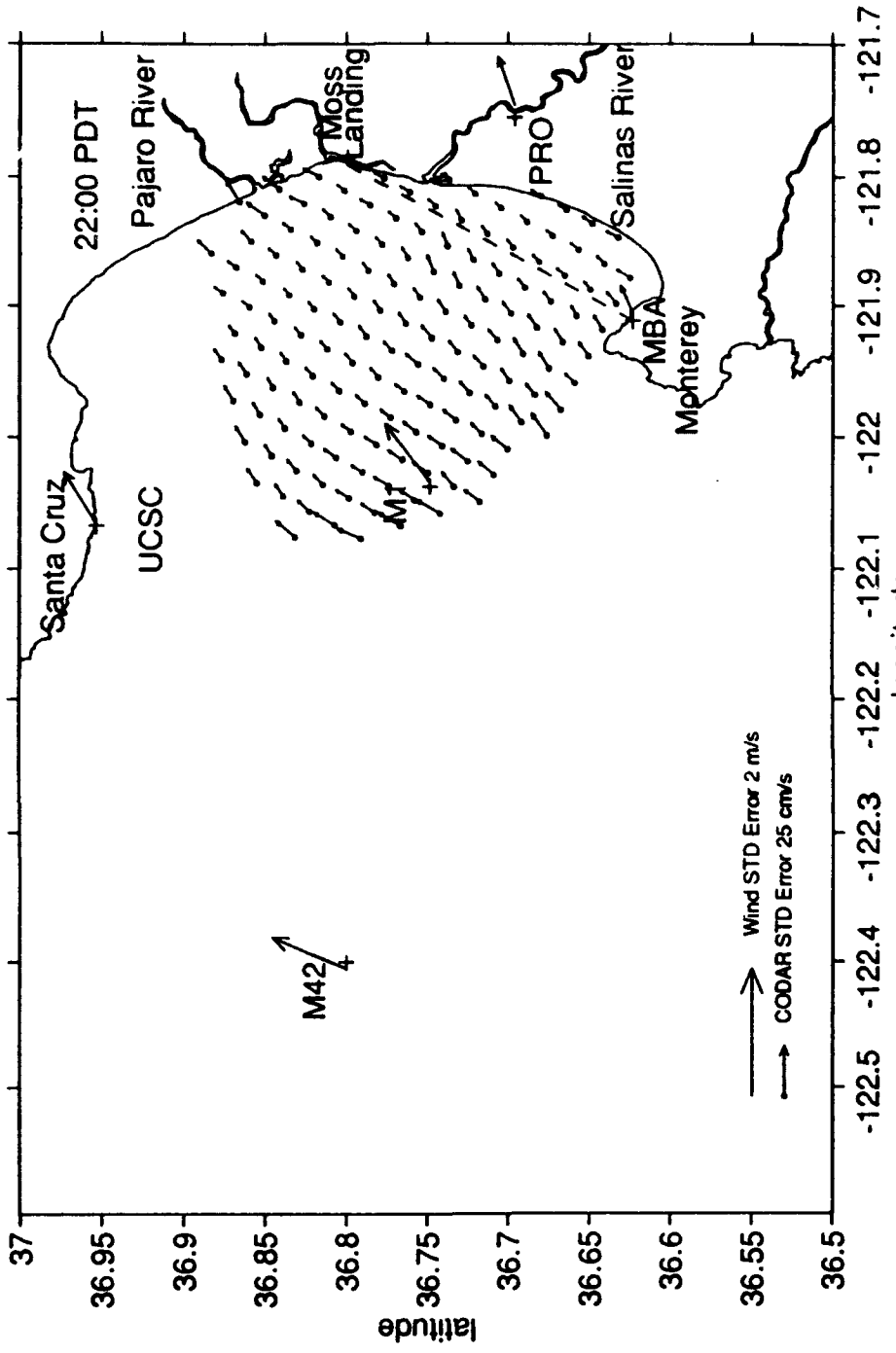

Figure 40. CODAR STD Error Velocity fields for 2200 PDT in September 1992.

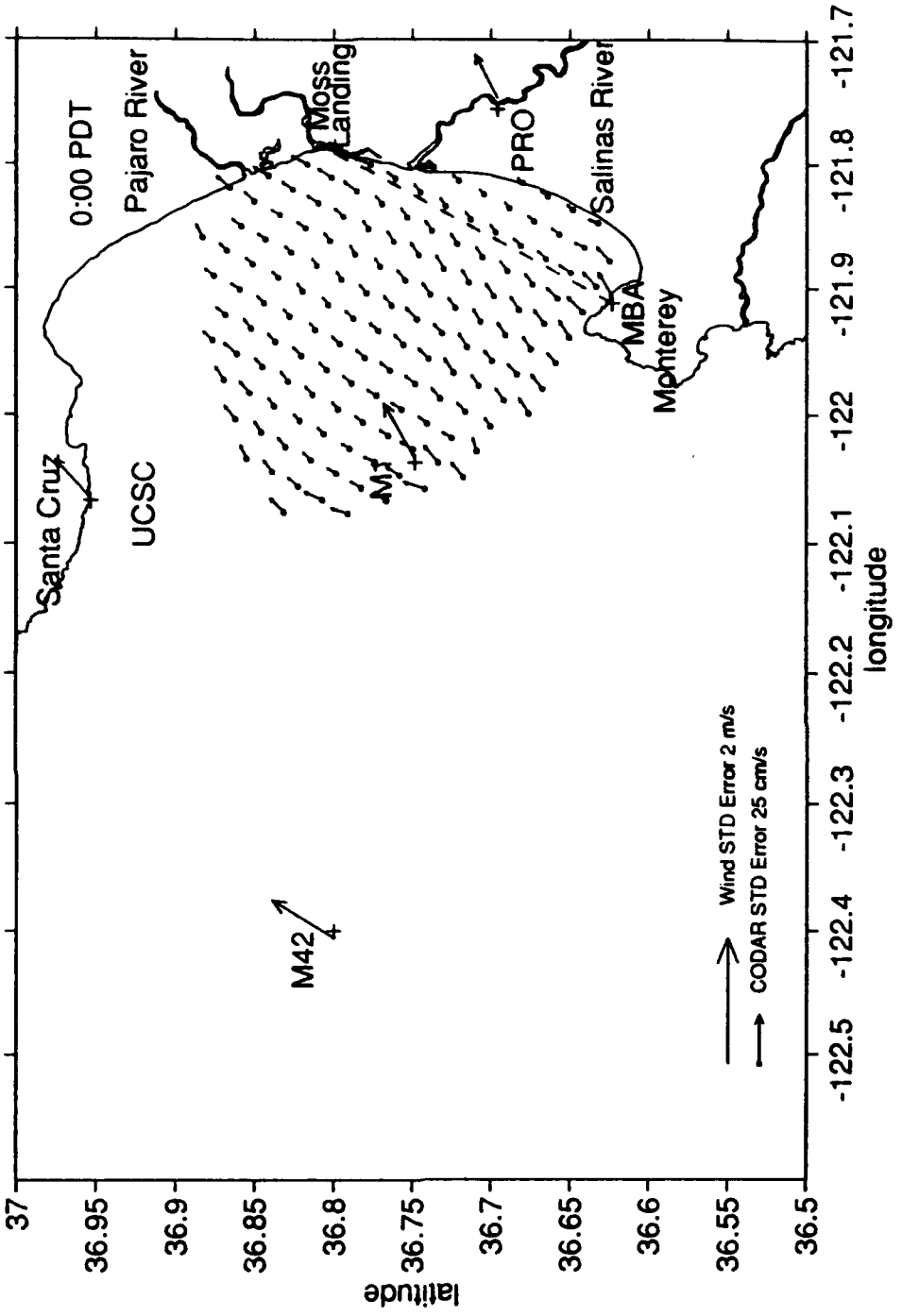

Figure 41. CODAR STD Error Velocity fields for 0000 PDT in September 1992.

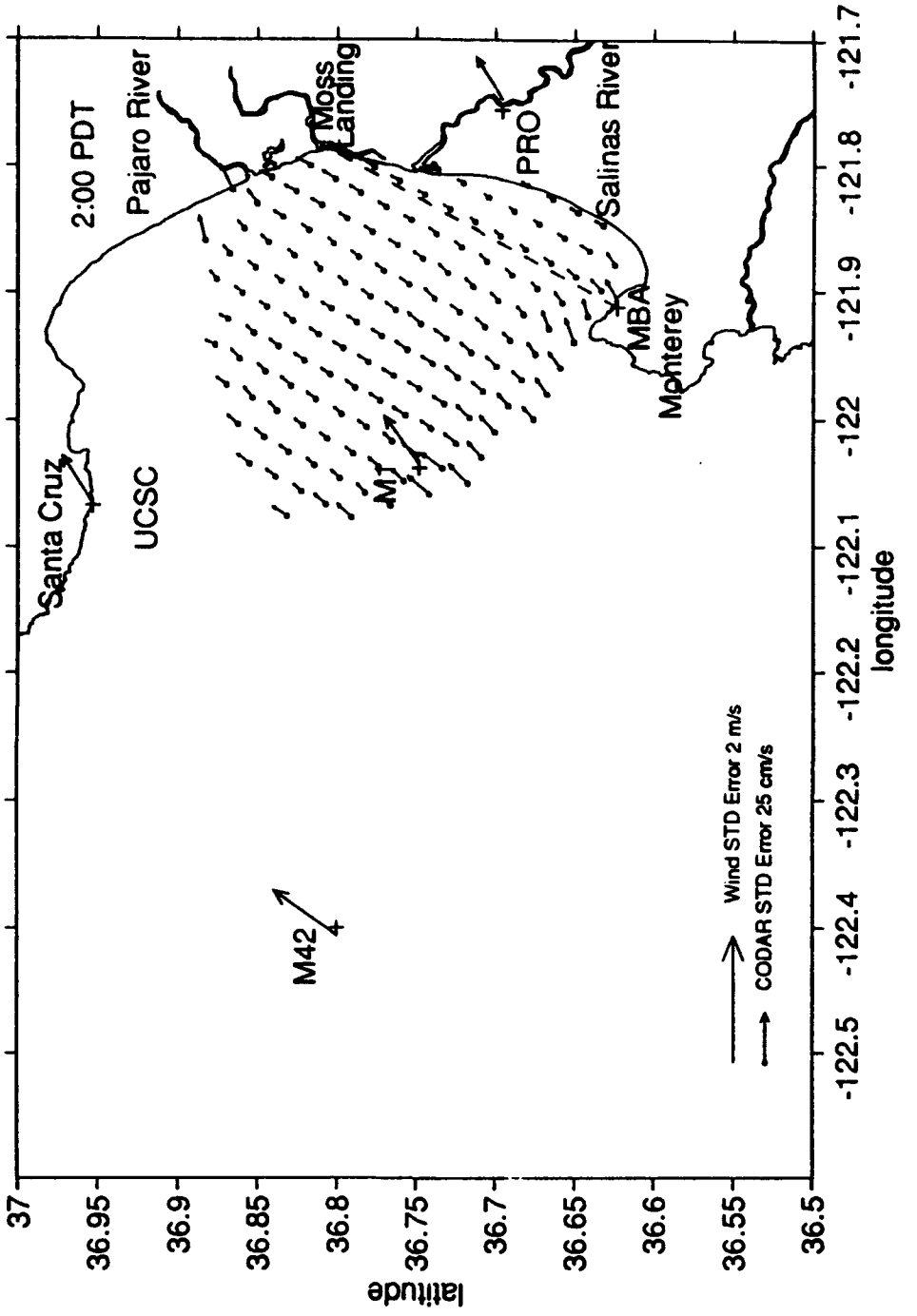

Figure 42. CODAR STD Error Velocity fields for 0200 PDT in September 1992.

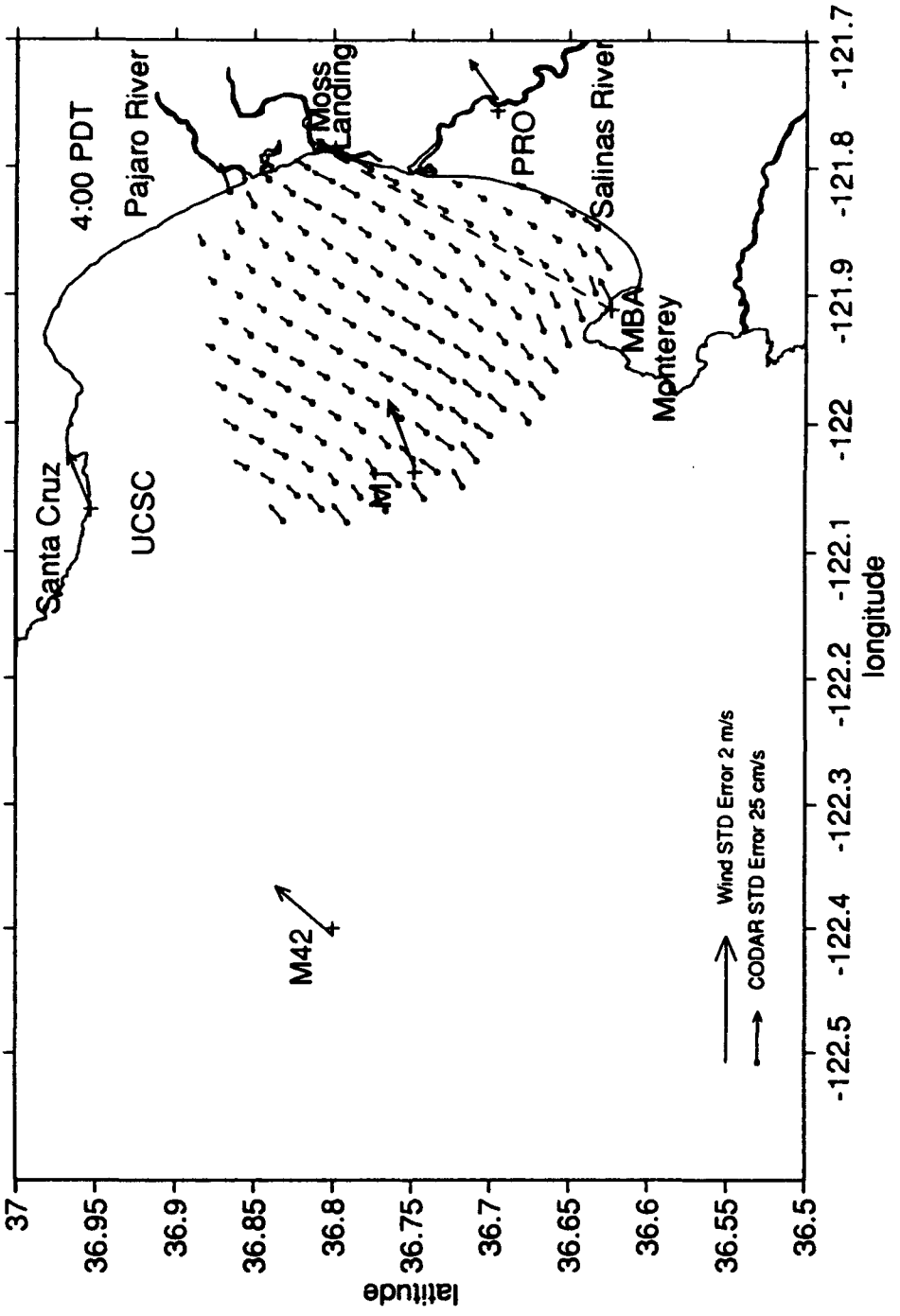

Figure 43. CODAR STD Error Velocity fields for 0400 PDT in September 1992.

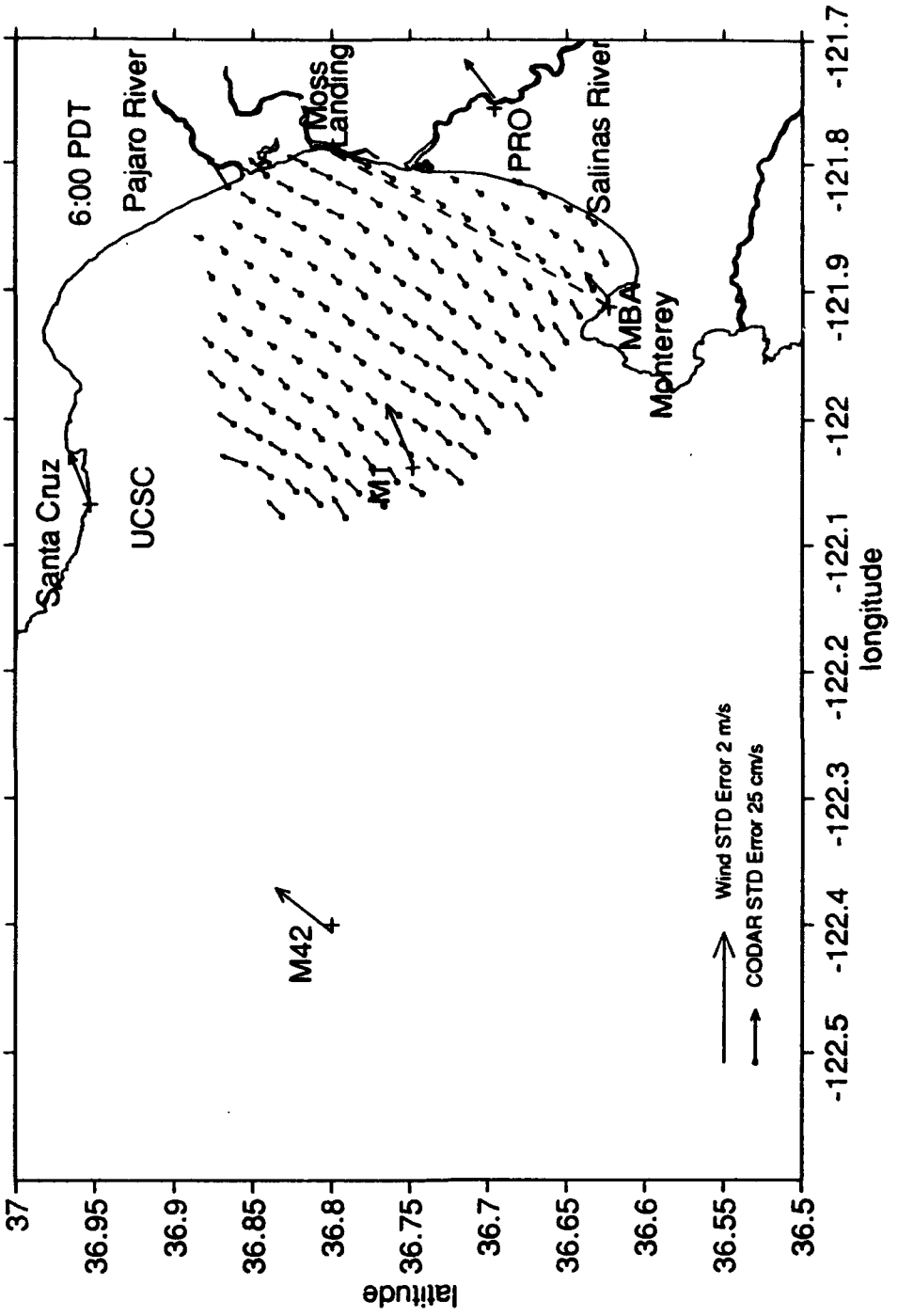

Figure 44. CODAR STD Error Velocity fields for 0600 PDT in September 1992.

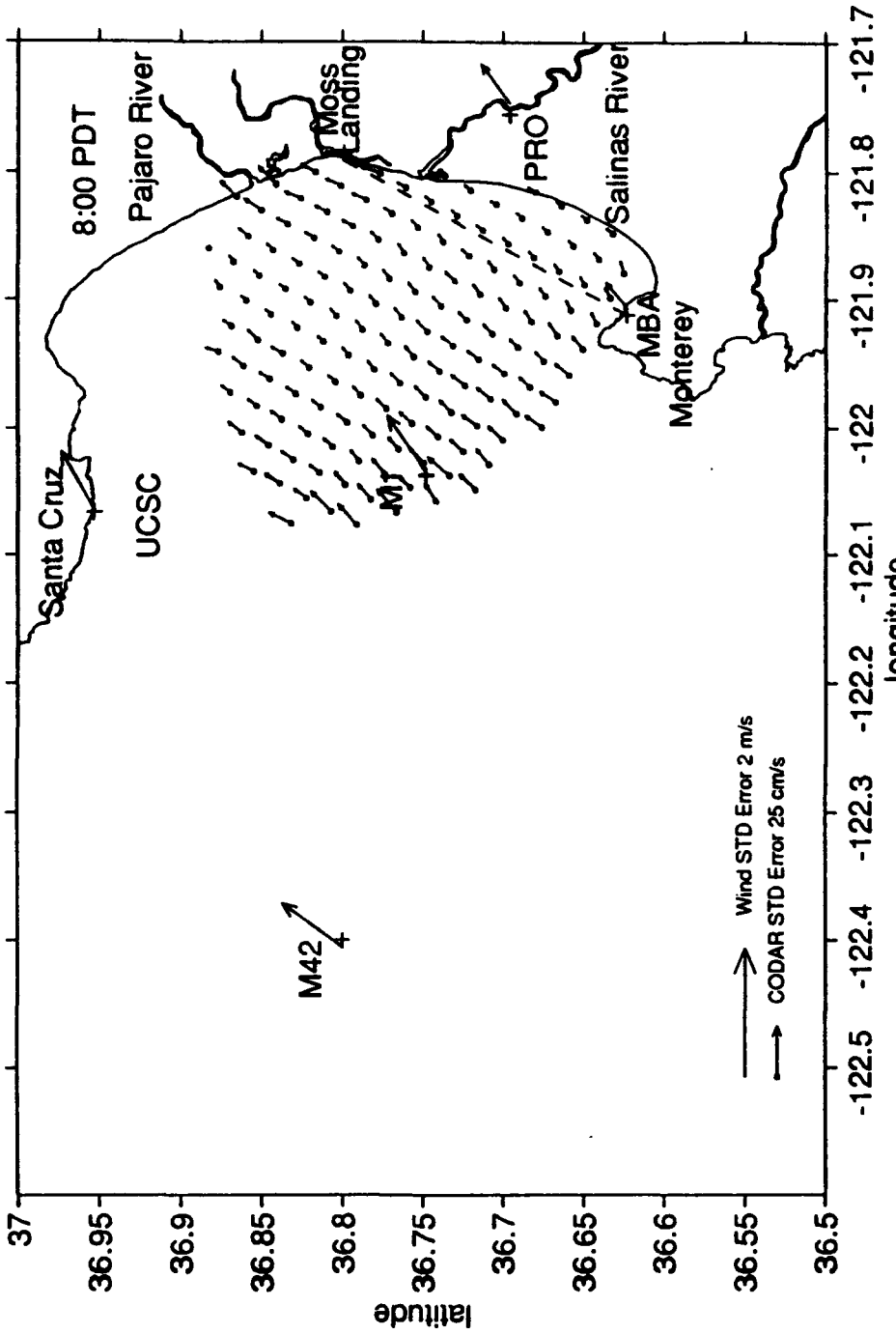

Figure 45. CODAR STD Error Velocity fields for 0800 PDT in September 1992.

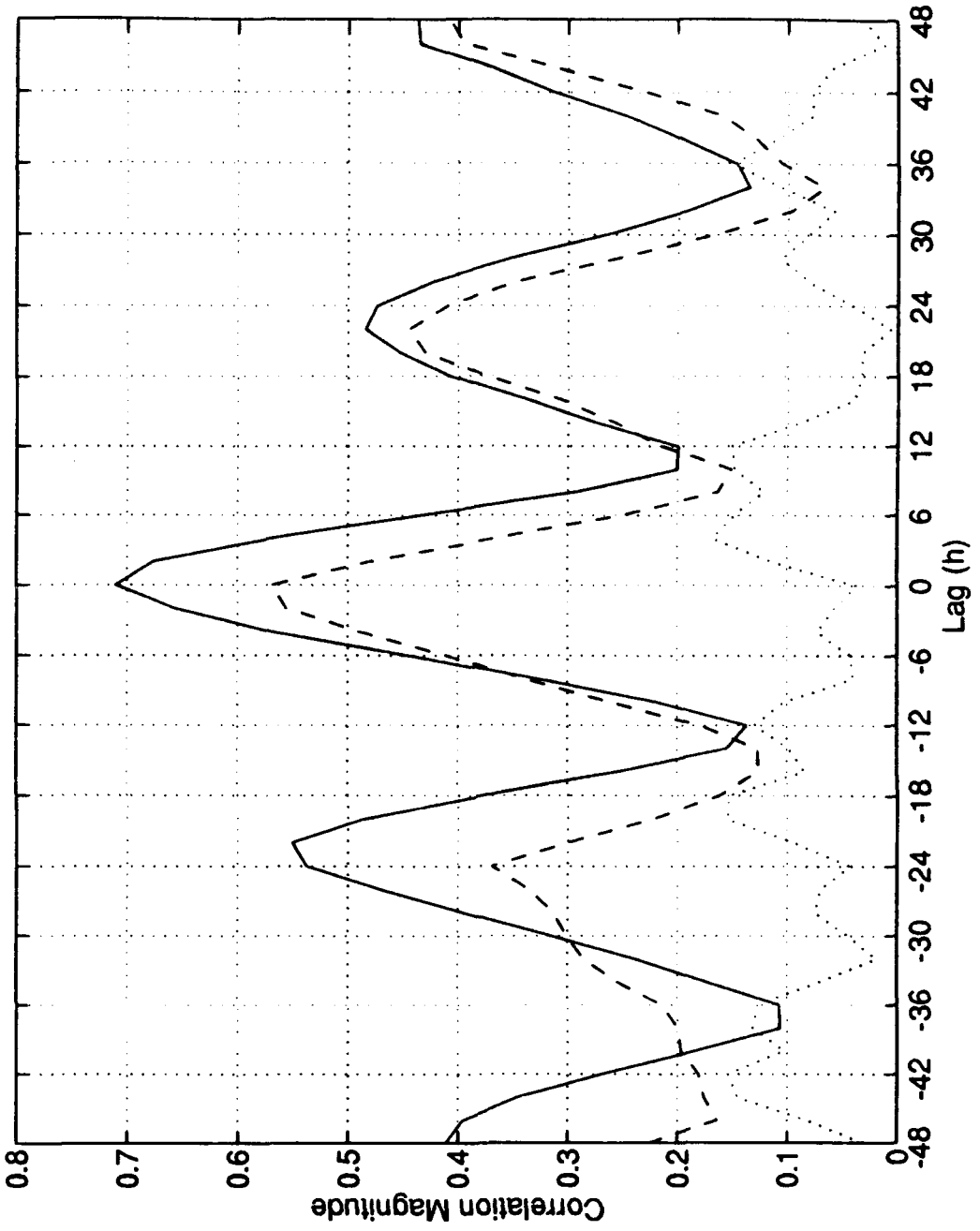

Figure 46. Magnitudes of the lagged complex correlation between selected CODAR derived current records. The solid line represents the correlation between gridpoints 1409 and 1709. The dashed line represents the correlation between gridpoints 1409 and 1305. The dotted line represents the correlation between gridpoints 1409 and 1803.

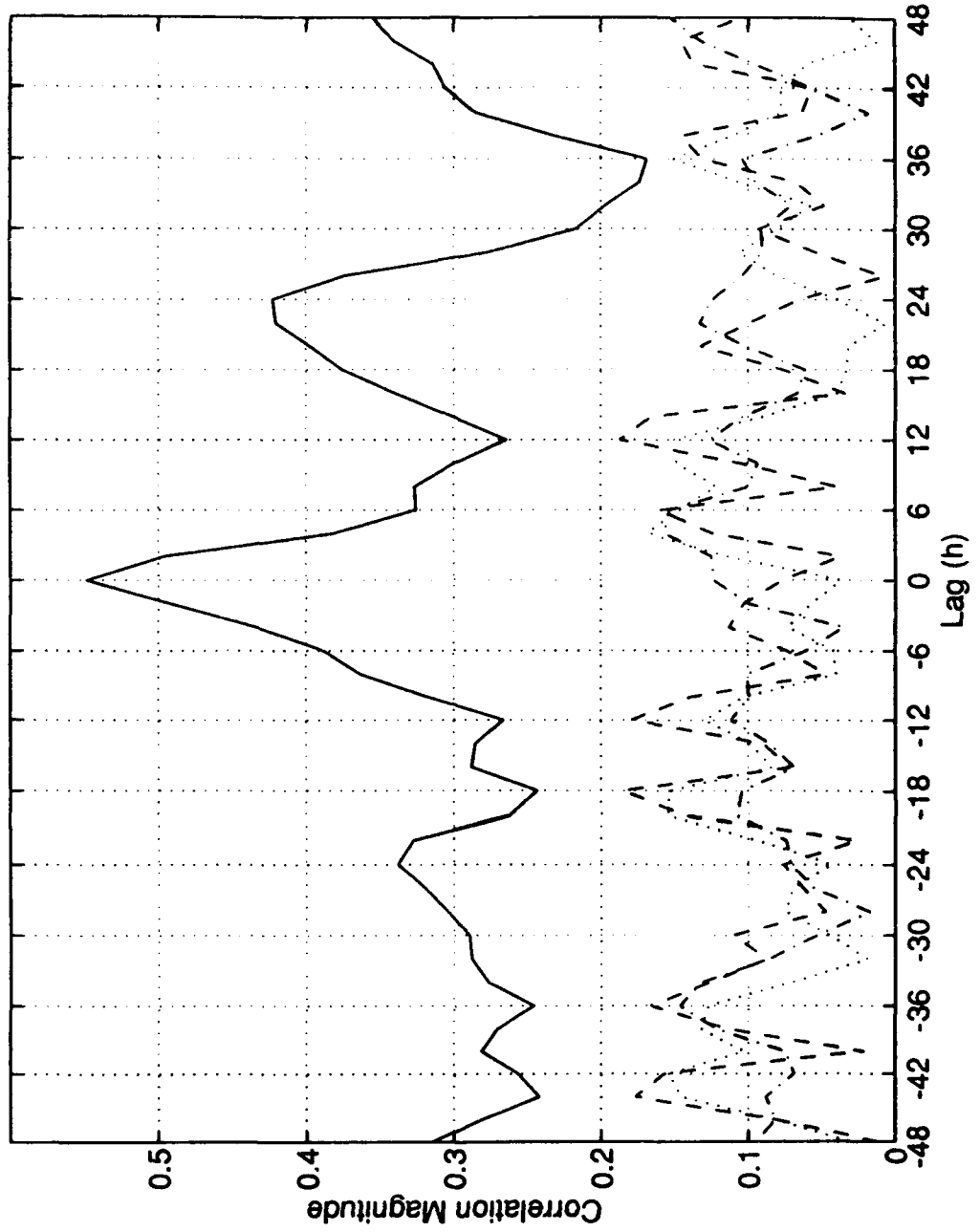

Figure 47. Magnitudes of the lagged complex correlation between selected CODAR derived current records. The solid line represents the correlation between gridpoints 1305 and 1709. The dashed line represents the correlation between gridpoints 1803 and 1305. The dotted line represents the correlation between gridpoints 1409 and 1803. The dash-dotted line represents the correlation between gridpoints 1709 and 1803.

V. CURRENT EFFECTS AS A RESULT OF SEA BREEZE

A. GENERAL DATA CONSIDERATIONS

The final consideration of the combined wind and current data set used in this study attempted to understand the effect of the winds on the currents. (The winds used in this section were reduced to two-hour resolution to correspond with the sampling rate of the CODAR observations.) The CODAR-derived currents seem to be highly sensitive to the effects of the sea breeze. Current velocities orient themselves with the wind flow pattern with the onset of the sea breeze in Monterey Bay (recall Figure 23). The speeds of the currents respond quickly with the changes in wind speeds due to the sea breeze. When larger wind speeds were observed in the late mornings and afternoons, however, the magnitudes of the currents did not increase in proportion, possibly due to momentum transfer of the wind stress into deeper layers of near-surface water. Decreased onshore wind flow during the nights corresponded to periods of current flowing out of Monterey Bay suggesting that there may be a minimum wind stress needed to produce current flows into Monterey Bay, especially in the presence of any offshore pressure gradient due to the build up of water along the coast. A significant current feature in this analysis is the clockwise rotation the currents throughout the late morning and afternoon, after the initial sea breeze impulse in the early morning in the outer portions of the Bay. This rotation occurs first in the outer portions of the Bay and is observed later in the evening closer to shore. It is not

known what causes this rotation of the currents in Monterey Bay. The direction of rotation is consistent with Ekman adjustment or inertial currents. (In this context, Ekman adjustment refers to the transition of the currents, as they proceed from initial downwind state toward the steady state Ekman balance, which is to the right of the wind. Inertial currents forced by the impulsive afternoon winds would rotate clockwise with a period of 20 hours at this latitude in the absence of friction. Observed rotation periods range from 17 to 33 hours.)

B. CURRENT TO WIND ANALYSIS

In order to quantify the relationship between the winds and the currents in Monterey Bay, again, two methods were used to correlate the winds at two shore sites and two ocean sites with CODAR derived currents at three points within the Bay (Figure 17). One method was the spectral analysis method which split the time series of each observation point into its U and V components and performed component-to-component analysis. The other method was to use a complex correlation applied to the vector winds. Both methods used two hourly data.

1. Longitudinal and Latitudinal Cross Spectra

In splitting the winds into the U and V components, it was found that the U components were more highly related to each other than the V components. This is due to the fact that sea and land breezes occur mostly in the east-west direction. Although spectral analysis was performed on all of the previously mentioned CODAR gridpoints, the current data at gridpoint 1409 correlated the highest with the current

data at the other three gridpoints using the complex correlation formulation. Since gridpoint 1409 is also closest to M1, it is used as the focal point for the current to wind analysis. The U and V component spectral analysis results for gridpoint 1409 and the four wind stations for the diurnal period are shown in Tables VI and VII, respectively.

Using the east-west (U) component alone, the currents at gridpoint 1409 lead the winds at all of the observing sites by two or more hours at a level of coherence greater than 95% confidence. Analysis of the currents at gridpoint 1409 indicates that the total peak magnitude of the currents (for both U and V components) occurs two hours later than the peak current in the U direction. Inspection of the time series indicates that the current vectors begin to rotate clockwise before the peak current speed is reached at some gridpoints (1409 and 1709). However, this maximum total current occurs at these gridpoints only two hours later. Even if the rotation of the currents is accounted for with the two hour phase shift, the currents at gridpoint 1409 would still lead the winds at all wind stations, except for MBA which would be in phase.

These statistical results suggest that the diurnal currents peak before the diurnal wind. These are surprising results. It could be explained if the statistical results are not significant. However, these results are found for many pairs of wind and CODAR-derived current observations. Neal (1992) found a similar relationship between wind and CODAR-derived current time series in which currents apparently led the winds. An alternate explanation is that diurnal winds and CODAR-derived

currents are not dynamically related. A possible mechanism for current forcing in Monterey Bay is diurnal tidal forcing, which is not related to the winds. Petruncio (1993) shows, however, that tidal currents in Monterey Bay are small when compared with the diurnal period fluctuations in this study.

It is possible to explain these surprising results due to the process of momentum transfer from the wind to the surface currents. In response to the wind forcing, the velocity of the thin surface slab of water, which is measured by CODAR, would increase initially. As the surface current speed increases, the slab of water would thicken, transferring momentum deeper into the ocean but not necessarily increasing its speed at the surface. Thus it might appear that the current velocities at one meter depth peak while the wind velocities are still increasing.

TABLE VI

U Analysis at f=0.0417 cph or 1.00 day	Phase Difference (degrees)	Phase Difference (h)	Coherence	95% Sig Level of Coherence
C-1409 leads MBA	28.5	1.9	.911	.726
C-1409 leads PRO	50.5	3.4	.942	.726
C-1409 leads M1	72.9	4.9	.983	.726
C-1409 leads M42	82.0	5.5	.915	.726

TABLE VII

V Analysis at f=0.0417 cph or 1.00 day	Phase Difference (degrees)	Phase Difference (h)	Coherence	95% Sig Level of Coherence
MBA leads C-1409	87.0	5.8	.902	.726
PRO leads C-1409	41.9	2.8	.909	.726
C-1409 leads M42	78.0	5.2	.766	.726
C-1409 leads M1	134.3	8.9	.866	.726

2. Complex Correlation

CODAR to wind complex correlations are shown in Figures 48 to 51. Correlation magnitudes for winds and currents at gridpoints 1409 and 1709 were the largest in the study, with the oceanic wind stations correlating highest with both gridpoints (see Figures 48 and 49). There are strong diurnal signals at M1 and, to a lesser extent, at M42 with very slight (within the sampling rate of the observations) lags required for maximum correlations. The correlations of the ocean currents at gridpoints 1305, 1409 and 1709 with the winds from the land stations were significantly less than the oceanic wind stations.

Currents at gridpoint 1305 were most correlated with the winds at M1 (Figure 50). This correlation is encouraging since the wind station and the CODAR gridpoint are near to one another. The land breeze does not reach M1, or as suggested by the high diurnal correlation, it also does not reach gridpoint 1305 either. The diurnal signal is also echoed by the winds at M42 although to a significant lesser extent. The correlation of the land breeze component at the PRO site with the currents

at gridpoint 1305 in the 6 to 12 hour lag time frame is notable, since the same signal is not echoed at MBA as expected.

The currents at gridpoint 1803 did not correlate well with the winds at the oceanic wind stations; but, correlated better with the winds at the land wind stations. Currents at gridpoint 1803 were best correlated with the winds at MBA with only slight lags (Figure 51). The diurnal signal of the sea and land breezes are quite evident in most of the wind correlations, possibly due to the fact that gridpoint 1803 is closest to the shore near Moss Landing. The correlations with the winds at M42 are very weak.

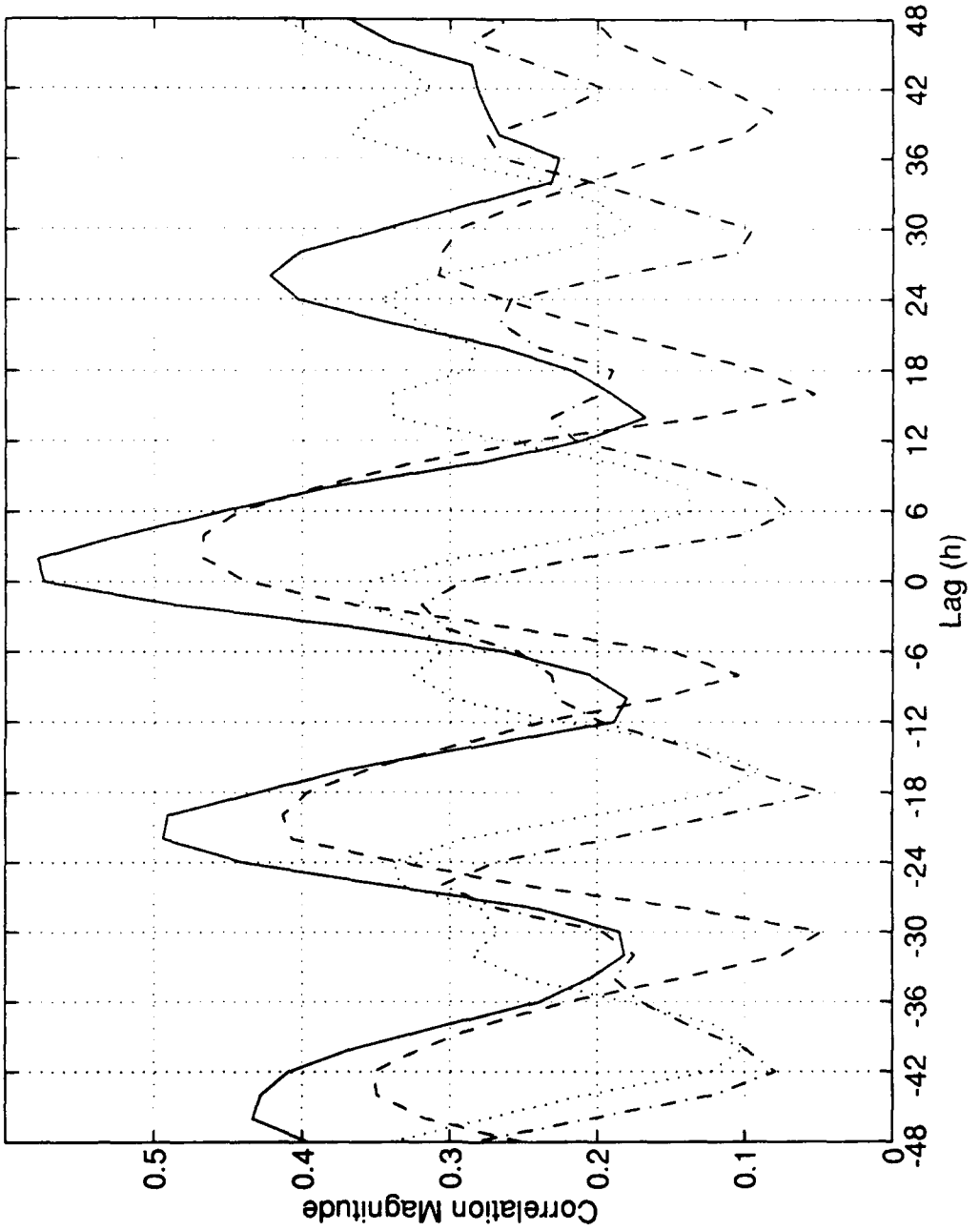

Figure 48. Magnitude of the lagged complex correlation between selected surface winds and CODAR-derived Currents at gridpoint 1709. The solid line represents the correlation between currents and winds at M1. The dashed line represents the correlation between currents and winds at M42. The dotted line represents the correlation between currents and winds at PRO. The dash-dotted line represents the correlation between currents and winds at MBA.

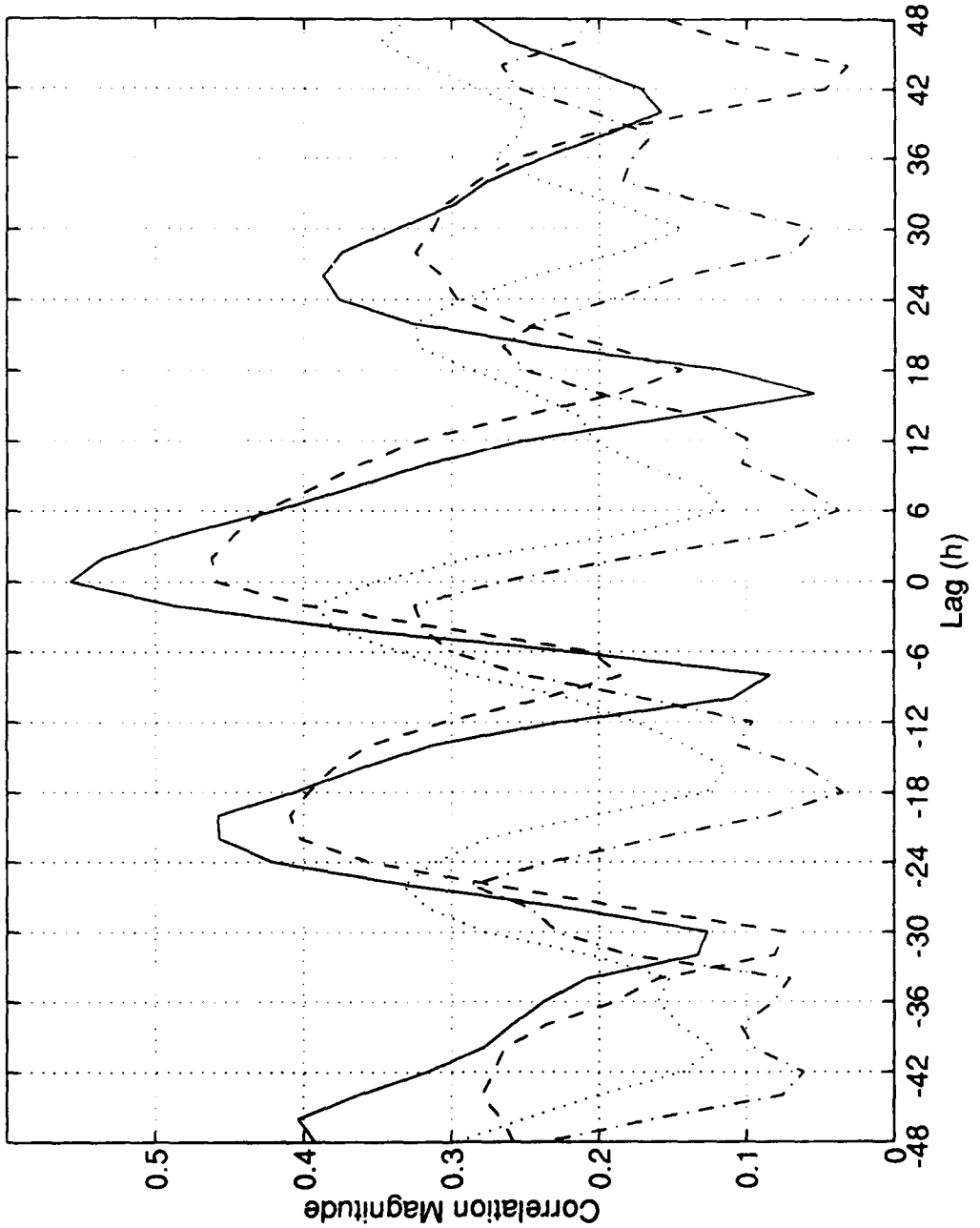

Figure 49. Magnitude of the lagged complex correlation between selected surface winds and CODAR-derived Currents at gridpoint 1409. The solid line represents the correlation between currents and winds at M1. The dashed line represents the correlation between currents and winds at M42. The dotted line represents the correlation between currents and winds at PRO. The dash-dotted line represents the correlation between currents and winds at MBA.

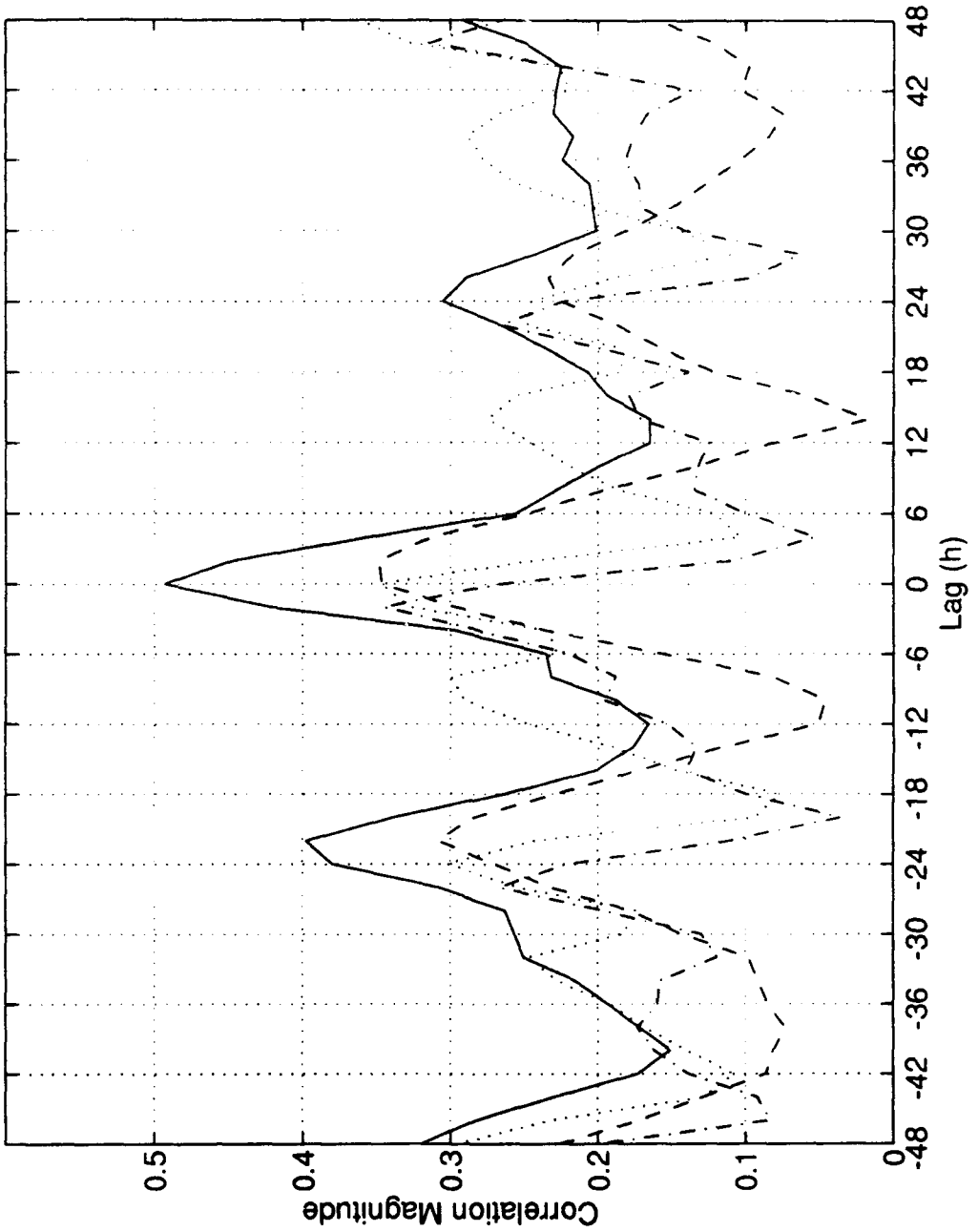

Figure 50. Magnitude of the lagged complex correlation between selected surface winds and CODAR-derived Currents at gridpoint 1305. The solid line represents the correlation between currents and winds at M1. The dashed line represents the correlation between currents and winds at M42. The dotted line represents the correlation between currents and winds at PRO. The dash-dotted line represents the correlation between currents and winds at MBA.

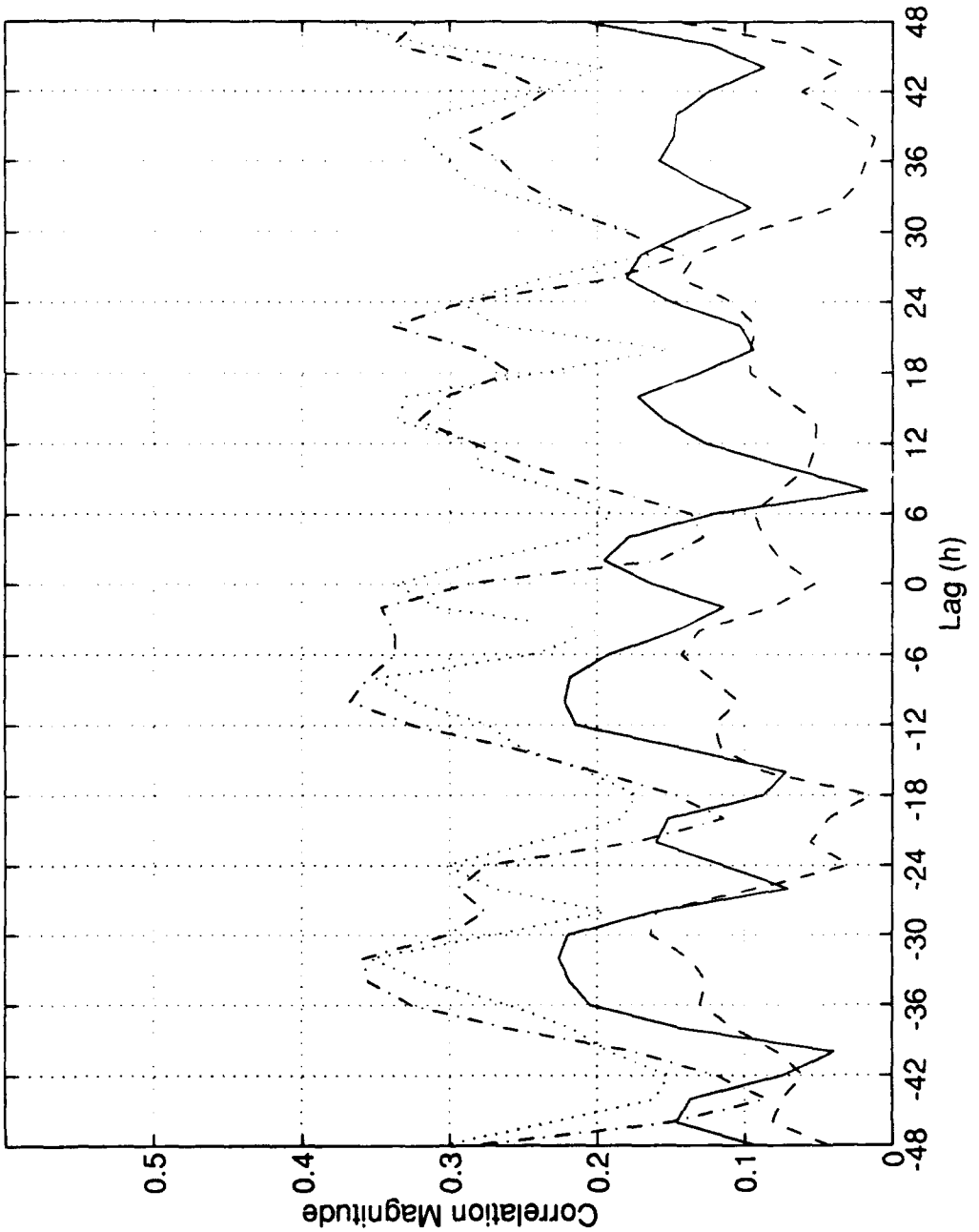

Figure 51. Magnitude of the lagged complex correlation between selected surface winds and CODAR-derived Currents at gridpoint 1803. The solid line represents the correlation between currents and winds at M1. The dashed line represents the correlation between currents and winds at M42. The dotted line represents the correlation between currents and winds at PRO. The dash-dotted line represents the correlation between currents and winds at MBA.

VI. CONCLUSIONS AND RECOMMENDATIONS

A. CONCLUSIONS

The understanding of the diurnal-period fluctuations of the winds and surface currents within Monterey Bay is a complicated process, requiring the interleaving of data from a variety of oceanic, terrestrial and remote-sensing sources. Data was collected and analyzed for the month of September 1992. Wind data from five observation stations (three land stations and two oceanic stations) indicate a complex wind circulation pattern that varies temporally and spatially. Analysis of the continuous wind observations indicates a growth in scale of the sea breeze circulation that explains the wind field at both coastal and oceanic wind stations. The sea breeze begins first along the coast with flow perpendicular to the coast line. The sea breeze grows by advancing inland and oceanward. Once the sea breeze is well established, the coastal wind flow alignment rotates toward the southeast under the influence of a larger-scale sea breeze circulation caused by intense heating in the Salinas and Santa Clara Valleys.

Once the nature of the diurnal wind influences were understood, the same descriptive and analytical techniques were applied to the surface currents in Monterey Bay. In general, it was found that the currents flowed into Monterey Bay during the daytime and out of the Bay at nighttime. Daytime currents respond quickly to sea breeze forcing, often in less time than can be measured by the two hour sampling

interval of the CODAR current measuring system. Under the influence of the sea breeze, the daytime currents across the entire Bay accelerate and orient themselves parallel to the Salinas Valley. In the afternoon, the offshore currents rotate clockwise while the surface winds continue their onshore (easterly) flow. As the day progresses, the clockwise rotation of the currents spreads into the interior of the Bay. The nighttime currents are not directly influenced by surface winds since they flow out of the Bay, opposite the weak nighttime winds at most locations. The uniform clockwise rotation of the currents within the outer portions of Monterey Bay may be due to Ekman adjustment or inertial currents as discussed in Section V.A.

The mean monthly and canonical day CODAR-derived current fields indicate a complicated eddy pattern within Monterey Bay that could be induced by the coastal boundary and/or the Monterey Canyon (see Figure 17). A weak, small cyclonic eddy in the mean monthly current field is centered northwest of Moss Landing over the Monterey Canyon. A weak cyclonic eddy is also visible in the canonical day current fields over the Monterey Canyon, varying its position from near M1 to northwest of Moss Landing depending upon the time of day. This weak eddy in the average fields suggest that the steady onshore current flow within the Bay during the daytime interacts with the coastal boundary to generate pressure gradients that produce surface currents that flow contrary to surface winds in late afternoon and nighttime.

B. RECOMMENDATIONS

It is recommended that this study be repeated again for a different observational period. The data at M1 is under suspicion since the wind direction sensor failed at some unknown point in its deployment. Also, additional wind data is available in the Bay for other time frames. MBARI mooring buoy M2 was not available in September 1992 due to routine maintenance, but will be available for other time frames. Also, recently the CODAR network within Monterey Bay has been improved with another CODAR installation at UCSC so that currents can be determined in the northern portions of the Bay as well as the northern approaches to the Bay.

Due to the fact that the surface current response occurs so quickly, the two hour sampling interval of the CODAR current measuring system is too large to get a very accurate picture of the exact initiation times of the current response to sea breeze forcing. It is recommended that the sampling interval of the CODAR stations in Monterey Bay be shortened to 30 minutes or one hour if the computer resources are sufficient.

It is also recommended separate the confirmed "sea breeze" days from the "non-sea breeze" days in accordance with sea breeze statistical delimiters outlined by Round (1993) in order to eliminate the contamination of atypical or non sea breeze events in the data set.

It is likely that a complete description of diurnal surface winds and currents in Monterey Bay will require a complicated set of physics and parameters. The simple notion of thermally-direct forcing of the sea breeze winds holds for Monterey Bay but

the scale of the phenomenon grows throughout the day. Certainly the ultimate size and strength of the sea breeze is controlled by the larger-scale synoptic winds.

In terms of the diurnal surface currents, direct forcing by the sea breeze winds accounts for only a small part of the daily current patterns. Afternoon currents clearly align with the strong afternoon winds but then quickly rotate clockwise while the winds continue their thermally-directed onshore flow. Pressure gradient forcing due to piling up of water at the coastline, direct wind forcing, and tides all play a role. A simple one-dimensional upper ocean model might be used to identify those parts of the diurnal currents that are entirely locally forced. A numerical model that incorporates observed episodic wind forcing, coastline shape, and observed tidal currents may be successful in describing the complete diurnal cycle of surface currents, particularly if direct current information is available over more of the Bay from additional HF radar sites to verify and time model parameters.

LIST OF REFERENCES

Banta, R. M., Oliver, L. D., and Levinson, D. H., "Evolution of the Monterey Bay Sea-Breeze Layer as Observed by Pulsed Doppler Lidar," *Journal of the Atmospheric Sciences*, submitted 1993.

Barrick, D. E., and Growler, J. F. R., "Panel Discussion Summary," *IEEE Journal of Oceanic Engineering*, vol. OE-11, no. 2, pp. 147-149, 1986.

Barrick, D. E., Evans, M. W., and Weber, B. L., "Ocean Surface Currents Mapped by Radar," *Science*, 198, pp. 138-144, 1977.

Crombie, D. D., "Doppler Spectrum of Sea Echo at 13.56 Mc/s," *Nature*, vol. 175, pp. 681-682, 1955.

Elliott, D. L., and O'Brien, J. J., "Observational Studies of the Marine Boundary Layer over an Upwelling Region," *Monthly Weather Review*, vol. 105, pp. 86-98, 1977.

Fernandez, D. M., *High-Frequency Radar Measurements of Coastal Ocean Surface Currents*. Ph.D. Dissertation, Stanford University, San Francisco, California, 1993.

Gill, A. E., *Atmospheric-Ocean Dynamics*. Academic Press, New York, 1982.

Holton, J. R., *An Introduction to Dynamic Meteorology*, Academic Press, San Diego, California, 1979.

Hsu, S. A., *Coastal Meteorology*. Academic Press, San Diego, California, 1988.

Krauss, W., and Böning, C. W., "Lagrangian Properties of Eddy Fields in the Northern North Atlantic as Deduced from Satellite-tracked Buoys," *Journal of Marine Research*, vol. 45, no. 2, pp. 259-291, 1987.

Kundu, P. K., "Ekman Veering Observed near the Ocean Bottom," *Journal of Physical Oceanography*, vol. 6, pp. 238-242, 1976.

Neal, T. C., *Analysis of Monterey Bay CODAR-Derived Surface Currents*. M.S. Thesis, Naval Postgraduate School, Monterey, California, September 1992.

Nuss, W., interview between W. Nuss, Naval Postgraduate School, and the author, November 1993.

Petruncio, E. T., *Characterization of Tidal Currents in Monterey Bay from Remote and In-Situ-Measurements*. M.S. Thesis, Naval Postgraduate School, Monterey, California, December 1993.

Round, R. D., *Climatology and Analysis of the Monterey Bay Sea Breeze*. M.S. Thesis, Naval Postgraduate School, Monterey, California, September 1993.

Stewart, R. H., and Joy, J. W., "HF Radio Measurement of Surface Currents," *Deep Sea Research*, vol. 21, pp. 1039-1049, 1974.

INITIAL DISTRIBUTION LIST

		No. Copies
1.	Defense Technical Information Center Cameron Station Alexandria, VA 22304-6145	2
2.	Attn: Library, Code 52 Naval Postgraduate School Monterey, CA 93943-5000	2
3.	Superintendent Attn: Chairman, Department of Meteorology (Code MR/HY) Naval Postgraduate School Monterey, CA 93943-5000	1
4.	Superintendent Attn: Chairman, Department of Oceanography (Code OC/CO) Naval Postgraduate School Monterey, CA 93943-5000	1
5.	Superintendent Attn: Professor C. H. Wash (Code MR/WX) Naval Postgraduate School Monterey, CA 93943-5000	2
6.	Superintendent Attn: Assistant Professor J. D. Paduan (Code OC/PD) Naval Postgraduate School Monterey, CA 93943-5000	2
7.	Lieutenant Commander Michael D. Foster 5 Mervine Street Monterey, CA 93940	1
8.	Superintendent Naval Research Laboratory 7 Grace Hopper Avenue Stop 2 Monterey, CA 93943-5502	1

9. Chairman
Oceanography Department
U. S. Naval Academy
Annapolis, MD 21402 — 1

10. Office of Naval Research (Code 420)
800 N. Quincy Street
Arlington, VA 22217 — 1

11. Library
Scripps Institution of Oceanography
P.O. Box 2367
La Jolla, CA 92037 — 1